	MAPP	

Titel: **MAPP Algorithm Theoretical Basis Document**

Project: MAPP

Doc. No.: MAPP-ATBD

Issue: 2

Revision: 0

Date: 27.3.2000

	Function	Name	Organisation	Signature	Date
Author:		MAPP Team			

Copyright © 2000 Brockmann Consult

Internal Distribution

Name	Organisation	Qantity
R. Doerffer	GKSS	1
H. van der Piepen	DLR	1
J. Fischer	FUB	1
A. Neumann	DLR	1
C. Brockmann	Brockmann Consult	1

External Distribution

Name	Organisation	Quantity
M. Edelwirt	PT-UKF	2
K. Schmidt	DLR	1

Change Record

Issue	Revision	Date	Changes
1	0	8.3.1999	initial issue
2	0	27.3.2000	updated ATBDs 1,4,5 new ATBDS 12,13,14,15,16

Copyright © 2000 Brockmann Consult

MAPP

Algorithm Theoretical Basis Documents

1 GUIDE

This document is the foundation of the theoretical basis of the algorithms and associated products developed within the MERIS Application and regional Products Project, MAPP.

The overview about the different algorithms and products, their interdependencies and their integration within a single software processor is described in the System Architecture Theoretical Basis Document, SATBD, which is the first in the sequence of the following detailed text sections. The sections 2 – 8 describe the operational Level 2 algorithms and products, their physical background, a mathematical description, implementation details and validation plans. The Level 3 products are described in sections 10 an 11. For most products, a general method will be applied which is outlined in section 10, while for the cloud and water vapour level 3 products a different approach is foreseen which is described in section 11. Finally, sections 12 – 16 include the ATBDs for the experimental products.

Copyright © 2000 Brockmann Consult

This page is intentionally left blank

Copyright © 2000 Brockmann Consult

Document Overview

Index No.	Doc. No.	Title	March 99 Issue No.	March00 Issue No	
1	MAPP-SATBD	MAPP System Architecture Theoretical Basis Document	1.0	1.1	
2	MAPP-ATBD-WC1	Regionalized Case-II Water Products and Algorithms	1.0		
3	MAPP-ATBD-WC2	Chlorophyll Concentration, Sediment Scattering and Gelbstoff Absorption derived from MERIS Normalised Water Leaving Reflectances using Principal Component Inversion (PCI)	1.0		
4	MAPP-ATBD-AER	Optical Depth of “Fine” and “Coarse” Aerosols, total Aerosol Optical Depth, Optical Depth of Thin Cirrus and Water Leaving Reflectance	1.1	2.0	
5	MAPP-ATBD-LCC	Land Cover / Land Use Classification	1.1	1.6	
6	MAPP-ATBD-NDVI	AVHRR Compatible NDVI	-	1.0	
7	MAPP-ATBD-CACO	Cloud Albedo and Cloud Optical Thickness	1.1		
8	MAPP-ATBD-CTP	Cloud Top Pressure	-	1.0	
9	MAPP-ATBD-WV	Water Vapour	1.1		
10	MAPP-ATBD-GENL3	Generic algorithms for Level 3 products	1.0		
11	MAPP-ATBD-CLWVL3	Cloud and Water Vapour Level 3 Products	1.0		
12	MAPP-ATBD-ARF	Aerosol direct Radiative Forcing	-	1.0	
13	MAPP-ATBD-CMP	Cloud Microphysical Properties	-	1.0	
14	MAPP-ATBD-CMAP	Chlorophyll Map	-	1.0	
15	MAPP-ATBD-PCLASS	Phytoplantkon Classification	-	draft	
16	MAPP-ATBD-PP	Primary Production	-	draft	

Copyright © 2000 Brockmann Consult

Copyright © 2000 Brockmann Consult

Title: **MERIS-VA System Architecture Theoretical Basis Document**

Doc. no:

Issue: 1

Revision: 1

Date: 16.3.2000

	Function	Name	Company	Signature	Date
Prepared:		C. Brockmann	SCICON		
		N. Fomferra	SCICON		
Approved:	Project Manager	C. Brockmann	SCICON		
Released:					

Copyright © 1999 SCICON

External Distribution

Name	Quantity

Change Record

Issue	Revision	Date	Description	Approval
1		1.3.99	initial issue	
1	1	16.3.2000	Level 2 ADD added Appendix 1: CRR added	

Copyright © 1999 SCICON

Table of Contents

1 INTRODUCTION 4

1.1 GENERAL 4
1.2 PURPOSE AND SCOPE 4
1.3 DEFINITIONS, NOTATIONS AND CONVENTIONS 5

2 REFERENCES AND ABBREVIATIONS 6

2.1 APPLICABLE DOCUMENTS 6
2.2 REFERENCE DOCUMENTS 6
2.3 ABBREVIATIONS 6

3 ARCHITECTURE OVERVIEW 8

3.1 SYSTEM CONTEXT 8
3.2 SUBSYSTEMS 11
3.2.1 Level 2 Data 12
3.2.2 Level 3 Data 12
3.2.3 Visualizion of Validation Data 12
3.2.4 Formatting 12
3.3 AUXILIARY DATA PRODUCTS 12
3.4 THE MERIS-VA GRID 12

4 ARCHITECTURE DESCRIPTION 13

4.1 LEVEL 2 DATA 13
4.1.1 Architectural breakdown 13
4.1.1.1 Detailed Description 14
4.2 LEVEL 3 DATA 20
4.2.1 Level 3 plug-in management 20
4.2.2 Level 3 database management 21
4.3 GENERATION OF GENERIC LEVEL 3 PRODUCTS 22
4.4 GENERATION OF LEVEL 3 CLOUD AND WATER VAPOUR PRODUCTS 23
4.5 GENERATION OF LCC 23

5 LEVEL 2 ADD (DRAFT) 25

5.1 USE CASES 25
5.2 LOGICAL STRUCTURE 27
5.3 PHYSICAL STRUCTURE 27
5.4 ARCHITECTURE DETAILS 28

6 APPENDIX 31

6.1 COMPUTATIONAL RESOURCE DOCUMENT 31
6.1.1 Scope of the document 33
6.1.2 Applicable Documents 33
6.1.3 disk space requirements 33
6.1.3.1 MERIS-VA Products Overview 33
6.1.3.2 Input Products 33
6.1.3.3 Level 2 intermediate products 34
6.1.3.4 Level 3 intermediate products 34
6.1.3.5 User products 37
6.1.3.6 Summary 37
6.2 PLUG – IN CONCEPT FOR THE MERIS-VA PROCESSOR 38
6.3 MEMORY MAPPED FILE I/O FOR LARGE FILES 38

Copyright © 1999 SCICON

1 INTRODUCTION

1.1 General

This document is the system architecture theoretical basis document for the MERIS-VA processor. It covers the processing for the generation of the MERIS-VA Level 2 and Level 3 products, as defined in MERIS-VA Input /Output Data Definition document (RD1).

The definition of the MERIS instrument processing software for the routine on ground processing of MERIS Value Added data is a key activity in the overall definition and implementation of the MAPP subproject “operational products”.

1.2 Purpose and Scope

This document provides a complete architectural overview of the MERIS-VA processing chain. It provides upper level information relevant to and supporting the MERIS processing specification documentation which is shown in diagram 1.2-1 below.

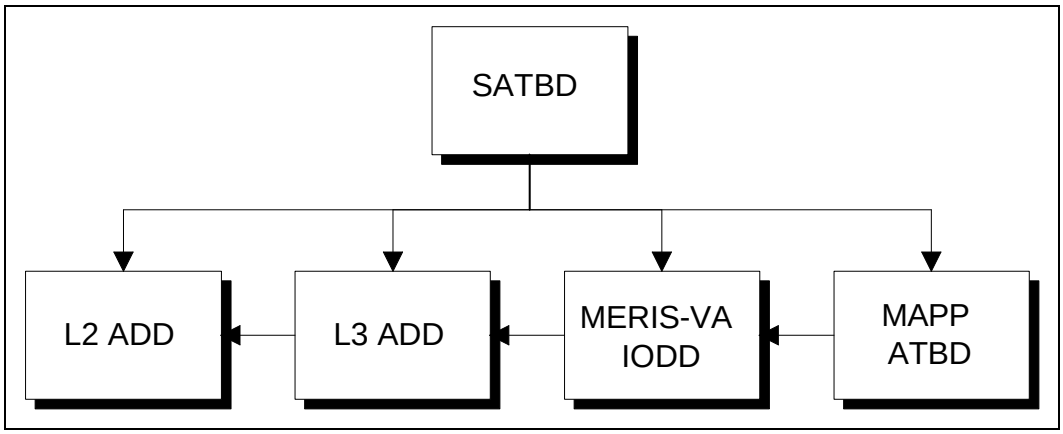

Figure 1 MERIS-VA Processing documentation tree

The processing model is described, based on objectives and current knowledge. A top-down structured analysis (SA) breakdown is performed into basic functional elements and identifying all interfaces. Each of these basic elements is described in detail in the relevant Algorithm Theoretical Basis Document and in the Detailed Processing Model Document (RD2, RD3).

For each basic functional element, a critical review is performed, and a global algorithm assessment is provided under the form of a summary table, which gives:

1. the criticality of the function : how fundamental the function is in the overall processing chain: rated from **low** to **critical**;
2. the complexity of the algorithm : rated from **simple** (about 50 statements or less) to **complex** (more than 200 statements);
3. the maturity /stability of the algorithm, rated **research** for unsolved problem as of today, **semi-operational** for specific aspects still subject to changes, and **operational** for purely engineering operations;
4. the level of complexity of the interface, from **simple** to **complex**.

Copyright © SCICON 1999

1.3 Definitions, Notations and Conventions

A Product is a data set identified within the MAPP project, and whose description exists in the Input /Output Data Definition (RD1).
There are **input products** : MERIS standard Level 1 and 2 products, auxiliary products, and **output products**: Level 2 products, Level 3 products, browse product (TBC).

A **Line** is

a set of data simultaneously acquired by MERIS
by extension, the instant where these data are acquired

A **Sample** is a single MERIS measurement or derived quantity (column, band, line in the Level 1 and Level 2 products).

A **Pixel** is the set of samples representing all the bands at a given place sampled by MERIS (column, line) or in the product (column, line).

A **grid cell** is the set of samples included in one box of the MERIS-VA Level 3 grid (see section 3.4).

The subscripts used shall be b: band; k: column; f: frame. * represents the whole range of an index.

In all SA – data flow diagrams the following symbols are used as specified in Figure 2.

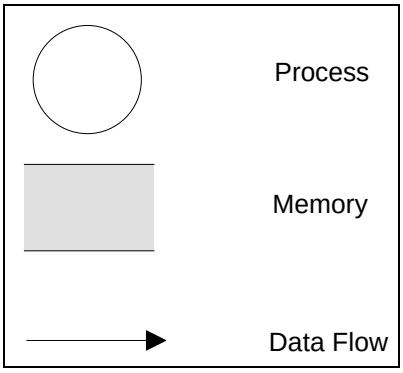

Figure 2 Definition of symbols used in flow diagrams

Physical notations shall follow the conventions in the "6S User Guide" (RD4).

For each basic functional element, a summary table is given, which in the example shown below means that the function has a high criticality, an operational simple algorithm, and a simple interface :

Criticality	LOW	MEDIUM	**HIGH**
Algorithm complexity	**SIMPLE**	MEDIUM	COMPLEX
Maturity / stability	**OPERATIONAL**	SEMI OPERATIONAL	RESEARCH
Interface	**SIMPLE**	MEDIUM	COMPLEX

Copyright © SCICON 1999

2 REFERENCES AND ABBREVIATIONS

2.1 Applicable Documents

none

2.2 Reference Documents

RD1. Input / Output Definition Document (in preparation)
RD2. Algorithm Theorectical Basis Document
RD3. Detailed Processing Model (in preparation)
RD4. Second Simulation of the Satellite Signal in the Solar Spectrum (6S) User guide v.1, Laboratoire d'Optique Atmospherique
RD5. Tables Generation Requirement Document (in preparation)

2.3 Abbreviations

AD	Applicable Document
AVHRR	Advanced Very High Resolution Radiometer
BOAVI	Bottom Of Atmosphere Vegetation Index
CCD	Charge Coupled Device
CD-ROM	Compact Disc, Read Only Memory (trade mark)
DDV	Dense dark vegetation
DEM	Digital Elevation Model
DFD	Deutsches Fernerkundungsdatenzentrum
DPM	Detailed Processing Model
ESA	European Space Agency
FR	Full Resolution
GS	Ground Segment
IODD	Input /Output Definition Document
JPEG	Joint Photographic Experts Group
L1b	Level 1 b
L2	Level 2
LCC	Land cover classification
MDS	Main data set
MERIS	Medium Resolution Imaging Spectrometer
MJD2000	Modified Julian Day 2000
MTF	Modulation Transfer Function
NDVI	Normalised Differential Vegetation Index
NN	Neural net
PCD	Product Confidence Data
PCI	Principle Component Inversion
PSM	Processing System Management
RD	Reference Document
RR	Reduced Resolution
SA	Structured Analysis
sqq.	and the following ones
TBC	To Be Confirmed
TBD	To Be Defined

Copyright © SCICON 1999

TOA	Top Of Atmosphere
TOAR	Top Of Atmosphere Radiance
TOAVI	TOA Vegetation Index
UTC	Universal Time Coordinate
VA	Value added
WGS	World Geodetic Standard

Copyright © SCICON 1999

3 ARCHITECTURE OVERVIEW

3.1 System Context

In Figure 3, the context of the MERIS-VA processor, i.e. its relationship with the external environment, is shown. The MERIS-VA main process (ID 0) has the objective to generate the MERIS-VA products. The production requests are either issued by an Operator or a Controlling Process. The latter will be probably the PSM (Processing System Management) of the DFD facility.

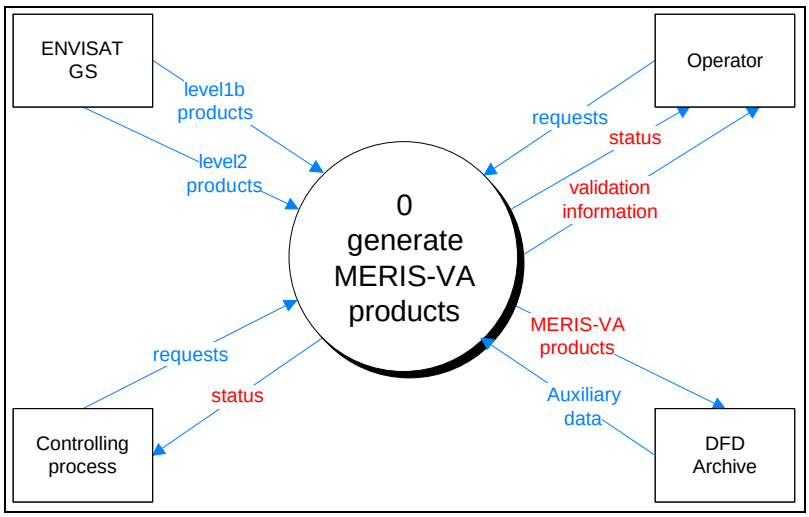

Figure 3 MERIS-VA Context

The Main Process gets the required Level 1b and Level 2 products for a processing request from the ENVISAT Ground Segment (ENVISAT GS), i.e. the ESA – MERIS processor. In addition, data tables with auxiliary parameters (e.g. coefficients for data conversion, atmospheric parameters, previously generated Level 2 products needed for Level 3 products) are retrieved from the DFD Archive. In the latter, the final results of the process, i.e. the Level 2 and 3 products are written.

If the PSM is used, the retrieval of all input parameters as well as the proper storage of the output parameters is performed by that system. All data exchange is performed through a Cache area, and the main Process uses this Cache area as a single input / output storage location.

The MERIS-VA processess work of the Standard Level 1b and Level 2 products generated by the ESA processor. Table 1 and Table 2 summarise these basic input data. The Level 1b product consists of calibrated top of atmosphere reflectances in all 15 MERIS bands and a set of flags indicating the data quality. In addition, on a sub grid (every 16th pixel) the geo-location, the viewing geometry and meteorological data are available. The Level 2 product depends on the surface type of the viewed pixel. Therefore, in Table 2 the contents of some main data sets depends on the surface type. The different types are shown in Figure 4: Water, Land and Clouds. Waters are further separated into Case-I and Case-II, and Land into DDV and non DDV, but without influence on the product content (however, with strong influence on the standard processing). Above all surfaces, the surface reflectances in all bands except the

Copyright © SCICON 1999

O2A and water vapour absorption bands are given. Also, quality flags are specified for all surface types.

MDS s	*Ocean*
MDS-1	TOA reflectance 412.5
MDS-2	TOA reflectance 442.5
MDS-3	TOA reflectance 490
MDS-4	TOA reflectance 510
MDS-5	TOA reflectance 560
MDS-6	TOA reflectance 620
MDS-7	TOA reflectance 665
MDS-8	TOA reflectance 681.25
MDS-9	TOA reflectance 705
MDS -10	TOA reflectance 753.75
MDS-11	TOA reflectance 760
MDS-12	TOA reflectance 775
MDS-13	TOA reflectance 865
MDS-14	TOA reflectance 890
MDS-15	TOA reflectance 900
MDS-16	Quality flags

Table 1 MERIS Standard Level 1b products. MDS is the Main Data Set and can be understood as a record in the product. TOA stands for Top Of Atmosphere.

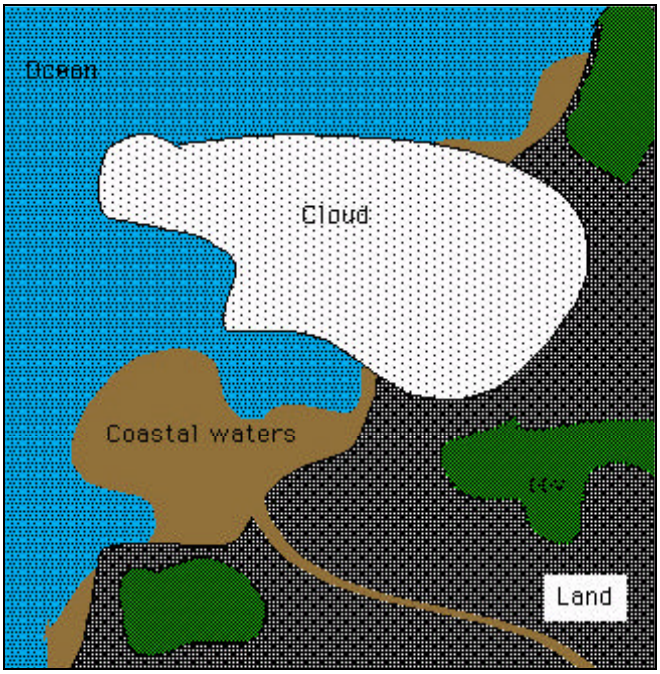

Figure 4 MERIS Standard Surface Types

Copyright © SCICON 1999

MDS s	*Ocean*	*Land*	*Coud*
MDS-1	rs 412.5	rs 412.5	rs 412.5
MDS-2	rs 442.5	rs 442.5	rs 442.5
MDS-3	rs 490	rs 490	rs 490
MDS-4	rs 510	rs 510	rs 510
MDS-5	rs 560	rs 560	rs 560
MDS-6	rs 620	rs 620	rs 620
MDS-7	rs 665	rs 665	rs 665
MDS-8	rs 681.25	rs 681.25	rs 681.25
MDS-9	rs 705	rs 705	rs 705
MDS –10	rs 753.75	rs 753.75	rs 753.75
MDS-11	rs 775	rs 775	rs 775
MDS-12	rs 865	rs 865	rs 865
MDS-13	rs 890	rs 890	rs 890
MDS-14	Water Vapour Content	Water Vapour Content	Water Vapour Content
MDS-15	Algal pigment I	TOAVI	Cloud top pressure
MDS-16	TSM - YS	Spare	Spare
MDS-17	Algal pigment II	BOAVI	Spare
MDS-18	FPAR	Surface pressure	Cloud albedo
MDS-19	Aerosol t & e	Aerosol t & e	Cloud t & type
MDS-20	Flags	Flags	Flags

Table 2 MERIS Standard Level 2 Products. MDS is a Main Data Set. RS is a surface reflectance. TSM is total suspended matter, FPAR the Fractional Photosynthetically available radiation, TOAVI and BOAVI the Top of Atmosphere and Bottom of Atmosphere Vegetation Indices.

Table 3 shows the MERIS-VA Level 2 and Level 3 products which are generated by the processor. The Level 2 products are provided in satellite coordinates with geolocation appended. The Level 3 products are resampled to a standard grid, which is introduced in section 3.4 and described in detail in ATBD 10.

All Level 2 and Level 3 products are described in the related ATBDs.

	Level – II	*Level – III*
Wasser	• Chlorophyll, • Gelbstoff, • Schwebstoff • (Nordsee, Ostsee, Bodensee)	• Ostsee: wie L2, monatl. Mittelwerte • M1 Karte
Atmosphere	• Aerosoltyp, • optische Dicke in der Küstenzor	• wie L2, monatl. Mittelwerte. • M8 Karte
	• Wolkenhöhe • optische Dicke von Wolken • Wolkenalbedo • Wasserdampf	• ISCCP Wolkentypen (oder Erweiterung) • Wasserdampf in ISCCP Wolken Kategorien

Copyright © SCICON 1999

		• Statistik in vertikalen Schichten:
		  • Wolkenhäufigkeit
		  • optische Dicke von Wolken
		  • Wolkenhöhe
		  • Wasserdampf
		  • M16 Karte

Land	• NDVI	• NDVI monatl. & jährl. Mittel • Landbedeckungsklassifikation • M1 Karte

Table 3 MERIS-VA Level 2 and Level 3 products

3.2 Subsystems

The main process introduced before has 4 subsystems (Figure 5):
1. The generation of Level 2 data
2. The generation of Level 3 data
3. The visualisation of validation data
4. The ouput product formatting

The first two sub processes receive the external processing request. The level 2 data generation needs from external both the Level 1b and Level 2 products, while the Level 3 process only requires Level 2 standard products. Both processes deliver validation data for inspection and quality control to the visualisation process.

A key element in this level are two storages, one for the produced MERIS-VA level 2 and one for the Level 3 data. The Level 2 storage contains for every pixel a data structure with all available information, i.e. Level 1b, Level 2 standard and VA, geolocation, geometry, etc. The level 3 storage contains on the MAPP Level 3 grid the Level 3 products and statistical information.

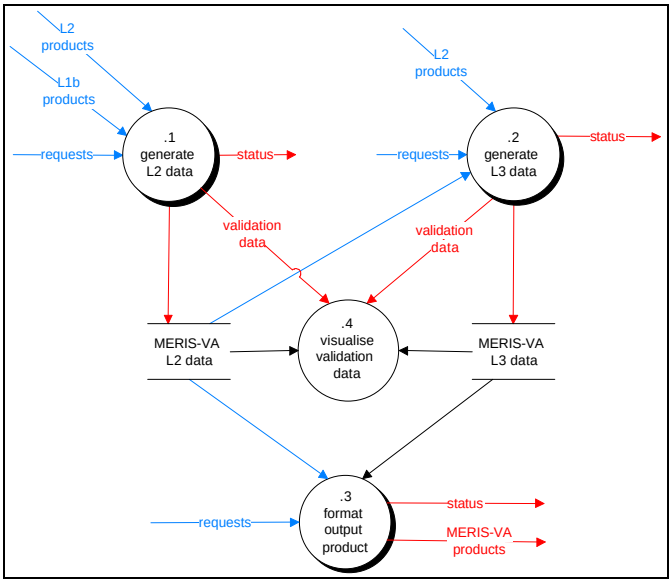

Figure 5 MERIS-VA subsystems

Copyright © SCICON 1999

3.2.1 Level 2 Data

The level 2 generation process is triggered by production requests, which include the products to be generated and their time and geographical specification. Status information is provided back to the invoking process, and the resulting products are stored in the level 2 data storage.

3.2.2 Level 3 Data

The level 3 generation process is triggered by production requests, which include the products to be generated and their time and geographical specification. Status information is provided back to the invoking process, and the resulting products are stored in the level 3 data storage.

3.2.3 Visualizion of Validation Data

The visualisation process is an interactive user interface which permits a visualisation of the data in the two storages for quality control. It will be an independed process which can be run in any remote environment which has access to the data storages.

3.2.4 Formatting

The formatting works on the Level 2 and Level 3 data storages and performs two types of processing: the transformation of the data into any of the TBD projections and then the packing into any of the TBD user product formats.

3.3 Auxiliary Data Products

Data bases of input parameters for MERIS processing are also called "data tables" throughout this document. The detailed format of these data tables is provided in RD1; their contents and generation is described in RD5.

3.4 The MERIS-VA Grid

The basis for the generation of the MERIS-VA level 3 products is the Level 3 grid Figure 6. See also ATBD 10 and 11 for details of the generation of the Level 3 products on that grid.

The grid is consists of 12800 x 12800 grid cells with 300m extension in both directions. It has an extension of 3840 km x 3840 km. The receiving station Neustrelitz is in the centre of the grid, which covers the whole area of reception. The transformation of a geographical location into the corresponding grid cell is given in ATBD 10.

This grid is called the M1 grid. A coarser grid, where n grid cells in every direction are combined, is called the Mn grid. Such a grid has a grid size of n x 300m in every direction and has 12800/n grid cells in every direction. For example, the M5 grid has 2560 x 2560 grid cells with a size of 1500 x 1500m.

It is possibly forseen to extend the grid in all directions slightly in order to cover also those areas, where Neustrelitz still receives some data.

Copyright © SCICON 1999

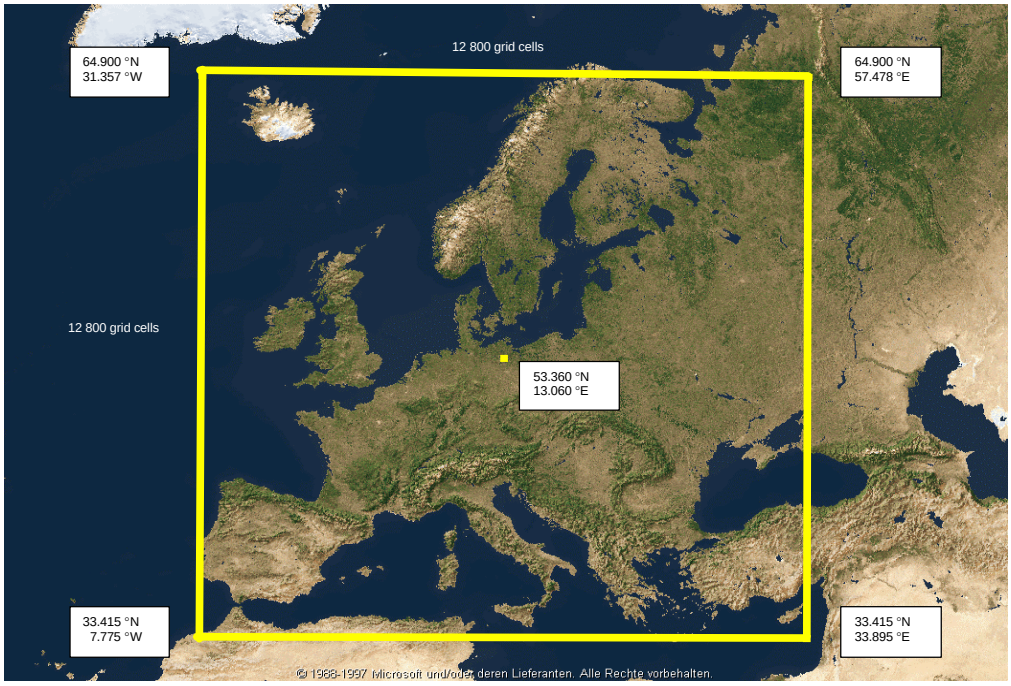

Figure 6 MERIS-VA Level 3 grid

4 ARCHITECTURE DESCRIPTION

4.1 Level 2 Data

4.1.1 Architectural breakdown

The top level breakdown of the MERIS Level 1 Architecture is represented schematically in figure Figure 7below.

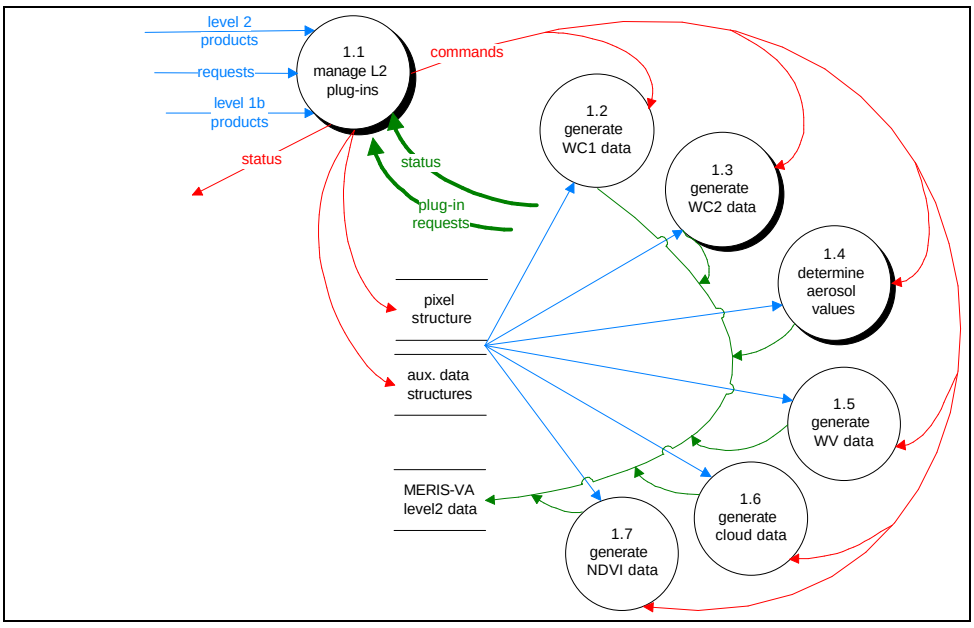

Figure 7 Generation of Level 2 Data

Copyright © SCICON 1999

Every module which generates a specific Level 2 product will be implemented following common rules concerning the interface and accessing the internal storages. They are called plug-ins. In this way, the list of level 2 product modules or plug-ins must not be fixed. The plug-ins are organized by a specific module, the Level 2 plug-in manager. This issues the commands to the plug-ins and organizes the data for them.

4.1.1.1 Detailed Description

The following sections provide, for each of the top level breakdown units shown above, a description of the unit's function, inputs, outputs.

4.1.1.1.1 Plug-In Management

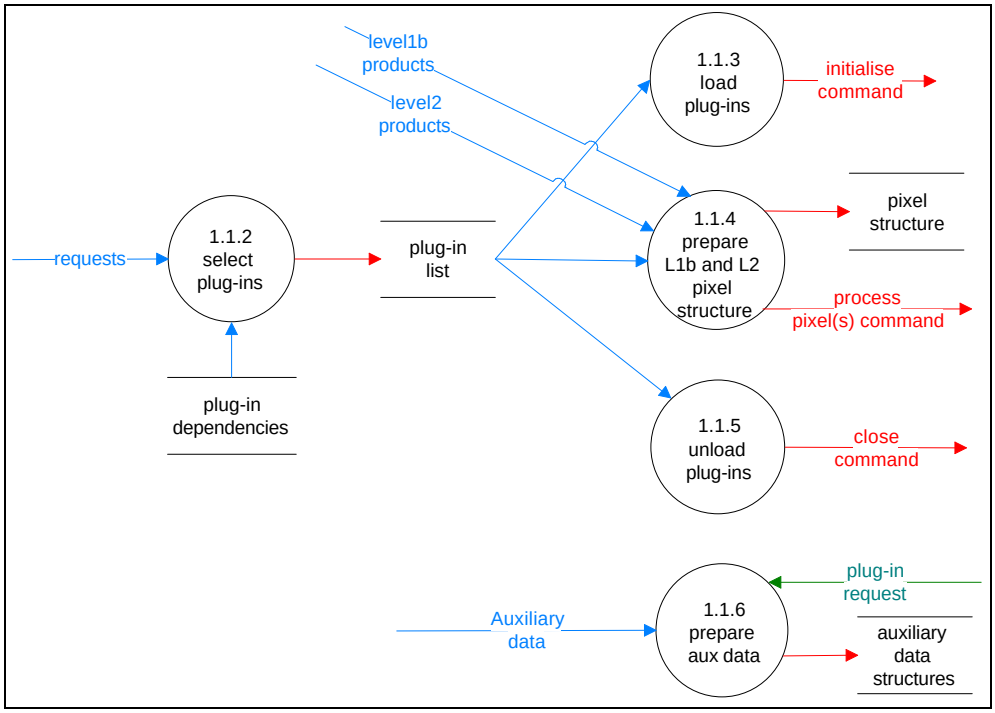

Figure 8 Level 2 Plug-In Management

A request includes the specification of which Level 2 products need to be generated. Based on this, the plug-in manager selects the required plug-ins, regarding the dependencies (i.e., if a specific plug-in needs another to be executed before, this one will also be included in the list of selected plug-ins even if it is not directly requested). These plug-in dependencies are maintained in an auxiliary data table “plug-in dependencies”.

The plug-in manager then has to load the plug-in, to prepare the Level 1b and Level 2 data into a pixel structure internal storage and issue the commands to generated the VA Level 2 product for that pixel structure. In this sense, the plug-in manager loops through the whole image while the plug-in works only on the pixel structure (which can have any number of individual pixels. This depends on the one hand on the requirements of the plug-ins, e.g. window processes, on the other on performance requirements).

Finally, the plug-in manager has to unload the plug-in.

Copyright © SCICON 1999

Details on implementing the plug-in concept under UNIX and on the memory management for large files are given in the appendices to this SATBD.

Algorithm Assessment

Criticality	LOW	MEDIUM	**HIGH**
Algorithm complexity	SIMPLE	MEDIUM	**COMPLEX**
Maturity / stability	OPERATIONAL	**SEMI OPERATIONAL**	RESEARCH
Interface	SIMPLE	MEDIUM	**COMPLEX**

4.1.1.1.2 Water Constituents 1

The generation of total suspended matter, yellow substance and chlorophyll concentration using the Neural Network approximated Inverse Modelling Technique is shown in Figure 9. It refers to ATBD 2.

There are two different products forseen for that application. One consists of a Java application together with the Level 2 standard product (water leaving radiance reflectances). This is totally generated in the formatting module because it requires no data processing but only binding of existing code and data. The second application is described here.

Different neural nets are available for different geographical and temporal conditions (e.g. spring in the North Sea). Depending on the actual time and geography, which is included in the pixel structure, the proper Neural Net is selected and executed. The resulting concentrations of water constituents are checked for possible errors before stored in the main Level 2 product storage.

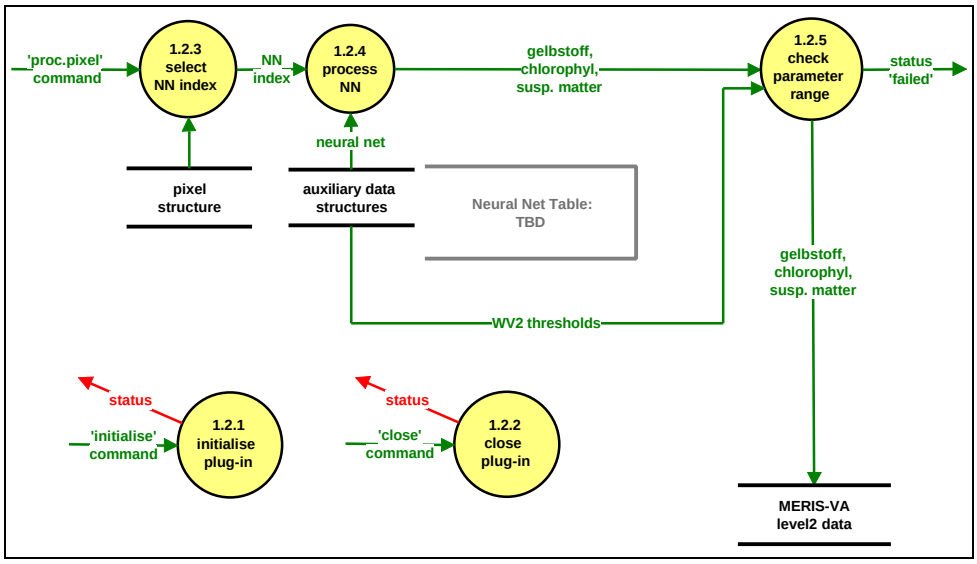

Figure 9 Water Constituents 1 (NN Method)

The neural nets will be stored in a tabulated format following the ESA Neural Net format.

Copyright © SCICON 1999

Algorithm Assessment

Criticality	LOW	**MEDIUM**	HIGH
Algorithm complexity	SIMPLE	**MEDIUM**	COMPLEX
Maturity / stability	**OPERATIONAL**	SEMI OPERATIONAL	RESEARCH
Interface	**SIMPLE**	MEDIUM	COMPLEX

4.1.1.1.3 Water Constituents 2

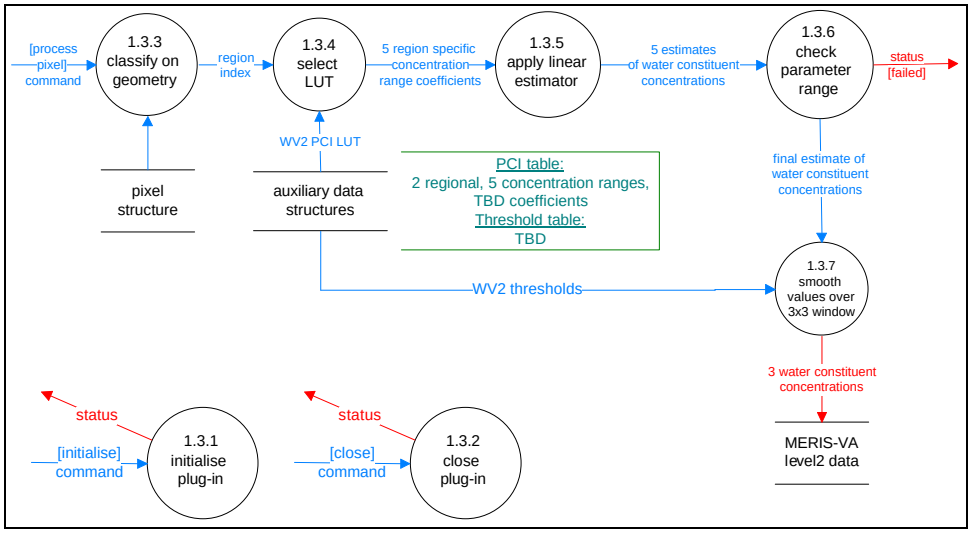

Figure 10 Calculation of water constituents 2 (PCI method)

The derivation of the concentration of water constituents with the PCI method is shown in Figure 10and refers to ATBD 3. Basis for the method are tables including the parameters of the PCI regression formular (linear estimator). Theses are stored in an auxiliary data table, and the proper tables are selected based on geometry information. The linear estimates are derived for 5 differend concentration ranges, and the correct one is selected based on the results of the estimates. Finally the values are smoothed over sliding window.

Algorithm Assessment

Criticality	LOW	**MEDIUM**	HIGH
Algorithm complexity	SIMPLE	**MEDIUM**	COMPLEX
Maturity / stability	OPERATIONAL	**SEMI OPERATIONAL**	RESEARCH
Interface	**SIMPLE**	MEDIUM	COMPLEX

Copyright © SCICON 1999

4.1.1.1.4 Aerosol Properties

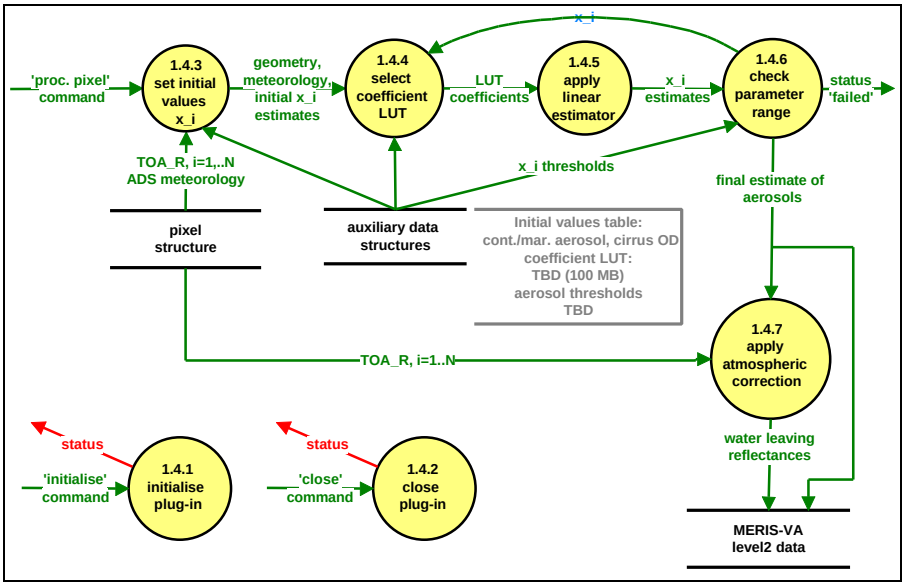

Figure 11 Calculation of aerosol properties

The generation of Aerosol properties is shown in Figure 11and refers to ATBD 4. The method is based on a linear estimate of the aerosol properties from Level 1b measurements. Additionally, the water leaving radiance reflectance is derived as an internal product.

The parameters for the linear estimation are read from an auxiliary data table, and the proper coefficients are selected according to geometry and meteorological conditions, which are available in the pixel structure. Also, initial values for the aerosol properties have to be assigned. If these are not available from a previous pixel, they have to be read from auxiliary data.

Algorithm Assessment

Criticality	LOW	**MEDIUM**	HIGH
Algorithm complexity	SIMPLE	**MEDIUM**	COMPLEX
Maturity / stability	OPERATIONAL	**SEMI OPERATIONAL**	RESEARCH
Interface	**SIMPLE**	MEDIUM	COMPLEX

4.1.1.1.5 Water Vapour

The water vapour calculation is shown below in Figure 12and refers to MAPP-ATBD-WV. The water vapour will be retrieved with a trained neural net. The parameters for the net are read from an auxiliary data table.

Copyright © SCICON 1999

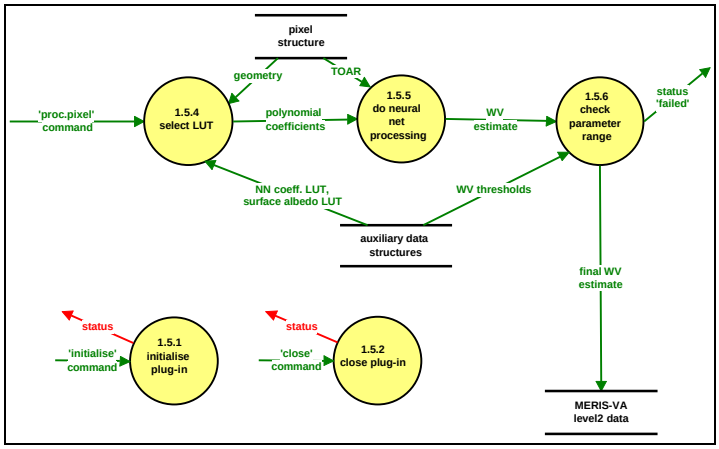

Figure 12 Calculation of water vapour

Algorithm Assessment

Criticality	LOW	**MEDIUM**	HIGH
Algorithm complexity	SIMPLE	**MEDIUM**	COMPLEX
Maturity / stability	OPERATIONAL	SEMI OPERATIONAL	**RESEARCH**
Interface	**SIMPLE**	MEDIUM	COMPLEX

4.1.1.1.6 Cloud Products

The cloud products include cloud optical thickness, cloud albedo and cloud top height. Their generation is shown in Figure 12. They are described in MAPP-ATBD-CACO and MAPP-ATBD-CTP.

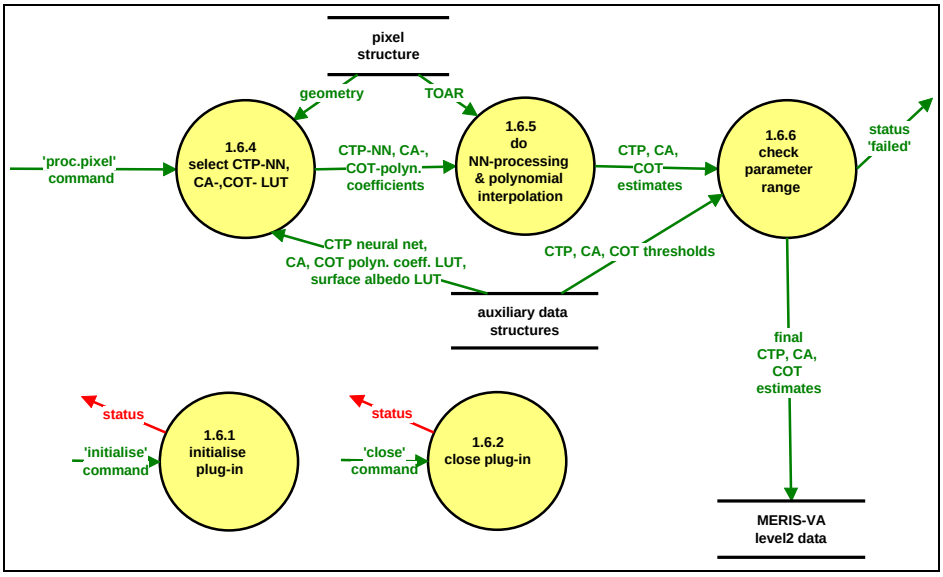

Figure 13 Calculation of cloud products

The generation of cloud albedo and cloud optical thickness uses polynomial expressions, while the cloud top height is calculated by a neural net. However, all algorithms require coefficients,

Copyright © SCICON 1999

which are either the polynomial coefficients or a tabulated neural net. These are retrieved based on geometry. Also, the surface albedo is required by the algorithms.

Algorithm Assessment

Criticality	LOW	**MEDIUM**	HIGH
Algorithm complexity	**SIMPLE**	**MEDIUM**	COMPLEX
Maturity / stability	**OPERATIONAL**	SEMI OPERATIONAL	RESEARCH
Interface	**SIMPLE**	MEDIUM	COMPLEX

4.1.1.1.7 NDVI

The retrieval of the NDVI is a simple procedure which interpolates the channels of the AVHRR from proper MERIS Level 1b data and computes the NDVI.

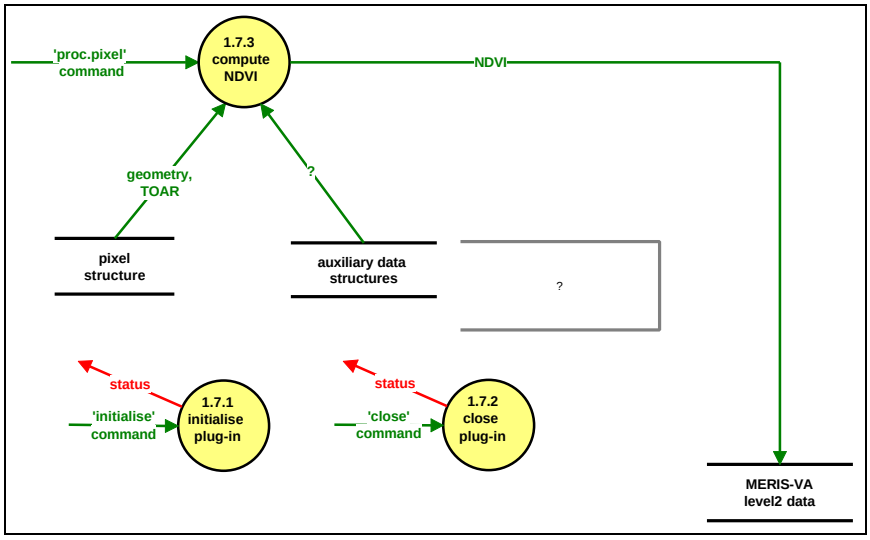

Figure 14 Calculation of NDVI

Algorithm Assessment

Criticality	LOW	**MEDIUM**	HIGH
Algorithm complexity	**SIMPLE**	MEDIUM	COMPLEX
Maturity / stability	OPERATIONAL	SEMI OPERATIONAL	**RESEARCH**
Interface	**SIMPLE**	MEDIUM	COMPLEX

Copyright © SCICON 1999

4.2 Level 3 Data

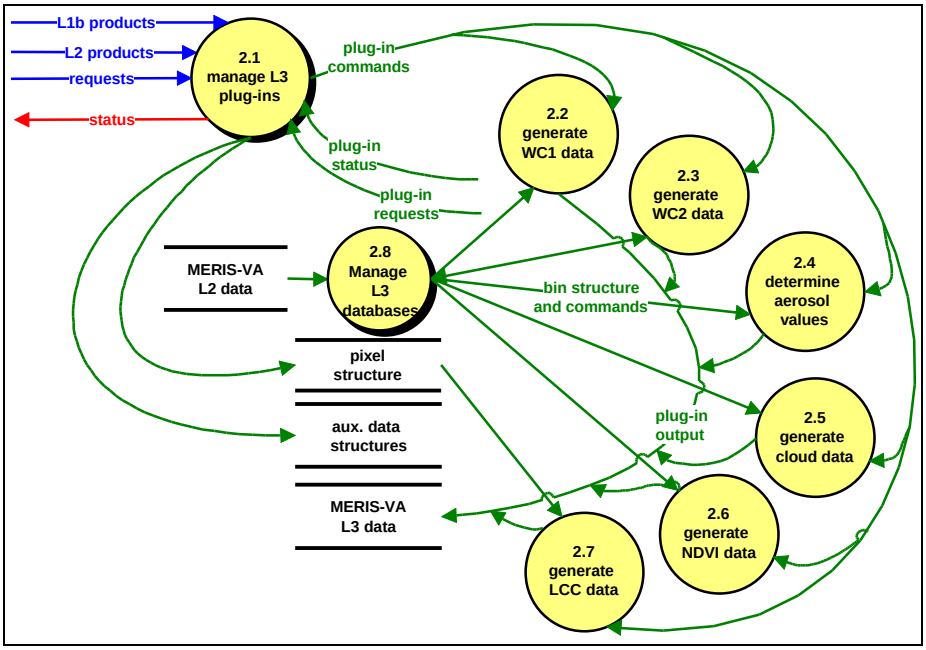

Figure 15 Level 3 product generation

The generation of the Level 3 data implements the same plug-in concept as the generation of the Level 2 data. The individual Level 3 modules have a common interface structure and are initiated and managed by the plug-in manager. The latter acts in the same way as the Level 2 plug-in manager but is supported by the Level 3 database manager, which maintains the three main data storages: the pixel structure which contains the set of pixels to be processed, a storage for auxiliary data, e.g. polynomial coefficients, and the Level 3 product storage.

4.2.1 Level 3 plug-in management

A request includes the specification of which Level 3 products need to be generated. Based on this, the plug-in manager selects the required plug-ins, regarding the dependencies (i.e., if a specific plug-in needs another to be executed before, this one will also be included in the list of selected plug-ins even if it is not directly requested). These plug-in dependencies are maintained in an auxiliary data table “plug-in dependencies”.

The plug-in manager then has to load the plug-in, to prepare the Level 1b and Level 2 data into a pixel structure internal storage and issue the commands to generated the VA Level 3 product for that pixel structure. In this sense, the plug-in manager loops through the whole image while the plug-in works only on the pixel structure (which can have any number of individual pixels. This depends on the one hand on the requirements of the plug-ins, e.g. window processes, on the other on performance requirements).

Finally, the plug-in manager has to unload the plug-in.

Details on implementing the plug-in concept under UNIX and on the memory management for large files are given in the appendices to this SATBD.

Copyright © SCICON 1999

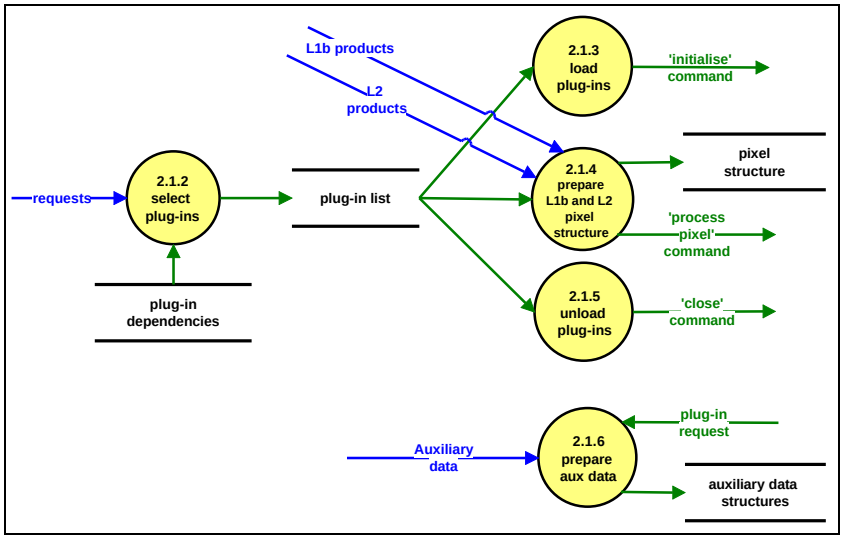

Figure 16 Level 3 Plug-In management

Algorithm Assessment

Criticality	LOW	MEDIUM	**HIGH**
Algorithm complexity	SIMPLE	MEDIUM	**COMPLEX**
Maturity / stability	OPERATIONAL	**SEMI OPERATIONAL**	RESEARCH
Interface	SIMPLE	MEDIUM	**COMPLEX**

4.2.2 Level 3 database management

While the Level 2 processes work only on simple pixel structures, which is a set of 1 or more samples together with all relevant information for that pixel (geometry, location, ...), the data structure for the Level 3 processes are more complex and must be regarded together with the operations performed on it. The mathematical background is described in MAPP-ATBD-GENL3.

The generation of the generic Level 3 products includes the binning into the MAPP-Level 3 grid (Mn grid) and the spatial and temporal integration of the corresponding data following the procedure described in MAPP-ATBD-GENL3. This is shown schematically in Figure 17The spatial processing includes the computation of the bin index i from the geographical location of a given pixel. The logarithm and the squares of the logarithms of the parameters of concern of all pixels belonging to a bin are summed up ($S1_i$ and $S2_i$ matrix). Further, for every bin (still for one overpass), the number of samples per bin (n_i matrix) is stored.

Copyright © SCICON 1999

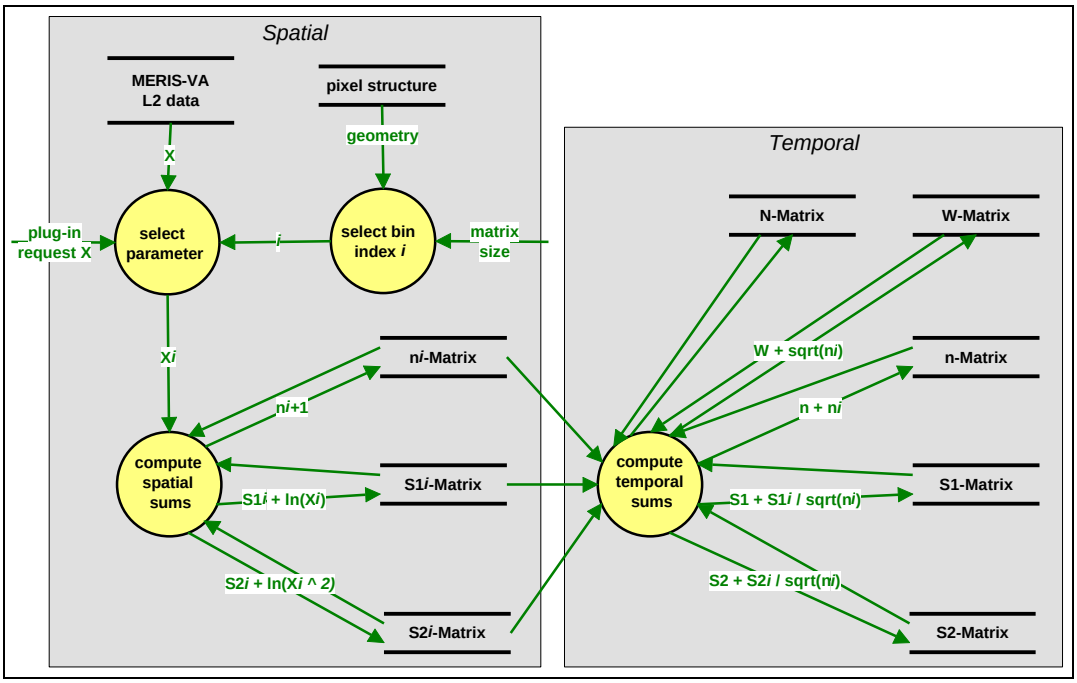

Figure 17 Level 3 database management

The temporal integration then computes temporal sums for every bin using the choosen weighting: the N-matrix contains the total number of samples, the W-matrix the sum of the weights (in Figure 17the weights are the inverse root of of number of samples), the n-matrix the number of samples per bin and the S1 and S2 matrices the weighted sums of the individual sum and squares matrices.

Algorithm Assessment

Criticality	LOW	MEDIUM	**HIGH**
Algorithm complexity	SIMPLE	MEDIUM	**COMPLEX**
Maturity / stability	OPERATIONAL	SEMI OPERATIONAL	**RESEARCH**
Interface	SIMPLE	MEDIUM	**COMPLEX**

4.3 Generation of generic Level 3 products

The so called “generic” Level 3 products are those, which are a direct spatial and temporal integration of the corresponding Level 2 products, and for which the procedures are already implemented in the Level 3 database management.

At present, these products are the Water Constituents 1 and 2, the aerosol properties and the NDVI. These modules only need to define the temporal and spatial integration parameters for the database management module.

Algorithm Assessment

Criticality	LOW	MEDIUM	**HIGH**

Copyright © SCICON 1999

Algorithm complexity	**SIMPLE**	MEDIUM	COMPLEX
Maturity / stability	OPERATIONAL	**SEMI OPERATIONAL**	RESEARCH
Interface	**SIMPLE**	MEDIUM	COMPLEX

4.4 Generation of Level 3 cloud and Water Vapour products

The Level 3 cloud and water vapour products are derived statistical products which differ from their corresponding Level 2 products. In an ISCCP compatible way, the fractional cloud cover, the cloud top pressure, cloud optical depth and water vapour content are calculated. The data will be stored in a M16 grid, but the mathematics to fill the data table differs from the generic method, so that an own database handling will be used.

Algorithm Assessment

Criticality	LOW	**MEDIUM**	HIGH
Algorithm complexity	SIMPLE	**MEDIUM**	COMPLEX
Maturity / stability	OPERATIONAL	SEMI OPERATIONAL	**RESEARCH**
Interface	SIMPLE	**MEDIUM**	COMPLEX

4.5 Generation of LCC

The LCC is a product which has no direct corresponding Level 2 product, It is directly generated from MERIS L2 surface reflectances. The processing includes three steps:

1. A classification of every pixel of an overflight. The classification result is binned and stored for step 2.
2. A multitemporal, monthly analysis of the stored overflight values (monthly LCC).
3. A multitemporal, yearly analysis of the monthly LCC.

In the first step, the geolocation values of the pixel structure are used to select the spectral signature covariance matrix from an auxiliary data table, which is used in the maximum likelihood classification. This assigned a class number to every pixel.

In the second step, after the period of one month, for every bin the most and second most frequent class number are selected as the resulting classes for that month and stored as monthly LCC.

In the third step, the series of 12 monthly mean NDVI values for a given bin are compared with typical NDVI time series of the 17 classes used for the final classification. This time signal is an additional information, which is used together with the 12 monthly classes in order to determine the final class for that bin. This gives the yearly LCC class.

Copyright © SCICON 1999

Algorithm Assessment

Criticality	LOW	MEDIUM	**HIGH**
Algorithm complexity	SIMPLE	MEDIUM	**COMPLEX**
Maturity / stability	OPERATIONAL	**SEMI OPERATIONAL**	RESEARCH
Interface	SIMPLE	MEDIUM	**COMPLEX**

Copyright © SCICON 1999

5 LEVEL 2 ADD (DRAFT)

5.1 Use Cases

Three actors have been identified:

1) The main actor is the Processing System Management (PSM). This software generates the operational and recurring processing requests and controls the MERIS-VA processor.
2) An operator, which is a real person and who is responsible for the processor.
3) A validator who performs off-line quality control.

These actors perform the following use cases with respect to the processor (see Figure 1):

The operator maintains the processor which includes mainly the installation of new Plug-Ins. Then, he controls the processing, which the generation of the various product types of the processor in exceptional cases, e.g. during campaigns or for a re-processing. Finally, he inspects and and verifies each processing job for its correct performance.

In addition to this verification, a more intensive validation is done by the validator. This is a scientific assessment of the quality of the products. For this, it should be able to generate intermediate variables of the processing.

The generation of the Level 2, Level 3 and User products are the main use cases. During normal operations, these include the whole processing chain from the ESA Level 1b and 2 to the MERIS-VA products.

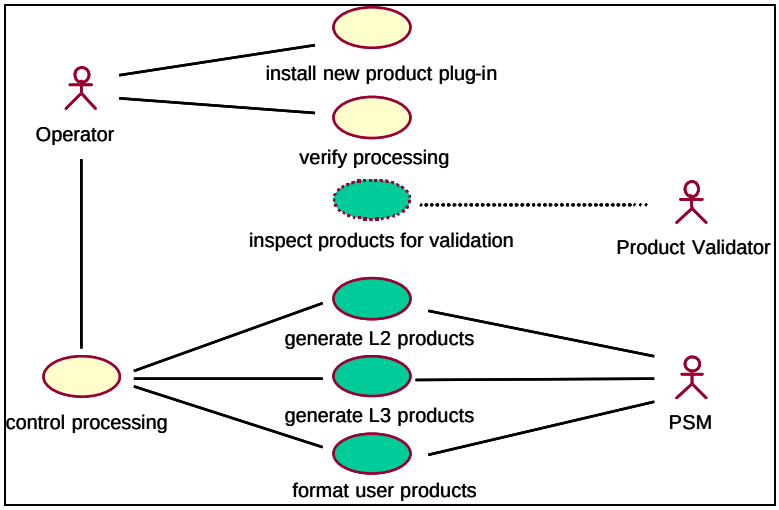

Figure 1: Use Cases for the MERIS-VA Processor

These use cases are reflected in the architecture as individual sub-processors, which have a common interface to the PSM. This is reflected in Figure 2, which shows the co-operation between DIMS/Product Library, the processing system, which includes the PSM and the MERIS-VA processor, and the operator through an operating tool.

Copyright © SCICON 1999

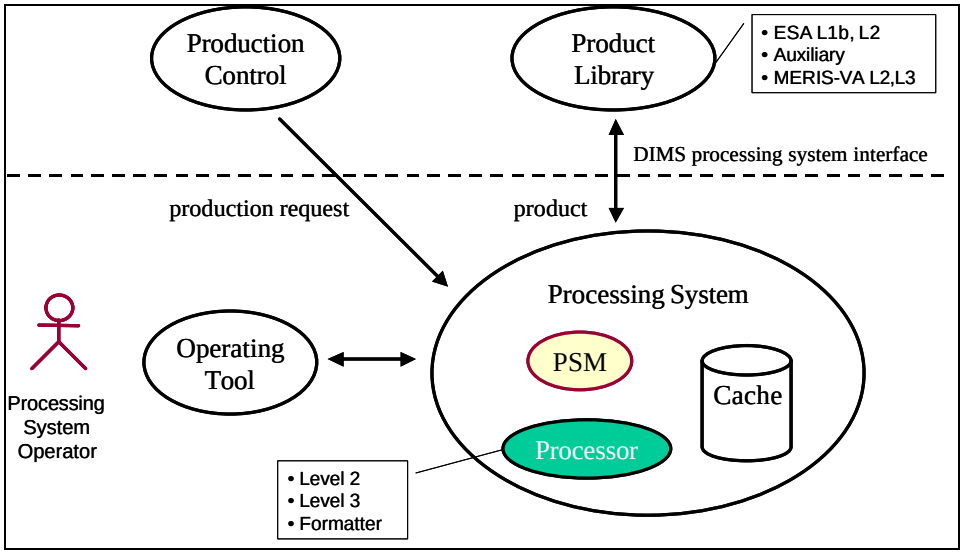

Figure 2: Co-operation between DIMS and processing system.

DIMS has the overall control. Production requests are submitted by the production control to the PSM. This retrieves the required input and auxiliary products from the product library and puts it into a cache space, which is connected with the processor. The PSM the invokes the processor. This is detailed in Figure 3.

The PSM initialises the MERIS-VA processor body. This reads its configuration from a file (cfg), which includes – among others – the available Plug-Ins. After successful initialisation, which is reported back to the PSM, this starts the processor with the details of the processing requests, i.e. the requested products and its parameters. The processor reads the necessary parameters, e.g. coefficients for Plug-Ins, and the Input products from the cache space. During generation of the products, the processor may submit status information to the PSM, and this suspend or revoke the processor. Finally, when the output products have been written, the processor reports its completion to the PSM, which gives the output products to the product library (not shown here) and terminates the processor.

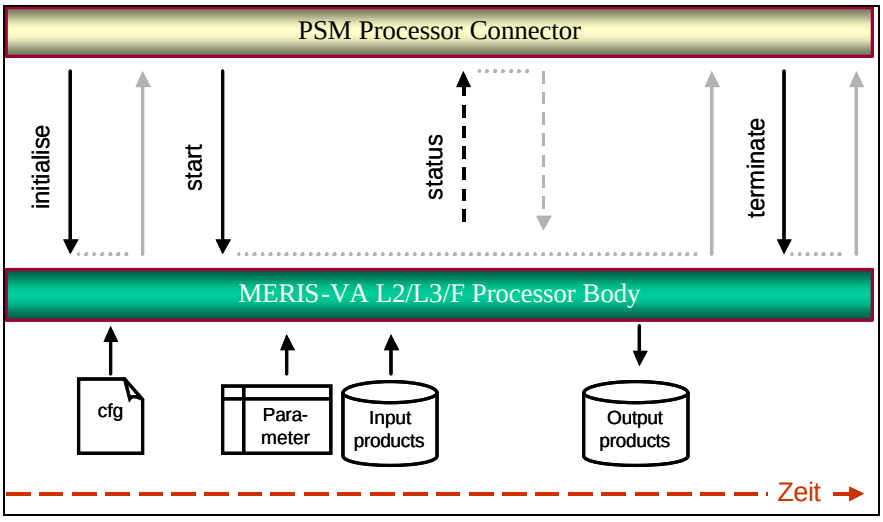

Figure 3: Communication between PSM and processor body for a processing request.

Copyright © SCICON 1999

5.2 Logical Structure

The MERIS-VA processor has a top-level structure which reflects the use cases (see Figure 4). In three packages are the sub-processors for the generation of Level 2 (meris_va_l2), Level 3 (meris_va_l3) and User Product Formatting (meris_va_f) organised. These depend on reusable basis classes, which are grouped in the two packages for basic MERIS-VA classes (meris_va_base) and the standard Brockmann Consult Classes (bc_std). This includes mainly existing basic functionality. E.g., it depends on the commercially availably Tera-Scan API, the public domain hdf API and the neural net classes of BC.

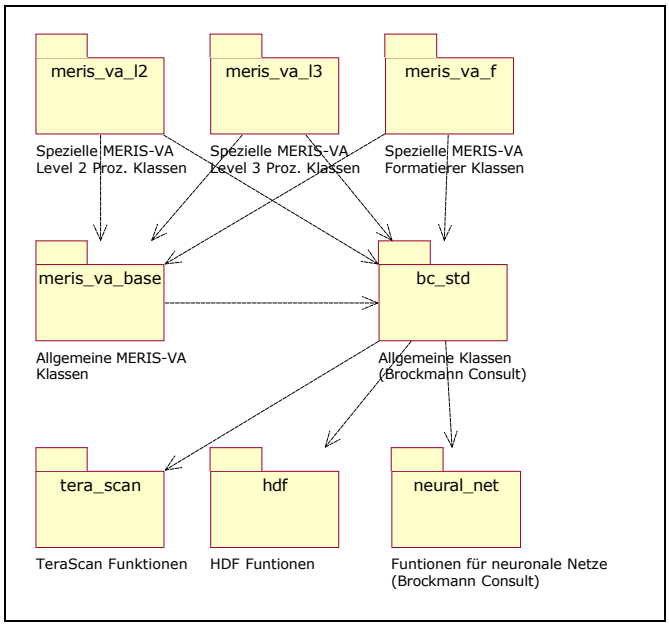

Figure 4: Package structure of the MERIS-VA processor

5.3 Physical Structure

The external interface of the MERIS-VA is the DIMS connection layer. This has been established by DFD in form of the PSM. This layers handles the processing requests and the interfacing with the product library.

The three top level packages of the logical structure are reflected in corresponding APIs. This means, that the PSM can call each of the subprocessors individually. By this, the individuality of the use cases is correctly implemented. The Plug-Ins are also separate elements which interface with the Level 2 and Level 3 sub-processors. It becomes clear here that the sub-processor and the Plug-Ins are individual and separate elements, and the sub-processors call the Plug-Ins (and vice versa) if demanded.

The MERIS-VA base layer is a combination of the Base API, which implements the meris_va_base package, and the BC-STD API. This interfaces directly with the processor body layer and also with the Base API. Finally, off-the-shelf software is used where possible (COTS layer).

Copyright © SCICON 1999

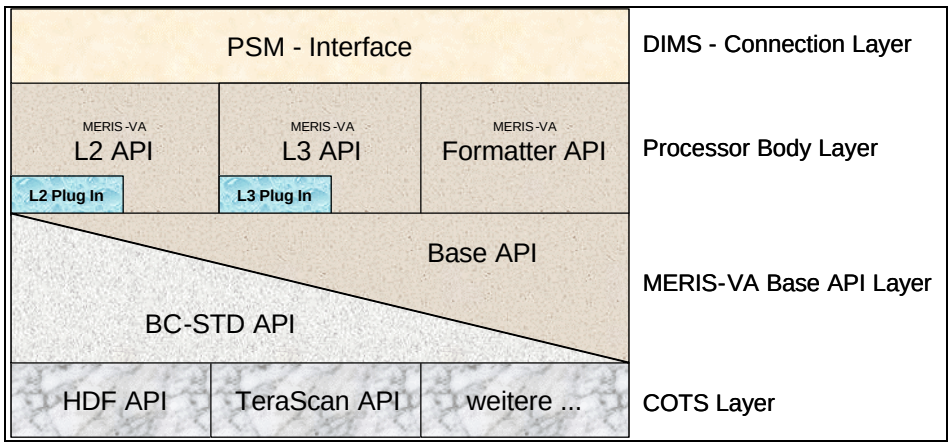

Figure 5: Physical Layers of the processor software

5.4 Architecture Details

The model for the Processor-Class is shown in Figure 6. This is the basic class from which the L2 Processor, L3Processor and Formatter Classes are derived. It processes a ProductionRequest, which is the connection to the PSM.

A Processor has one PlugInManager,which is detailed in Figure 7. He has the responsibility to create an ActivePlugInList, which is the list of those PlugIns, which are required to fulfil the production request. In order to create this list, the PlugInManager has to get the PlugInDescriptors for all requested products and those, which depend on already required PlugIns (Dependency Class of the PlugInDescriptor). With this list and the corresponding PlugInDescriptors, the PlugInManager can then call the Plug-Ins, which itself only need to process a Pixel or a set of Pixels, a so called Granule.

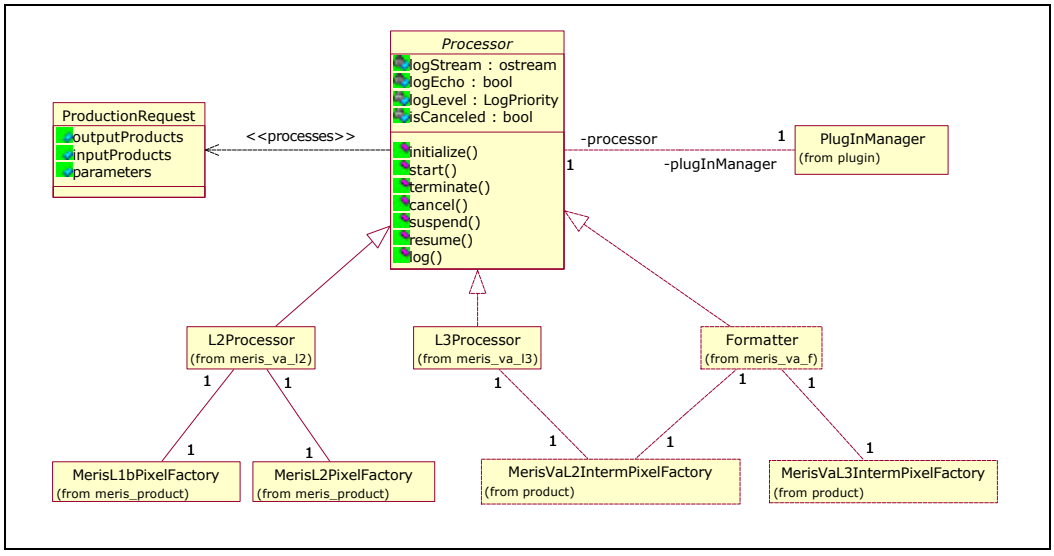

Figure 6: The Processor Class

Copyright © SCICON 1999

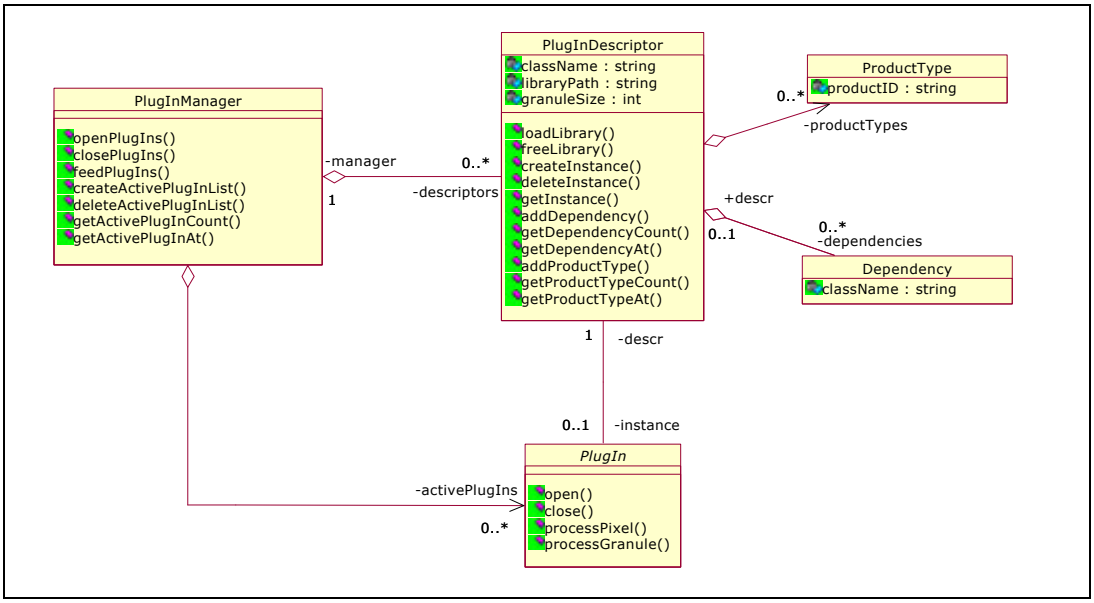

Figure 7: The Plug-In Classes

The pixel (or granule) needs to be prepared before it can be given to a Plug-In. The concerned classes are shown in Figure 8 and Figure 9. The MerisPixelFactory is the basis class for MERISL1bPixelFactory and MERISL2PixelFactory, which are associated with the Processor (see Figure 6).

The MerisPixelFactory is a MerisProductReader, because the MERIS Products have a structure which makes it possible to deduce generalised methods. The MerisPixelFactory basically is responsible to sample all the pixel relevant information from the different locations in the MERIS product files (e.g. GADS – Global Annotation Data Set, LADS – Location Annotation Data Sets, which are better known as Tie-Point annotations), and to associate them with every pixel correctly. This includes of course the interpolation of the LADS data to pixel resolution.

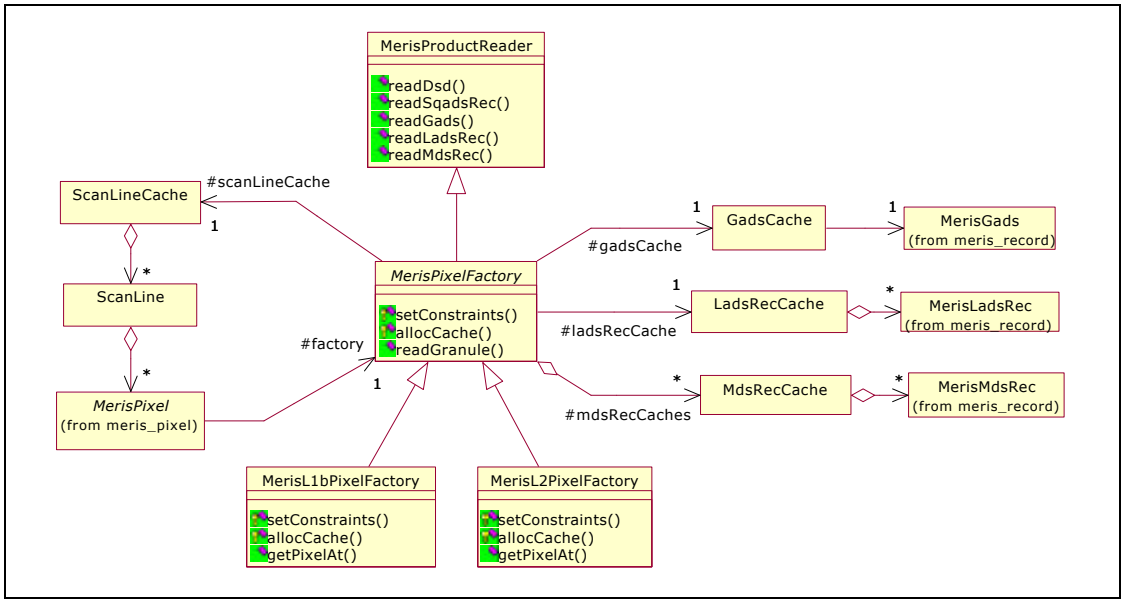

Figure 8:The MERIS Pixel Factory

Copyright © SCICON 1999

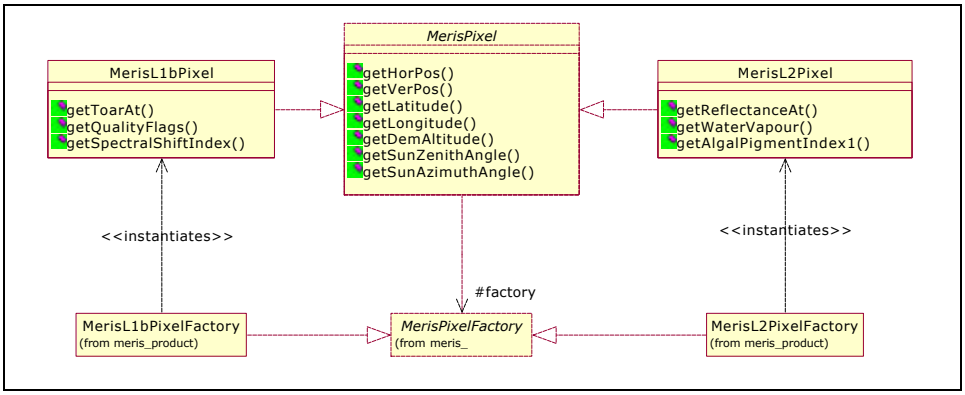

Figure 9: The MERIS Pixel Class

So, finally, a MERISPixel class has methods to provide all revelant information common to Level 1 and 2 products, which are its position in the image and in geographical coordinates, its sun and viewing geometry etc. The deduced MerisL1bPixel and MerisLevel2Pixel classes have, additionally, methods to provide the specific values, i.e. the spectral radiances or geophysical parameters.

Consequently, a Plug-In is supplied with a Pixel, which knows everything about itself.

Copyright © SCICON 1999

6 APPENDIX

6.1 Computational Resource Document

Copyright © 1997 SCICON.

Titel: **MERIS-VA Computational Resource Requirements Document**

Project: MAPP

Doc. No.: TN-MAPP-CB-CRR

Issue: draft
Revision:
Date: 20.5.1999

	Function	Name	Organisation	Signature	Date
Author:		Carsten Brockmann	Brockmann Consult		
		Norman Fomferra	Brockmann Consult		

Copyright © 1997 SCICON.

6.1.1 Scope of the document

This document defines the hard- and software requirements for the MERIS-VA processor. The document will evolve in the same way as the algorithm definitions and the system architecture change.

6.1.2 Applicable Documents

AD1 MAPP Algorithm Theoretical Basis Document. MAPP ATBD 1.0, 8.3.1999

6.1.3 disk space requirements

6.1.3.1 MERIS-VA Products Overview

The MERIS-VA processor generates Level 2 and Level 3 products. The Level 3 products require the corresponding Level 2 products. Therefore, each received orbit must be processed up to Level 2, and some intermediate products (integrators for the Level 3 products) must be generated.
The Level 2 data and Level 3 integrators are stored in an internal format, which is optimised for processing efficiency. When products are requested by a user (which is regularly for final Level 3 products, but irregularly for Level 2 products), the formatting module of the processor generates the requested area and time from the internal format. Therefore, the Level 2 and 3 products must be permanently stored in the internal format.
The processor requires for the processing of a single orbit the Level 1b and Level 2 data of the ESA MERIS processor, and the integrators for the Level 3 products. During the processing, the Level 2 intermediate products must also be stored locally. After processing, the Level 2 products and the integrators must be stored in the DIMS products library.

6.1.3.2 Input Products

Input to the processor are the ESA MERIS Level 1b and Level 2 products. The characteristics of these are specified in Table 1. A complete orbit is divided into 84 scenes because of the product specifications of the ESA processor. Each MERIS line has 4484 samples, while a product includes only 1940 samples, so that 3 products are necessary to reproduce a full swath. An orbit includes approximately 59200 scan lines, but a product inlcudes only 2200 lines. Consequently, 28 products are required to build the length of an orbit. In total this yields 3x28=84 ESA products for 1 orbit.
The total disk space requirement for the input data for 1 orbit is 7.5 Gbyte.

	ESA Produkt					
Level	*Width*	*Height*	*Samples*	*Lines*	*size / MB*	*Products*
L1b	582 km	650 km	1940	2200	41	1
L2	582 km	650 km	1940	2200	50	1
	Orbit					
L1b	1345 km	17760 km	4484	59200	3444	3x28=84
L2	1345 km	17760 km	4484	59200	4200	84
Sum Orbit					7644	

Table 1: Product specifications of the ESA MERIS Lvel 1b and 2 products.

Copyright © 1997 SCICON.

6.1.3.3 Level 2 intermediate products

In the worst case, every Level 2 product is generated for every pixel of an orbit, and it is stored in a plain binary array of a floating point variable. The resulting requirements for disk space is specified in Table 2.
The disk space requirements for the Level 2 intermediate products will not exceed 16.8 Gbyte.

Parameter	*Produkt*	*Pixel (max)*	*Größe max, 4 Byte / pixel*	
Chlorophyll Konzentration Nordsee	WC1	265.452.800	1012,62207	MB
Schwebstoffkonzentration Nordsee	WC1	265.452.800	1012,62207	MB
Gelbstoff Nordsee	WC1	265.452.800	1012,62207	MB
Chlorophyll Konzentration Ostsee	WC2	265.452.800	1012,62207	MB
Schwebstoffkonzentration Ostsee	WC2	265.452.800	1012,62207	MB
Gelbstoff Ostsee	WC2	265.452.800	1012,62207	MB
Optische Tiefe Aerosol	AER	265.452.800	1012,62207	MB
Mischungsverhältnis Aerosol	AER	265.452.800	1012,62207	MB
NDVI	NDVI	265.452.800	1012,62207	MB
Optische Tiefe Wolken	CO	265.452.800	1012,62207	MB
Albedo Wolken	CA	265.452.800	1012,62207	MB
Wolkenoberkantendruck	CTP	265.452.800	1012,62207	MB
Wasserdampf	WV	265.452.800	1012,62207	MB
LCC interm	LCC	265.452.800	1012,62207	MB
Geometry	GEO	265.452.800	1012,62207	MB
Auxiliary	AUX	265.452.800	1012,62207	MB
Flags	FLAG	265.452.800	1012,62207	MB
Summe			16,8	GB

Table 2: Disk space requirements of the Level 2 intermediate products in the worst case.

6.1.3.4 Level 3 intermediate products

M1 Matrix			
samples	*lines*	*cells*	*size / MB*
12800	12800	163 840 000	625
spatial statistic			
Matrix	*Byte/pixel*	*Größe / MB*	
ni	1	156	
S1i	4	625	
S2i	4	625	
Sum		1.406	
temporal statistic			
Matrix	*Byte / pixel*	*Größe / MB*	
N	2	313	

Copyright © 1997 SCICON.

n	2	313
W	4	625
S1	4	625
S2	4	625
Sum		2.500

Table 3: Basic data for the M1 grid.

Byte per Klassifikation	4	
Größe einer klassifizierten Szene	14	MB
Größe einer klassifizierten M1 Matrix	625	MB
Anzahl M1 Matrizen für monatliche Auswertung	32	31 Tage + Monatsmatrix
Größe des Speichers für monatlichen Auswertung	19,5	GB
Anzahl M1 Matrizen für Jahresauswertung	12	
Größe des Speichers für Jahresauswertung	7,3	GB
Maximale Speichergröße	19,5	GB

Table 4: Basic data for LCC processing.

Copyright © 1997 SCICON.

alle Parameter auf M16 Gitter, d.h. 640 000 pixel				
ISCCP compatible product				
Parameter	Bytes / bin	Anzahl	Größe / MB	
Nk	2	10	12	Number of observation in a cloud class k
CTPk	4	10	24	avarage CTP in class k
VAR_CTPk	4	10	24	variance CTP in class k
CODk	4	10	24	avarage COD in class k
VAR_CODk	4	10	24	variance COD in class k
Summe			110	
high vertical resolution product				
Nv	2	19	23	Number of observation in a vertical class v
CTPv	4	19	46	avarage CTP in class v
VAR_CTPv	4	19	46	variance CTP in class v
CODv	4	19	46	avarage COD in class v
VAR_CODv	4	19	46	variance COD in class v
WVPv	4	19	46	avarage WVP in class v
VAR_WVPv	4	19	46	variance WVP in class v
Summe			302	
Gesamtsumme WolkenWasserdampf			411	
Zeitliche Auflösung:	Wochenmittel und Monatsmittel			
um die auszurechnen, braucht man jeden Parameter 2 mal				
Gesamtsumme für Wochen- und Monatsmittel			823	

Copyright © 1997 SCICON.

Parameter	*Produkt*	*temporär*	*permanent*	
Chlorophyll Nord/Ostsee	WC	1.406	5.000	MB
Schwebstoff Nord/Ostsee	WC	1.406	5.000	MB
Gelbstoff Nord/Ostsee	WC	1.406	5.000	MB
Optische Tiefe Aerosol	AER	1.406	5.000	MB
Mischungsverhältnis Aerosol	AER	1.406	5.000	MB
NDVI	NDVI	1.406	5.000	MB
LCC	LCC		20.000	MB
WolkenWasserdampf	ATM		823	MB
Summe		8	50	GB

Table 5: Disk space requirements for the intermediate Level 3 products in the worst case.

6.1.3.5 User products

Not defined at present.

6.1.3.6 Summary

Gruppe	*GB*
ESA input	7,5
MAPP Level 2	16,8
MAPP Level 3	57,9
Prozessor Tabellen	2,0
Virtueller Speicher	2,0
Prozessor Software	1,0
Summe	87,1

Table 6: Estimate of total disk space requirements for the processing of one orbit.

Copyright © 1997 SCICON.

6.2 Plug – In Concept for the MERIS-VA Processor

6.3 Memory Mapped File I/O for Large Files

Copyright © 1997 SCICON.

	MAPP

Titel: **Regionalized Case-II Water Products and Algorithms ATBD**

Project: MAPP

Doc. No.: MAPP-ATBD-WC1

Issue: 1

Revision: 1

Date: 30.3.2000

	Function	Name	Organisation	Signature	Date
Author:		R. Doerffer	GKSS		
		H. Schiller	GKSS		

Copyright © 1997 SCICON.

Internal Distribution

Name	Organisation	Qantity

External Distribution

Name	Organisation	Quantity

Change Record

Issue	Revision	Date	Changes
1	0	31.3.1998	initial issue
1	1	30.3.2000	Addendum 1 added

Copyright © 1997 SCICON.

MAPP Data Products Definition and Algorithm Specification

Algorithm Theoretical Basis Document (ATBD)

Regionalized Case-II Water products and algorithms

ATBD 1.00

Regionalized pigment index, sediment and *gelbstoff* retrieval from directional water leaving radiance reflectances using inverse modelling technique

- **Version 1.1**
- **March 30, 2000**
-
-

- **Roland Doerffer, Helmut Schiller,**
- **GKSS Research Centre**
- **21502 Geesthacht, Germany**

-

Copyright © 1997 SCICON.

2. ABSTRACT 6

3. PREFACE 7

3.1 ATBD 1.00 HISTORY 7

4. INTRODUCTION 7

5. ALGORITHM OVERVIEW AND BACKGROUND INFORMATION 9

5.1 ALGORITHM IDENTIFICATION 9

5.2 ALGORITHM OVERVIEW 9

6. 7. ALGORITHM DESCRIPTION 12

7. ALGORITHM DESCRIPTION 13

7.1 THEORETICAL DESCRIPTION 13

7.2 PHYSICS OF THE ALGORITHM 13

7.2.1 The Monte Carlo Radiative transfer model 14

7.2.2 Wavelengths used for simulations 16

7.2.3 The atmosphere 16

7.2.4 Air/sea interface 19

7.2.5 Water properties 19

7.2.6 Ancillary data 20

7.2.7 Concentration and angular range 21

7.3 MATHEMATICAL DESCRIPTION OF THE ALGORITHM 22

7.3.1 Standard inverse modelling technique 22

7.3.2 Parametrization of the inverse modelling technique by a multiple non-linear regression technique ("Neural Network"). 24

7.3.3 Construction of a ffNN for inverting MERIS data 28

7.3.4 Results of testing the NN 31

7.3.5 Application to Case I water 34

7.3.6 Typical concentrations for North Sea water 35

7.3.7 Robustness against random errors of the input 37

7.4 PRACTICAL CONSIDERATION 41

7.4.1 Programming and Procedural Considerations 41

7.4.2 Computational effort 41

7.4.3 Calibration, Initialisation, and Validation 42

7.4.4 Quality Control and Diagnostics 42

7.4.5 Operational runtime checks of the ffNN 42

7.4.6 Exception Handling 42

7.4.7 Regional differences 43

7.4.8 Data Dependencies 43

7.4.9 Dependencies on other procedures 43

7.4.10 Output Products 43

8. ASSUMPTIONS AND CONSTRAINTS 44

9. TEST AND VALIDATION OF THE PROCEDURE 44

9.1 TEST OF THE MONTE CARLO MODEL 45

9.2 TEST OF THE NEURAL NETWORK 45

9.3 TEST WITH REAL DATA 45

10. FUTURE ACTIONS 45

11. 12. REFERENCES 46

12. REFERENCES 47

Copyright © 1997 SCICON.

13. 14. APPENDIX A: EXAMPLE OF A FFNN PROCEDURE (C - LANGUAGE) 49

14. APPENDIX A: EXAMPLE OF A FFNN PROCEDURE (C - LANGUAGE) 50

14.1 EXAMPLE FOR THE USAGE OF THE NN 50
14.2 EXAMPLE OF THE SUBROUTINE WHICH CHECKS THE ERRORS AND CALLS THE NN GENERATOR 51
14.3 EXAMPLE OF A SUBROUTINE PRODUCED BY THE NN GENERATOR 52
15. 16. APPENDIX B: VALIDATION PLAN FOR CASE II WATER ALGORITHM 53

16. APPENDIX B: VALIDATION PLAN FOR CASE II WATER ALGORITHM 54

16.1 REFERENCE DOCUMENTS 54
16.2 INTRODUCTION 54
16.3 BASIC SCOPE OF THE ALGORITHM 54
16.4 VALIDATION 55
16.4.1 Validation with simulated data 55
16.4.2 Validation with field measurements 56
16.4.3 Validation with airborne measurments 56
16.4.4 Validation with MOS data 57
16.5 OUT OF SCOPE TESTS 57
16.6 DETERMINATION OF ERRORS 57
16.7 DETERMINATION OF THE SCOPE OF ALGORITHM 58
17. 18. APPENDIX C: CASE II WATER MODEL (BY M. BABIN AND R. DOERFFER) 58

18. APPENDIX C: CASE II WATER MODEL (BY M. BABIN AND R. DOERFFER) 59

18.1 1. - PURPOSE 60
18.2 2. - COASTAL WATER OPTICAL PROPERTIES 60
18.2.1 2.1 - Remotely sensed layer 60
18.2.2 2.2 - Water constituents 60
18.2.3 2.3 - Vertical distribution 61
18.2.4 2.4 - Inherent optical properties of water and its constituents 61
18.3 3 - SEA SURFACE STATE 68
18.4 4 - ATMOSPHERIC PROPERTIES 69
18.4.1 4.1 - Air pressure at ground 69
18.4.2 4.2 - Density Profiles & Rayleigh parameters 69
18.4.3 4.3 - Ozone layer 69
18.4.4 4.4 - Aerosol 70
18.5 18.6 5 - REFERENCES 71
18.6 5 - REFERENCES 72
ADDENDUM 1 74

•

Copyright © 1997 SCICON.

2. Abstract

The document describes a procedure to retrieve for different regions and/or different seasons the concentrations of phytoplankton pigment, suspended matter and *gelbstoff* from water leaving radiance reflectance data of the Medium Resolution Imaging Spectrometer (MERIS), which will be operated on the environmental remote sensing satellite ENVISAT of the European Space Agency ESA. The key features of the presented algorithm are the capability to treat a wide range of concentrations which covers open ocean case I water as well as turbid case II waters, and to consider the non-isotropic character of the water leaving radiance, which depends on the solar and observation angles, the sea surface roughness as well as on the single scattering albedo, w_0, and the phase functions of the water and its constituents. In order to provide regionalized scopes of the algorithm, the optical properties of the three components of water constituents: phytoplankton pigment, suspended particles, and *gelbstoff* are measured for different regions and seasons. These measurements are used to calculate by a Monte-Carlo model the directional water leaving radiance reflectances, r_w, of 8 MERIS bands. The inversion of these regionalized models is emulated by (artificial) Neural Nets (NN).

The regionalized evaluation of MERIS data will be done by the user. For this the user will get

- the available set of NN's in form of Java code. The user can use just one of these NN's or a weighted mixture of some NN's to evaluate the concentrations of non absorbing suspended matter and phytoplankton pigment and the gelbstoff absorption at 440 nm.

- Input to the algorithm are the directional water leaving radiance reflectances, r_w, of 8 MERIS bands, which are defined as $r_w(q_v, Df_v)=L_w(q_v, Df_v)/E_d(q_s)$, with L_w, the water leaving radiance, and E_d, the downwelling irradiance just above the sea surface, and the three angles, q_v, the zenith angle of the observation angle, Df_v, the observation azimuth relative to the sun azimuth, and q_s, the solar zenith angle. This input interface requires data which are corrected for atmospheric effects including radiance which is specularly reflected at the water surface. The atmospheric correction procedure is described in another ATBD.

Output of the procedure are the concentrations of non absorbing suspended matter and phytoplankton pigment and the *gelbstoff* absorption at 440 nm.

The algorithm is a multiple non-linear regression method ("Neural Network"). Its coefficients are determined from a table of input (the 8 reflectances and 3 angles) and corresponding output variables (3 concentrations) using a feed forward backpropagation optimisation ("training") technique. The table of water leaving radiance reflectances as a function of the concentration of the 3 water constituents and the three angles is produced by radiative transfer simulations using a Monte Carlo radiative transfer model, which has been optimized for computing large data sets of upward directed directional water leaving radiance reflectances.

The test of the algorithm demonstrates:

- Concentrations of phytoplankton pigment, *gelbstoff* and suspended matter can be determined from randomly mixed compositions of these constituents over a large concentration range.

Copyright © 1997 SCICON.

- The error in the retrieval of a constituent at low concentration increases with increasing concentrations of the two other substances. This error and, thus, the scope of the algorithm for a given error range can be determined from the tests.

- Random errors in the input reflectances produce a similar error behaviour of the output concentrations.

- The algorithm works also for the retrieval of phytoplankton pigment at low concentrations of suspended matter and *gelbstoff* (case I water, as found in the open ocean) and shows a linear behaviour over the tested concentration range of four decades, i.e. < 0.003 to > 30 mg/m^3. Thus, the same algorithm covers case I and case II water with the maximum possible accuracy.

- The routine includes an algorithm to detect and flag reflectances and retrieved concentrations which are out of the NN training range.

- The computational performance of the NN is high and amounts to about 10^4 pixels/s (Ultra Sparc 1).

3. Preface

This Algorithm Theoretical Basis Document (ATBD) describes a procedure for retrieving concentrations of suspend matter, phytoplankton pigment, and *gelbstoff* of coastal and open ocean waters from directional water leaving radiance reflectance spectra. The procedure expects atmospherically corrected directional reflectance spectra. The algorithm is based on inverse modelling of the radiative transfer using a Monte Carlo photon tracing code. The parametrization is done by a multiple non-linear regression procedure ("neural network ", NN) which coefficients are determined from a table of reflectances, angles and the corresponding concentrations by the feed-forward back-propagation optimization technique. The training and test data sets are produced using Monte Carlo simulations for a concentration range which covers case I and case II waters and all potential illumination and observation angles of MERIS images.

The algorithm uses directional reflectances since the subsurface and the water leaving radiances are not isotropically distributed. The angular distribution depends on the solar zenith angle, the observation angle, the sea surface roughness and on the concentration and composition of the water constituents. Since the angular influence cannot be separated from the retrieval of the concentrations, the presented procedure uses a model and the parametrization of its inverse which includes the observation and sun angles.

3.1 ATBD 1.00 History

.

This is the first version.

4. Introduction

Coastal zones are attracting increasingly interest because they are the most populated and utilised areas of the earth. The development of the ecological quality of these zones including the quality of the coastal water is a key issue of coastal zone management. Investigation and monitoring require new approaches including remote sensing because of the heterogeneous

Copyright © 1997 SCICON.

distribution of water properties and their rapid changes. MERIS will be an instrument which specifically addresses the need of coastal zones.

Many coastal zones in Europe and in the world are characterised by high concentrations of suspended matter which is transported by rivers into the sea, or, in case of shallow seas, are stirred up from the ground by the shear stress of tidal or wind induced currents and waves. Furthermore, aeolian transport of desert dust can enrich the water with mineralic suspended material. The implication is that standard algorithms based on colour ratios which have been developed for the determination of phytoplankton pigments are not applicable to these types of water since suspended matter influences the whole blue to red spectral range.

A further important constituent which modifies the backscattered light of the ocean is yellow substance. It consists of various highly polymerized dissolved organic molecules which are formed from all kinds of degradation products of organisms. Its origin is partly marine plankton, but mainly it is transported by rivers into the coastal sea. These chemically uncharacterized fraction of organic constituents were named *gelbstoff* by Kalle (1949) who first investigated its influence on ocean optics. Beside its effect by contaminating the spectral signal of phytoplankton it is of increasing interest in global and regional carbon cycle studies since it amounts to 70% of the dissolved organic material in the ocean (Spitzy & Ittekkott, 1986). The resulting problem for remote sensing from these two water constituents is that they influence the water leaving radiance in addition to the effect of phytoplankton pigments. For these cases it is difficult to separate the influence of each substance. Model simulations for high concentrations of all three substances (as found in many coastal areas) show that a correct determination of one constituent is only possible if also the other constituents which determine the water leaving radiance are determined correctly. Furthermore it can be shown (Doerffer 1979, Doerffer & Schiller 1994) that the error of as well as the optimum spectral range for the retrieval of a substance depends on the concentrations of the others. Altogether one has to deal with a complex and highly non-linear system for which simple solutions based on empirically derived colour ratios are insufficient.

In order to solve the two problems, i.e. separation of the three groups of substances and atmospheric correction over turbid waters, an inverse modelling technique has been developed at the GKSS Research Centre which takes all 4 components into account. This technique has been successfully applied to ship and aircraft data and data of the Coastal Zone Colour Scanner CZCS, e.g. Doerffer and Fischer (1994). Although the CZCS had only 4 channels available for the retrieval and had only a rather limited accuracy, the inverse modelling technique turned out to be sufficiently robust even for these data. Using simulated MERIS data which were calculated from high resolution aircraft radiance spectra (GKSS 1994) it could be demonstrated that even in very turbid coastal waters of the German Bight the contribution by phytoplankton pigments, suspended matter, *gelbstoff* and aerosols could clearly be separated. However, the method requires the operation of a simplified radiance transfer model within an optimisation loop on a pixel by pixel bases. This approach has two limitations: (1) with presently available processors the computational effort exceeds the limits for an operational mass production for global coverage; (2) the simplification of the model, which is required to reduce the computational effort, limits the accuracy of the retrieval. Within this ATBD we have therefore investigated the use of a complex model and the parametrization of its inversion with a Neural Network as an alternative.

Copyright © 1997 SCICON.

The following document describes the algorithm for the retrieval of concentrations of phytoplankton pigment, total suspended matter and *gelbstoff* from water leaving radiance reflectance data of the Medium Resolution Imaging Spectrometer MERIS. The procedure includes the influence of the non-isotropic character of the water leaving radiance reflectance and its dependence on sun and observation angles as well as on the concentration of the water constituents. The angular dependence of the water leaving radiance and reflectance was identified as a major problem for accurate measurements and, thus, has been discussed in many publications (see e.g. Fischer & Graßl, 1984); a comprehensive analysis using Monte Carlo simulation is given by Morel & Gentili, 1991, 1993). Although the algorithm considers the complex nature of the water leaving radiance reflectance, its parametrization by the NN avoids any iterative procedures and, thus, provides the high computational efficiency which is required for the operational mass production of level - II concentration maps.

5. Algorithm Overview and Background Information

5.1 Algorithm Identification

Algorithm name

Inverse radiative transfer modelling technique with neural network parametrization (IRTM-NN)

Product names:

1. Phytoplankton pigment index expressed as chlorophyll-a concentration, unit: µg/l (MERIS.CASE2.PIG)

2. non-absorbing suspended particle concentration (NSP), unit: mg/l (MERIS.CASE2.NSP)

3. *Gelbstoff* (yellow substance) absorption at 440 nm, unit: m^{-1} (MERIS.CASE2.YS)

The spectral channels of MERIS enable that other variables may be retrieved in addition or as an alternative, but this extension has not yet been investigated:

- the organic fraction of suspended matter,
- separation of two types of yellow substance, originating from rivers or produced in the ocean and differing in their spectral exponents,
- "Red Tides", which are plankton blooms which discolour the water by carotinoids
- quantum efficiency of the sun light stimulated fluorescence when including the fluorescence channel at 682 nm.

5.2 Algorithm Overview

The widely applied algorithm used to determine the chlorophyll concentration in open ocean waters from radiance or reflectance data (such as of the Coastal Zone Color Scanner, CZCS[1])

[1] operated on the satellite Nimbus 7 from 1978 to 1986

Copyright © 1997 SCICON.

is based on the ratio of radiances or reflectances measured in one of the green channels between 520 and 550 nm and in the blue channel around 440 nm. This ratio describes the blue-green colour shift which occurs with increasing chlorophyll concentrations. The regression coefficients between the radiance ratios after atmospheric correction and the chlorophyll concentrations have been determined from numerous water samples taken by many researchers in various areas of the global oceans.

A further prerequisite for any algorithm is an accurate atmospheric correction, since the atmospheric contribution to the total radiance at the satellite surmounts 90%. Various papers have discussed different versions of this procedure; their underlying principles are summarised in an overview by Gordon and Morel [1983].

Most of the open ocean areas belong to case I water, where only one optical class of water constituents, i.e. chlorophyll and covarying substances such as detritus determine the colour ratio; all other waters with more than one constituent belong to case II, e.g. areas such as the North Sea, the Baltic Sea, and many other coastal regions of the world oceans.

A further problem of turbid waters is the atmospheric correction. Over case I water it is based on the assumption that the radiance in the NIR channels (where the absorption of water is very high) is only the atmospheric path radiance including the specularly reflected sky and sun light. This method cannot be applied to case II type waters with very high suspended matter concentrations which cause that the backscattering of water cannot be neglected. The inverse radiative transfer modelling technique (IRTM) is an approach to solve this problem.

In principle, a radiative transfer model is used which describes the process of remote sensing, that is, the flux of sunlight into the ocean and back to the sensor. By varying the concentrations and other parameters, such as the aerosol path radiance, with the help of an optimization procedure, the deviation between calculated and measured spectra is minimized.

The technique has first been applied by Jain and Miller (1976) to radiance spectra of water surfaces by using a two-flow approximation for describing the irradiance transport. A similar approach was applied to airborne radiances by Fischer (1984), who used a radiative transfer model based on the matrix operator method (MOMO). However, due to the high amount of computer time needed for the MOMO, the method could only be applied to single scan lines of the CZCS (Fischer & Doerffer, 1987). The combination of the highly accurate MOMO model with a simple and fast two-flow approximation for the inverse modelling has been successfully applied to full CZCS scenes by Doerffer and Fischer [1994]. Although the procedure did not contain any empirical relations between in situ and satellite data (besides the optical properties of the four parameters measured in part of the area of the CZCS scene), a comparison of a CZCS scene inversion with ship measurements showed an agreement of the results within the error range of the ship measurements (Puls et al., 1994).

However, even with a simple model this inversion method requires an amount of computational time which is not acceptable for the mass production of a ground segment. For a CZCS scene of 900 scan lines approximately 1h of computing time is used on a SUN Ultra Sparc 1. To increase the computational efficiency two techniques have been studied for the parametrization of the full model. One is the parametrization of the inverse model by Chebychev expansion. Depending on details of the parametrization and the desired accuracy, a reduction of computational time by up to a factor 100 is possible with this technique [Schiller

Copyright © 1997 SCICON.

and Doerffer, 1993]. The other possibility is the application of a neural network (NN), which is a multiple, non-linear regression technique (Buckton et al., 1995; Schiller and Doerffer, 1997). This approach leads to an even higher reduction, but requires a careful and elaborate determination of the multiple coefficients ("training phase").

Essential for inverse modelling but implicitly also for all other algorithms is the knowledge of the optical properties of the water constituents and aerosols. Therefore, work has to be focused on establishing data sets of the specific optical properties of water constituents and related spectral high resolution radiance spectra for different regions and seasons.

Copyright © 1997 SCICON.

6.

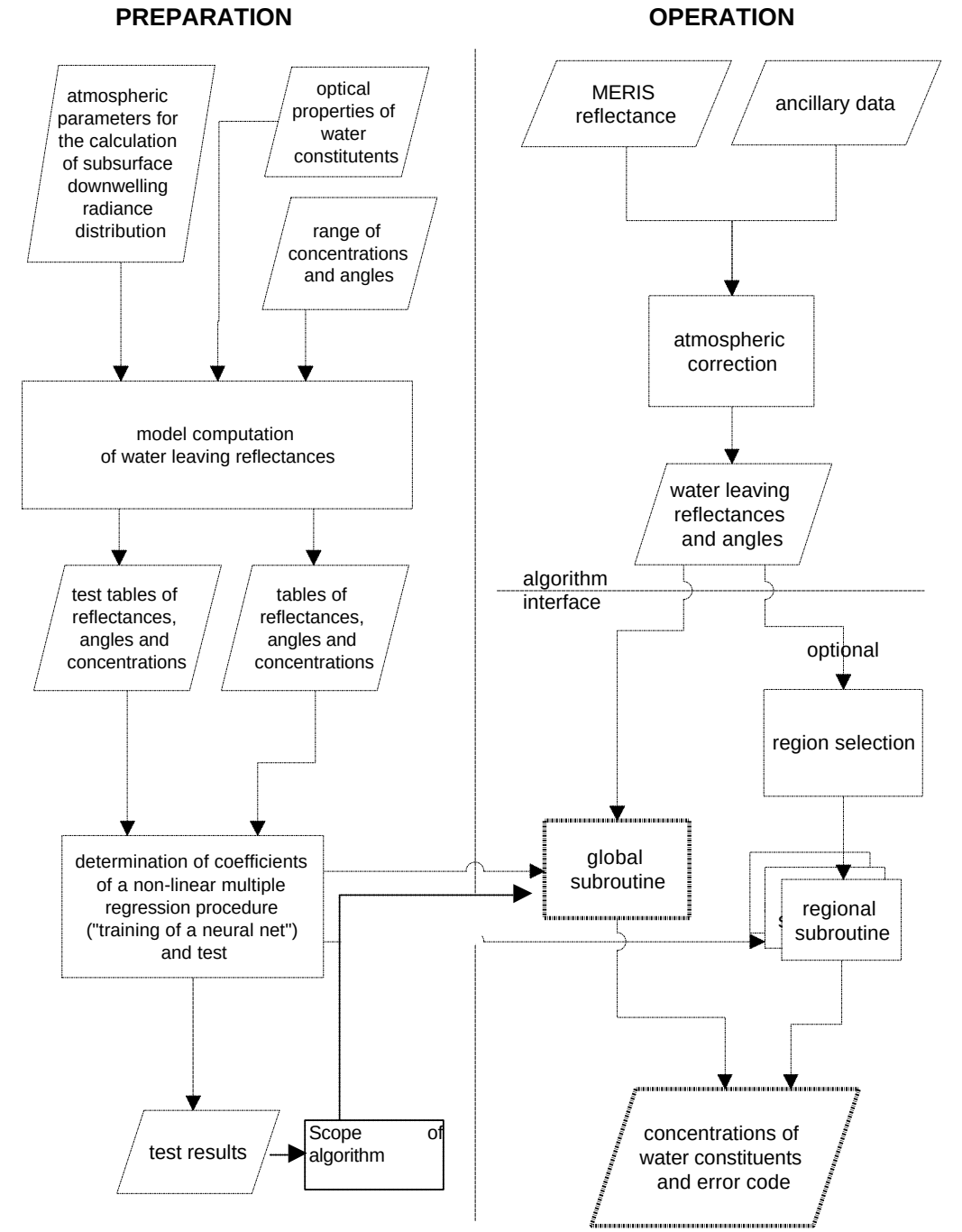

Fig. 1 Scheme of the algorithm based on inverse modelling of radiative transfer and its parametrization with a multiple non-linear regression procedure ("feed forward backpropagation neural network"). The scheme includes the option of different training sets for different coastal regions.

Copyright © 1997 SCICON.

7. Algorithm Description

This section describes the entire algorithm. The algorithm is based on directional water leaving radiance reflectances, i.e. using the actual solar and observation angle pixel-by-pixel. Reflectance is favoured because MERIS will be calibrated with a reflectance standard against the sun. The algorithm requires as input atmospherically corrected reflectance data and the actual solar and observation angle. The multiple non-linear regression procedure is developed from radiative transfer calculations which includes a wide range of concentrations to cover case I and case II water properties and the potential solar and observation angles. A scheme of the algorithm is given in Fig. 1

7.1 Theoretical Description

The following sections provide the theoretical basis of the algorithm. We discuss the basic physics of the algorithm, explain the inverse modelling approach and describe its parametrization by a neural network.

7.2 Physics of the Algorithm

The directional water leaving radiance reflectance $r_w(q_v, f_v)$ associated with the water leaving radiance $L_w(q,f)$ and the downwelling irradiance above the sea surface E_d is defined to be:

$$r_w(q_v, f_v) = L_w(q_v, f_v)/E_d(q_s)$$

where q_v and f_v are the zenith and azimuth observation angles respectively. E_d depends on the solar zenith angle, q_s, for the pixel under examination.

For convenience we will denote the wavelength dependency in the following chapters only where necessary.

In the procedure the contribution by sunlight induced fluorescence of *gelbstoff* and phytoplankton as well as the inelastic scattering caused by the Raman effect have been neglected.

The downwelling irradiance at the sea surface E_d is defined as:

$$E_d = t_0 F_0(q_s) + \int_0^{2p} \int_0^{p/2} L_{sky}(q_{sky}, f_{sky}) \cos q \sin q \, dq \, df$$

where F_0 is the extraterrestrial solar irradiance under the solar zenith angle q_s, t_o is the diffuse and direct transmission of sunlight through the atmosphere, L_{sky} is the sky radiance under the zenith angle q_{sky} and the azimuth angle f_{sky}.

Input to the algorithm are the water leaving directional radiance reflectances, which have to be derived from the reflectances at satellite altitude, r_{toa} .This procedure is described in another MERIS ATBD.

The water leaving directional radiance reflectance for the considered 8 MERIS bands depends on the following processes and quantities:

- spectral and angular distribution of the downwelling radiance just above the water surface, which is mainly a function of the solar zenith angle, the transmittance through the

Copyright © 1997 SCICON.

atmosphere including the ozone layer, Rayleigh scattering by air molecules and Mie scattering by aerosols,

- a rough sea surface, where part of the downwelling and upwelling radiance is reflected and the transmitted radiance is randomly refracted according to the wave slope distribution,
- scattering and absorption by pure water and its constituents in the water column.

7.2.1 The Monte Carlo Radiative transfer model

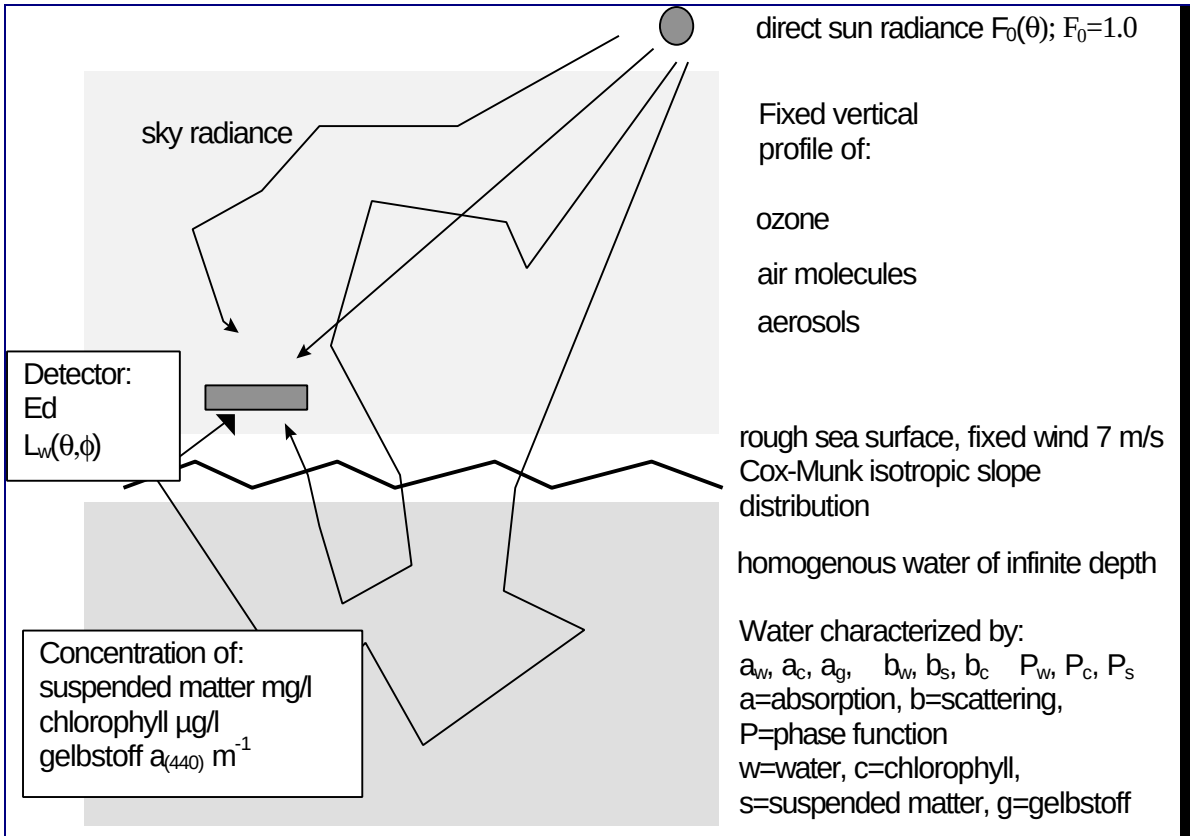

Fig. 2 Scheme of Monte Carlo Procedure for calculating water leaving reflectances

The procedure used to determine the relationship between the water constituents and the solar angle on one hand and the water leaving radiance reflectance and the observation angles on the other hand is an angular resolving ocean-atmosphere photon tracing Monte Carlo radiative transfer code which was developed by GKSS based on publications by Gordon (1994), Mobley(1994), Morel & Gentili (1991); the main processes are outlined in Fig. 2.

It has the following features:

- atmosphere with 50 layers using vertical profiles for scattering by air molecules (Rayleigh scattering), ozone absorption and scattering and absorption by three different aersols.
- air/sea interface with flat or wind dependent rough sea surface

Copyright © 1997 SCICON.

- unstratified water column
- bottom at a depth with no effect on water leaving radiance

Processes which are not included in the simulation are:

- polarization
- any inelastic scattering (fluorescence, Raman scattering)
- wind direction

The detector is positioned just above the water surface for counting the downwelling irradiance and the angular dependent upwelling radiance.

Photons start with a weight of unity (1) for all wavelengths at top of atmosphere (layer 51 of the model atmosphere) from a sun disc of 0.5 degree apparent diameter. The weight is multiplied with the cosine of the sun zenith angle. At each event the photon weight is multiplied with the single scattering albedo, ω_0, of the layer in which the event happens, to take into account for the probability of absorption. The travel distance between two interaction events is calculated from a random pull. The type of scattering is determined from the concentration mixture of the different media or constituents in water or air. Probability tables for the random pull of the type of scattering are pre-generated for each layer. The scattering angle, theta, at each event is randomly pulled from large tables which contain, for each media or constituent, the pre-calculated probabilities for the scattering angle in theta. The weights of photons which reach the air/sea interface layer in downwelling direction are counted for calculating the downwelling vector irradiance. All photons reaching the surface penetrate into the water , their weights are corrected for the probability of reflection. All photons which reach the interface layer from below the water surface in upward direction are split into two weights. The reflected photon survives in the water with the probability of reflection. The remaining refracted weight, after changing its direction according to the sea surface slope, is counted just above the surface together with its zenith and azimuth angle. The wave slope angles are randomly pulled from a probability table which is calculated using the Cox & Munk (1954) wind dependent sea surface slope distribution. This distribution is isotropic with respect to the azimuth, i.e. it does not take into account the wind direction.

The photon dies when its weight has decreased below a minimum weight. The predefined minimum weight is adapted from the first 2000 photons which have reached the radiance detector in order to reduce the variance. The simulation for one case and one wavelength is completed when a predefined number of photons have reached the radiance detector, i.e. the number of started photons is variable in order to account for strong differences in ω_0 of different concentration mixtures and wavelengths.

One major problem is the reduction of variance when calculating the angular distribution of the water leaving radiance. Standard photon counting with discrete small cones require a large number of photons which leads to an extreme high computational effort and can practically not be used for a mass production as required for the set up of training tables or simulation of images. Thus, we approximate the angular distribution of the photon by a series of spherical harmonics. Each arriving photon contributes to an update of the first and second moments of the spherical harmonics (the second moment allows the estimation of the standard deviations

Copyright © 1997 SCICON.

of the first moments). In the evaluation process the number of moments are reduced so that only moments remain with > 3 standard deviations apart from zero. The number of moments can be reduced separately for zenith and azimuth angles in the evaluation process. The resulting function can then be used to calculate the radiance at any observation angle without a new MC run. One important step in the development was to find the optimum cut-off of the approximating series for a correct description of the angular distribution and the corresponding number of photons which have to be collected to determine all the moments with the required statistical significance.

7.2.2 Wavelengths used for simulations

The following MERIS bands are used for the simulation:

Channel number	Wavelength [nm]
1	412
2	443
3	490
4	510
5	560
6	620
7	665
9	705

Furthermore, for producing the test data set, channels 13 (775 nm) and 14 (865 nm) were included. The chlorophyll fluorescence band at 681.25 nm has been omitted, since the fluorescence effect has not been considered in the present simulations.

7.2.3 The atmosphere

The atmosphere is modelled here only to determine the downwelling irradiance just above the sea surface, E_d, and a realistic downward directed radiance distribution just below the sea surface for different solar zenith angles. It is not used for atmospheric correction. Except the solar zenith angle all properties of the atmosphere are fixed for this purpose. The atmosphere model is a typical ocean atmosphere with maritime aerosol type with 70% humidity to meet the requirements of case I and case II water. No absorption by atmospheric gases is assumed for the considered 8 (10) MERIS bands. The atmosphere is defined in the document PO-TN-MEL-GS-0016, July 23, 1996, this project (ACRI, 1996).

The atmosphere is modelled with 50 layers, each 1 km thick, photons start at the top of layer 50. Fig. 3 shows the vertical distribution.

7.2.3.1 Pressure at ground

The atmospheric pressure at sea level is fixed to 1013.25 hPa (standard atmosphere).

Copyright © 1997 SCICON.

7.2.3.2 Rayleigh scattering

The vertical profile of the Rayleigh scattering coefficient (air molecules) is given by Elterman(1968) for the standard atmospheric pressure of 1013.25 hPa at sea level.

The profiles with 50 1 km-layers are tabulated for each MERIS channel in 8 files (rpmerxxx.txt, where xxx is the wavelength as listed above).

7.2.3.3 Ozone layer

The vertical ozone profile is taken from Elterman(1968). The density profile which is given in cm ozone per km for a surface pressure of 1013.25 hp is tabulated in the file ozprofel.txt. The total ozone column content is 0.34 cm. The extinction profiles with 50 1-km-layers are tabulated for each MERIS channel in 8 files (opmerxxx.txt, where xxx is the wavelenth as listed above). The ozone absorption spectrum is given in file ozspek1.txt.

7.2.3.4 Aerosol

To be consistent with case I water simulation and algorithms a maritime atmosphere is defined also for case II water. The vertical profiles and optical properties are taken from WMO report WCRP-112 (1986).

7.2.3.4.1 Aerosol types

Three aerosol types are used to model the case I and case II atmosphere:

- maritime aerosol with a humidity of 70% (Shettle & Fenn, 1979)
- continental aerosol (WMO report WCRP-112, 1986)
- stratospheric aerosol which is represented by a 75% solution of sulfuric acid in water (H2SO4) (WMO report WCRP-112, 1986)

The normalised extinction coefficients and single scattering albedos are tabulated for the 3 aerosol types and in addition for the urban aerosol type for each of the 8 MERIS bands in the files csmerxxx.txt, where xxx is the wavelength as listed above.

7.2.3.4.2 Aerosol phase functions

Aerosol phase functions and single scattering albedos were computed using the MIE code developed at LPCM[2], and the inputs (complex indices of refraction and particle size distribution) given in Shetlle & Fenn (1979) and World Climate Research Program, WMO document WCRP-112 (1986).

The single scattering albedos and the phase functions for the 8 MERIS channels are tabulated in the following files with xxx the wavelength:

- maritime aerosol 70% humidity: gm70_xxx.txt
- continental aerosol: gcon_xxx.txt
- stratospheric aerosol: ghso_xxx.txt

[2] the phase functions have been provided by David Antoine, LPCM

Copyright © 1997 SCICON.

The 75 angles of the aerosol phase functions are listed in file wink.txt. The single scattering albedos of these files are used for the calculations.

7.2.3.4.3 Aerosol vertical profile

The first two km (layers 1 and 2) consist of the maritime aerosol type with an aerosol extinction at 550 nm of 0.025 km^{-1}. The layers 3-12 consist of the continental aerosol type with an extinction of 0.0025 km^{-1} and the layers 13-50 of stratospheric aerosol type. The extinction of the stratospheric aerosol is altitude dependent (s.figure 3).

The vertical aerosol extinctions for these three types for 550 nm are tabulated in file profilma.txt.

Fig. 3 Attenuation of the model atmosphere at 510 nm (MERIS channel 4) as used for the simulation of this ATBD: Rayleigh scattering (Rayleigh), maritime aerosol with 70% humidity (Maritim), continental aerosol (Conti), stratospheric aerosol (Strato) and ozone (Ozone)

Copyright © 1997 SCICON.

7.2.3.5 Sun irradiance

As all calculations are done in terms of reflectances, sun irradiance is assumed to be equal 1 for all wavelengths.

7.2.4 Air/sea interface

The rough sea surface is modelled according to Cox & Munk (1954) for a wind speed of 7 m/s. A wind direction is not given; the azimuth distribution of the wave slopes is isotropic. Whitecaps are not accounted for.

The frequency distribution of wave slopes is of Gaussian type with $s^2 = 0.003 + 0.00512 v_w$, and v_w the wind-speed in m/s.

The relationship between random numbers $\rho_{\theta n}$ and $\rho_{\phi n}$ uniformly distributed on the unit interval (0,1) and the angle between the normal to the wave facet and the normal to the level surface, θ_n , and ϕ_n is:

$$r_{qn} = \frac{2}{s^2} \int_0^{q_n} \exp\left(-\frac{\tan^2 q_n}{s^2}\right) \tan q_n \sec^2 q_n \, dq_n$$

$$f_n = 2\pi r_{fn}$$

For calculating the specular reflectance at the air/sea interface $r(q_s)$ and $r(q_v)$, and transmittance through the interface, the law of refraction (Snell's law) is applied with a refractive index for seawater of 1.334.

7.2.5 Water properties

7.2.5.1 Depth of remotely sensed layer

We assumed that the water depth, z, is much larger than the signal depth z_{90}, which is the depth from which 90% of the signal measured at the surface comes from.

7.2.5.2 Water constituents

The path of the photon through the water column is determined beside pure seawater by 3 groups of substances. Composition and optical properties of case II water constituents are extremely variable on a global scale. Since a global algorithm was required, the water constituents are represented here by the following proxy components, which may not be identical with actual constituents: phytoplankton (and associated organic matter) is represented by the global pigment index of case I water (Morel, 1988), suspended matter by non-absorbing scattering particles (non-absorbing suspended particles, NSP) and non-chlorophyllous coloured dissolved and suspended organic matter by *gelbstoff* (yellow substance).

The concentration units are:

Copyright © 1997 SCICON.

Phytoplankton (and associated organic matter): expressed by the concentration of chlorophyll *a* (µg/l)

Non-chlorophyllous suspended matter: it is assumed that this component is solely represented by non-absorbing mineral particles. Its concentration is expressed by its total scattering coefficient at 550 nm [$b_p(550)$; m^{-1}]. It can be *a posteriori* converted into mass concentration per unit volume of suspended matter using a given mass-specific total scattering coefficient [$b_p^*(550)$]. According to Kronfeld(1988) we used a conversion factor of 0.125, i.e.

$$b_p(550) = [\text{NSP mg/l}]*0.125$$

Coloured dissolved organic matter (yellow substance or *gelbstoff*): expressed by its absorption coefficient at 440 nm [$a_y(440)$; m^{-1}]. It can be *a posteriori* converted into mass concentration per unit volume of dissolved organic matter DOC using a given mass-specific absorption coefficient [$a_y^*(440)$], for the North Sea this factor is in the order of 0.1.

7.2.5.3 Vertical distribution

Parameter	**Unit**	**Source**
wind speed	m/s	numerical weather model, weather maps
navigation data	time, position, sun and viewing angles	ENVISAT tracking
water depth	m	bathymetric maps

Table 1 Ancillary Data

It is assumed that all substances are homogeneously distributed in the water-column. For many coastal waters, this is a realistic assumption, especially within the z_{90} layer.

7.2.5.4 Inherent optical properties of water and its constituents

The properties adopted here are documented in the "Case II Algorithm Tests Specification", DOC Ref. No. PO-TN-MEL-GS-0016, s. Appendix C). The optical properties of phytoplankton are the same as for case I water. They are taken from the publication of Morel (1988), which describes a mean global case I water pigment index with concentration dependent spectral absorption coefficients. Thus, in case of the absence of suspended matter and *gelbstoff*, there is no difference between the case I and case II water model. This offers the opportunity to cover both water types with one inverse modelling algorithm.

7.2.6 Ancillary data

Since the atmospheric correction is not included in this version of the inverse modelling algorithm, only a few ancillary data are needed for the calculation of flags. However, these procedures are outside the scope of this ATBD. Also the decision for not passing a pixel to the algorithm by using these flags is made outside this algorithm. The following list contains variables which are needed to calculate these flags.

7.2.6.1 Wind speed

The wind speed is required for calculating the wave slope distribution, which in turn is used to calculate the sun glitter contribution L_g.and the contribution from whitecaps L_{wc} . A special

Copyright © 1997 SCICON.

procedure for coastal zones, where the whitecap distribution differs from that of open ocean areas, is not available.

The glint-mask flags sun glint - contaminated areas in a MERIS image which cannot be used for retrieval.

Data have to be taken from weather maps and numerical models.

7.2.6.2 Navigational data

The algorithm requires the knowledge of the sun and observation angles for each of the pixels. Exact navigational data are required as ancillary data to calculate these angles.

7.2.6.3 Water depth

The water leaving radiance of shallow coastal waters may also be effected by the reflection of the bottom. These areas have to be masked and flagged using bathymetric maps. The decision for not passing a pixel to the algorithm due to shallow water is made outside the described algorithm.

7.2.7 Concentration and angular range

The range of concentrations used for calculating the table and, thus, the scope of the procedure is given in table 2. Concentrations for the tables are randomly generated with constant probability from the log of the concentration within this range.

Copyright © 1997 SCICON.

Ranges of independent variables for calculating water leaving radiance reflectances			
Variable	concentration unit	min	max
phytoplankton pigment, chlorophyll *a*	µg/l	0.003	50
mineralic suspended matter	mg/l	0.03	50
gelbstoff, absorption at 440 nm	a(440) m^{-1}	0.002	2
solar zenith angle	degree	0	75
viewing zenith angle	degree	0	41
difference between solar and viewing azimuth	degree	0	180

Table 2 Ranges of variables for training the ffNN

7.3 Mathematical Description of the Algorithm

7.3.1 Standard inverse modelling technique

The inverse modelling procedure which has been developed for the evaluation of CZCS data of the North Sea and Baltic Sea is based on a simple model (single scattering in atmosphere, two-flow approximation for the radiative transfer in the water, s. chapter 4.2). The optimisation procedure is the simplex-algorithm developed by Nelder & Mead (1965). The procedure is applied on a pixel by pixel basis. Errors are calculated using the Hesse Matrix. The concentrations of total suspended matter, phytoplankton chlorophyll, *gelbstoff* and the aerosol path radiance at 670 nm are derived as independent variables. Due to the limited number of spectral channels and the absence of spectral channels in the near infrared spectral range, it was necessary to include the atmospheric correction implicitly into the procedure. The method as indicated in Fig. 4 is described in general in Doerffer (1992), and Doerffer & Fischer (1994). Comparison with ship data of experiments in 1979 and 1986 on a statistical basis show good agreement. The procedure has also been adapted to simulated MERIS data as derived from radiance spectra measured from an aircraft with the Airborne Optical Multichannel Analyzer (AR-OMA) over coastal waters of the North Sea.

Copyright © 1997 SCICON.

As seen from the scheme, the knowledge of the specific optical properties of the water constituents is a key issue for the success of an inversion. This has been tested for different parts of the Baltic Sea with different spectral absorption coefficients of phytoplankton.

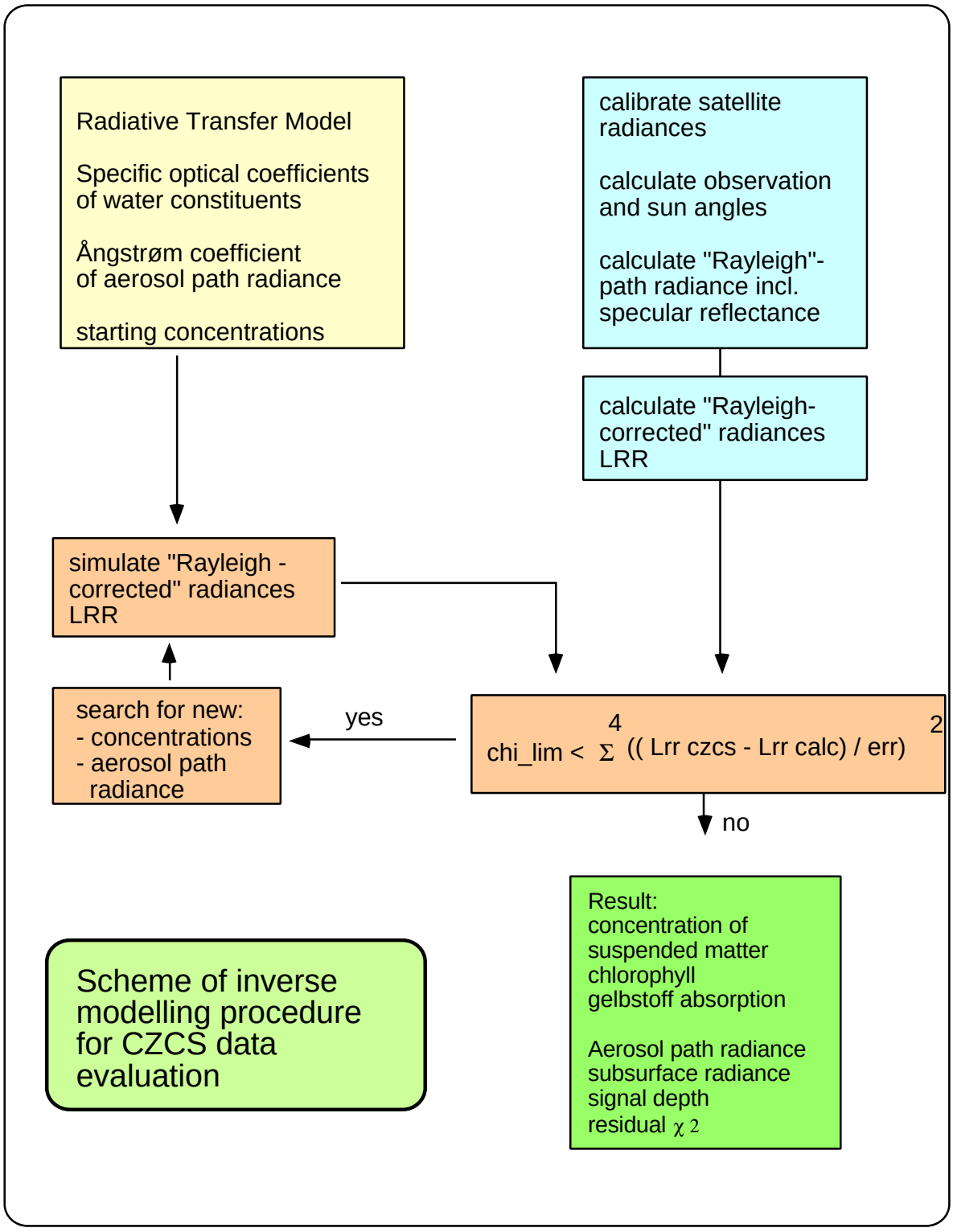

Copyright © 1997 SCICON.

Fig.4 Inverse modelling procedure for CZCS data

7.3.2 Parametrization of the inverse modelling technique by a multiple non-linear regression technique ("Neural Network").

This section describes our method for implementing the inverse modelling technique in form of a neural network (NN). The basic idea is to replace the optimisation loop within the inverse modelling procedure by a table of 6 independent input variables, i.e. the (1) concentrations of phytoplankton pigment, (2) *gelbstoff* and (3) suspended matter, (4) the solar zenith angle, (5) viewing zenith angle and (6) the difference between the solar and viewing azimuth angle, and 8 output variables, which are the water leaving radiance reflectances. This table is used to determine the coefficients of the non-linear multiple regression procedure ("neural network") by minimising the difference between the 3 concentrations used to compute the reflectances and the 3 corresponding concentrations which were produced by the neural network. The optimisation procedure, i.e. the feed forward backpropagation algorithm, is applied to a large data set ("training" of the NN).

7.3.2.1 Outline of the emulation technique

Suppose there is a radiative transfer model (RTF) f which calculates spectral reflectances $\vec{r}$ from concentrations $\vec{c}$ of n water constituents, such as phytoplankton pigments, *gelbstoff*, total suspended matter, and some parameters p

$$\vec{r} = f_{\vec{p}}(\vec{c})$$

In order to derive c from measured reflectances r_{meas} one needs the inverse model

$$\vec{c} = f_{\vec{p}}^{-1}(\vec{r}^{\,meas.})$$

The common procedure to realise the inverse model is the least square method. That means one iterates an optimisation loop until

$$c\,2(\vec{c}) = \sum \left(\frac{\vec{r}_i^{\,meas} .- r_i(f(\vec{c}))}{\Delta r_i^{\,meas.}} \right)^2 \rightarrow Minimum$$

The model is then inverted for the given reflectances if the minimisation is successful.

As stated above the utilisation of the inverse model is quite a heavy computational task since it has to be performed on a pixel by pixel basis. Therefore we look for possibilities to improve the performance:

The calculation of the inverse model can be regarded as an interpolation task. With the use of a RTM one can generate a large table with randomly chosen concentrations and parameters on one side and the calculated reflectances on the other side. In principle one could use this table to get the desired concentration from the combination of reflectances and parameters by interpolation. Technically this will not be feasible; the table would be simply too large due to it's high dimension. But there are a number of methods which can be used to construct an approximating function from such a table, like projection pursuit, neural networks, radial basis functions and tensor product methods. Once an approximating function is constructed it can

Copyright © 1997 SCICON.

be used to effectively do the desired interpolation. It will emulate the inverse model using much less computer time than the inverse model itself would need.

One way is the usage of a Chebyshev-Expansion of the inverse model. This method becomes intractable if more than three eigenvalues of the covariance matrix of the reflectances are significantly different from zero. It turned out that this method cannot reasonably be used for MERIS data for this reason, particularly for turbid coastal water when the atmospheric correction has to be solved implicitly in the retrieval procedure.

Another way for the approximation, which has been turned out as most effective, is the use of a neural network. This is mathematically a multiple non-linear regression technique. For the parametrization of the inverse model a feed forward error-backpropagation network (ffNN) was chosen for its simplicity (Rumelhard et al., 1986). In the following the essentials of this type of network is summarised.

7.3.2.2 The "neural network" procedure

ffNN are organised by layers with an input layer, an output layer and one or more hidden layer(s) between them. Each layer consists of `neurones': the input layer has as many `neurones' as there are input values, the output layer has as many `neurones' as there are output values necessary and the hidden layer(s) need a problem-dependent number of `neurones'.

Neighbouring layers are linked: each `neurone' in one layer has a link to each `neurone' of the next (neighbouring) layer. Each link has a weight (w).

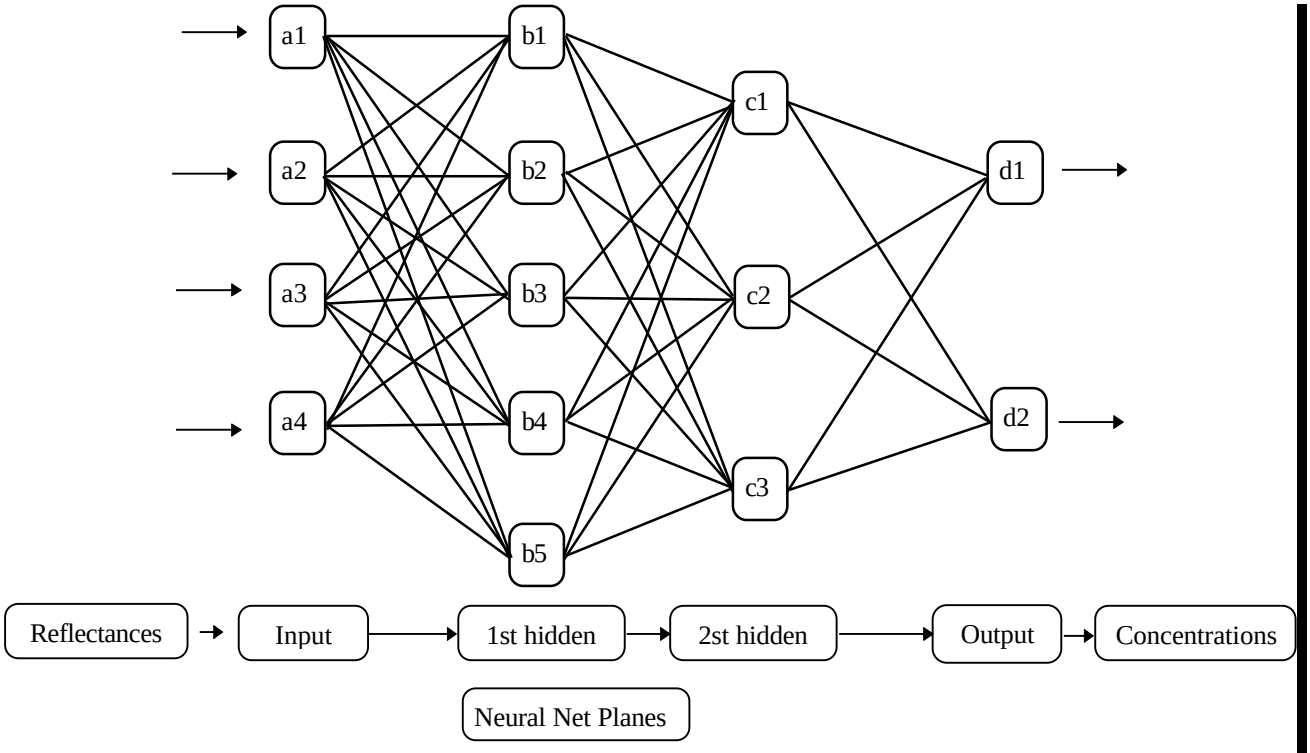

Fig. 5 Example of a Neural Net with two hidden layers. The used NN is more complex

Copyright © 1997 SCICON.

because of the 11 input 'neurones' (8 MERIS channels, 3 angles) and 3 output neurones (3 concentrations)

Copyright © 1997 SCICON.

Each 'neurone' calculates its output value *o* according to

$$o = s(-bias + \sum_{\text{incominglinks}} w_i x_i)$$

where

bias is a value specific for each neurone

w_i is the weight of the link

x_i is the output-value of the link in the preceding layer (the ´neurons´in the input-layer have only one incoming link and x_i are the output values of the input layer)

s is a non-linear function taking the form of a ´sigmoid´, that is, it assumes monotonically increasing values between 0 and 1 as the value of the argument goes from -∞ to ∞. The most popular choice (used also in this ATBD) is the logistic function (s. Fig. 6).

The ffNN works sequentially: at first the input-values are applied to the input-neurones and this is already the output of the first layer. Then all neurones of the first hidden layer calculate their outputs by summing up the weighted inputs, shifting this sum by the bias-value and applying the `sigmoid'. This is repeated for the next layer and so on until the output-layer is reached - giving the network-result for the applied input.

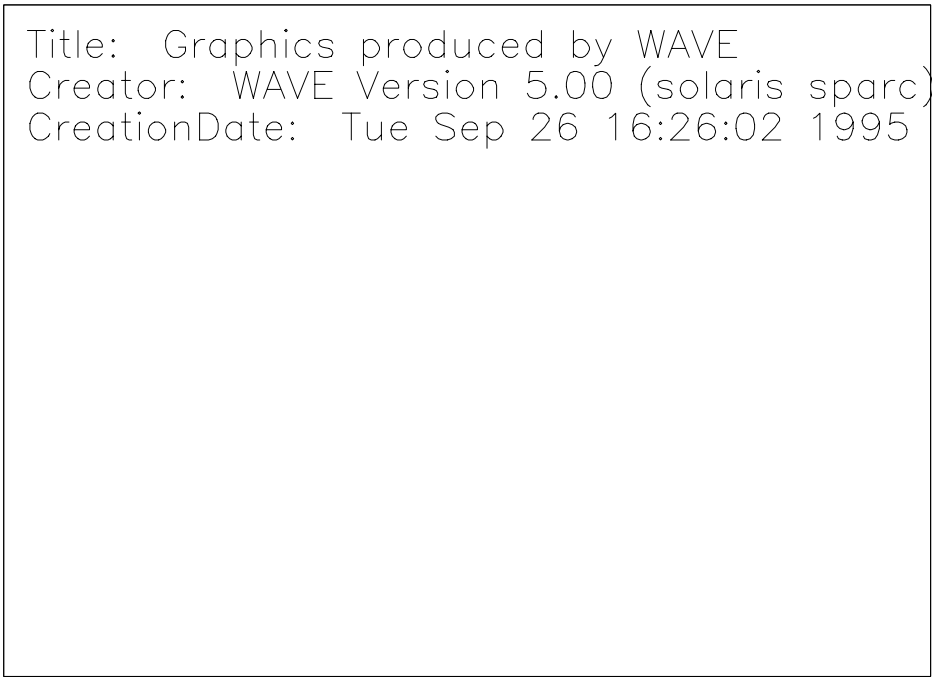

Fig. 6 The logistic function (sigmoid)

The multiple non-linear regression realised by the ffNN depicted in fig. 5 so reads

Copyright © 1997 SCICON.

$$y_l = s(-d_l + \sum_{k=1}^{3} w_{kl} \cdot s(-c_k + \sum_{j=1}^{5} v_{jk} \cdot s(-b_j + \sum_{i=1}^{4} u_{ij} x_i)))$$

For a useful ffNN one has to fit the diverse parameters (biases, link weights). It is the same problem as in a polynomial fit to a simple set of measurements - but due to the high dimensionality of the dependent as well as the independent variables the determination of the coefficients is more complex. One generates two sufficiently large sets of corresponding input-output-vectors - one set is used as `teaching'-sample and the other set as `test'-sample. During `teaching' the values of the biases of all neurones as well as the weights u,v,w,.... of all the links are changed so as to minimise an error-function. In the `teaching-phase the errors are propagated against the normal processing direction: they are backpropagated from the output-layer to the input-layer - this is why such nets also are called `backpropagation networks'. The criterion for a successful training is then the sum of squares of the difference between the output of the net *y* and the corresponding table entries:

$$\sum_{'teaching-sample'} \left(\vec{y}_{desired} - \vec{y}_{ffNN} \right)^2$$

After this minimisation-procedure it is necessary to check if the resulting net has `generalisation-power', i.e. if it is able to produce reasonable results also for input-values which were not `shown' to it before, i.e. data which were not included in the 'training set'. Like in a polynomial fit with too many parameters it could happen that the fit reproduces the points used to fit the parameters but shows bewildering behaviour at places between ("overtraining"). For this task the second (`test') set is used.

7.3.3 Construction of a ffNN for inverting MERIS data

For testing the behaviour and performance of the neural network a ffNN was designed for retrieving the concentrations of suspended matter, *gelbstoff* and phytoplankton pigment from MERIS radiance spectra by inverse modelling. Eight of the first 9 spectral channels which are presently under discussion but not yet fixed have been used for the inversion. The fluorescence and all "atmosphere channels" in the near infrared have been excluded. In subsection 5.3.3.1 the construction of the approximating ffNN for Meris data is described. Results from this ffNN are discussed in subsection 5.3.4. Aspects of the operational usage of the ffNN are presented in subsection 5.4.

7.3.3.1 The construction of the actual ffNN approximating the inverse model

Within this section we demonstrate the use of the ffNN procedure to derive concentrations from water leaving radiance reflectances and demonstrate its performance.

The Monte Carlo model as outlined in chapter 3 was used to calculate the water leaving radiance reflectances. The ranges of interest of the variables were defined to be those given in Table 2. The values were chosen to cover case I open ocean and turbid coastal waters. The software which was used for designing the ffNN is the Stuttgart Neural Network Simulator

Copyright © 1997 SCICON.

SNNS v3.1 (SNNS 1995). The steps to construct the emulating Neural Network for the inverse model for Meris data were as follows:

Copyright © 1997 SCICON.

Construction of the `teaching'- and test-data-set

`Teaching'-sample:

Values of each of the independent variables (3 concentrations and sun zenith distance were randomly pulled from their min - max range (see table 2); the concentrations were pulled from the logarithmic scale. Using these input data the water leaving radiance function was calculated with the Monte Carlo code. Five different observation angles from the predefined range (s. table 2) were then randomly pulled and the corresponding radiances were calculated, divided by the downwelling irradiance at the sea surface to get the water leaving radiance reflectances, i.e. for each MC run 5 reflectance spectra were calculated. Covering equidistantly the log(min)-log(max) - range leads to a higher density at small values of the variables rather than at large values, which reflects the real situation. So during the `teaching phase ' the ffNN is tuned more at small values thereby achieving roughly constant *relative* errors instead of roughly constant errors. Altogether 57240 MERIS spectra have been computed from which 45792 have been used for training of the NN.

Test-sample:

The test-sample, which were the remaining 11448 spectra, were again chosen as randomly (uniformly distributed) from the log(min)-log(max) -ranges.

In both samples the 3 concentration components were transformed to the range [0,1]. This transformation is done to adapt the input to the output-range of the ffNN and additionally eases the control of the errors.

Construction of the ffNN:

Preparation:

A feedforward/backpropagation-NN with 11 `neurones' in the input layer (reflectances in 8 MERIS bands + 3 angles), 50 `neurones' in the first hidden layer and 12 `neurones' in the second hidden layer was defined. The output layer contained three `neurones'. The NN became fully connected (each `neurone' of a layer connected with each `neurone' of the following layer) and was initialised by assigning random numbers (uniformly in (0,1)) to the weights and biases.

'Teaching':

For error-minimisation the backpropagation method with momentum and flat spot term was used. The `teaching'-sample was applied to the ffNN in random order. At start the control parameters were set as follows: learning factor 0.6, momentum factor 0.2 and flat spot term 0.02. Each time if the error-function did not decrease anymore the minimisation-parameters were divided by 3. The minimisation was continued until the error function was down to 211 corresponding to an average output error of 6.8%.

Test:

One problem in NN training is to find the right numbers of hidden layers and the number of `neurones' within these layers as well as the number of cases used for training in order to optimise the accuracy and avoid over-training which could weaken the interpolation power of the NN. The following procedure has been used to optimise the NN. During `teaching' it was

Copyright © 1997 SCICON.

checked that the error function of the test-sample agreed with the error function of the `teaching-sample' in proportion of the sample sizes. At the end of the minimisation the error function of the test-sample was at 54, indicating a good generalisation.

Usage:

The weights and biases obtained by the `teaching' of the ffNN were used to generate a C-function realising the ffNN with roughly no organisational overhead, i.e. the necessary expressions contained the numbers directly. Also the backtransformation from the (0,1)-interval for the components was built into this function. So this function could be used to derive the concentrations from the water leaving radiance reflectances of the test-sample for comparison as well as for timing (s. Appendix A).

7.3.4 Results of testing the NN

The above mentioned C-function was used to derive the concentrations (suspended matter, phytoplankton chlorophyll, *gelbstoff*) from the reflectances of the test-sample. The relationship between the test input for designing the neural network and the results from the ffNN are plotted in the following figures. It has to be mentioned here that due to the tight schedule for the development, the training and test data set were calculated with limited accuracy (20000 photons at detector), furthermore the training was not completed up to the optimal end. For the final version the accuracy will be improved.

We have first analysed the extreme case II waters in which all three substances can randomly vary within the range used for training the neural network (table 2). This kind of water would be typical for some turbid estuaries. Fig. 7 - 9 show the results on a logarithmic scale.

Copyright © 1997 SCICON.

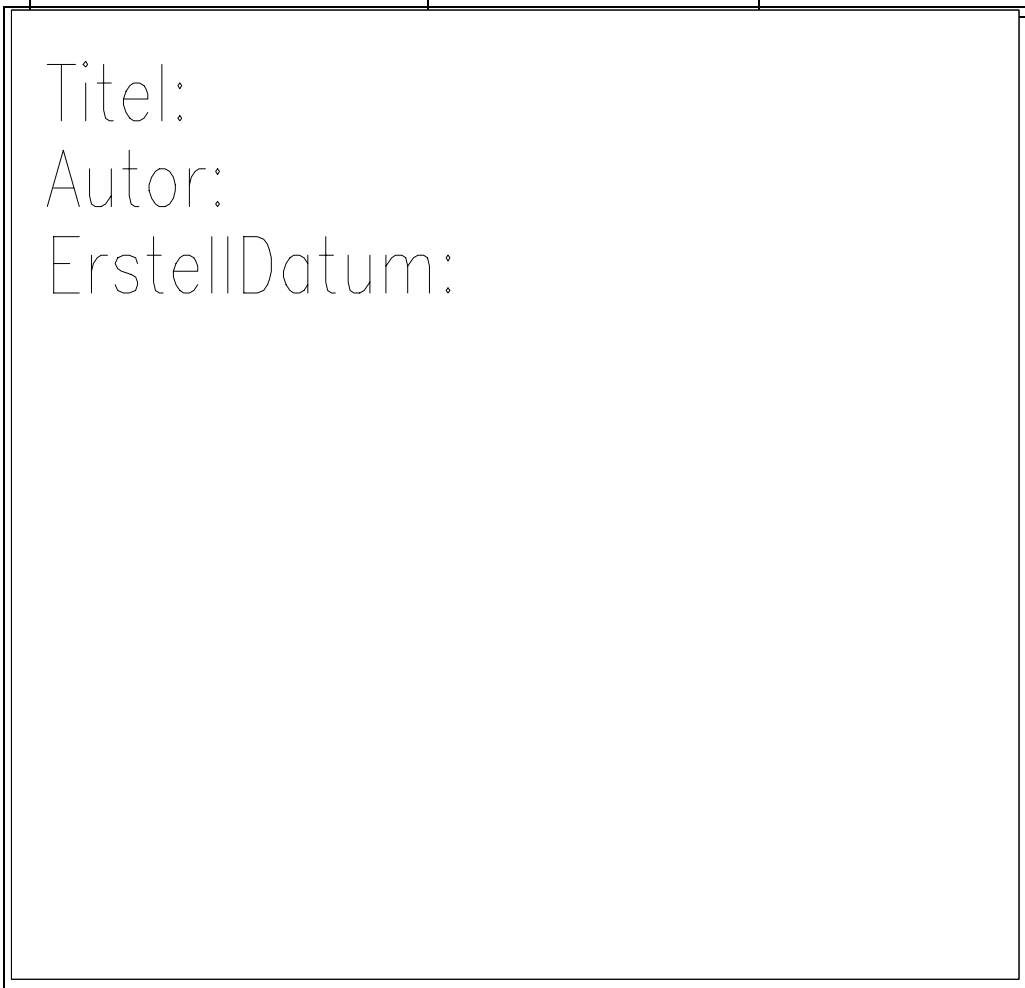

Fig. 7 Relationship between the input and NN derived concentration of Chlorophyll

Copyright © 1997 SCICON.

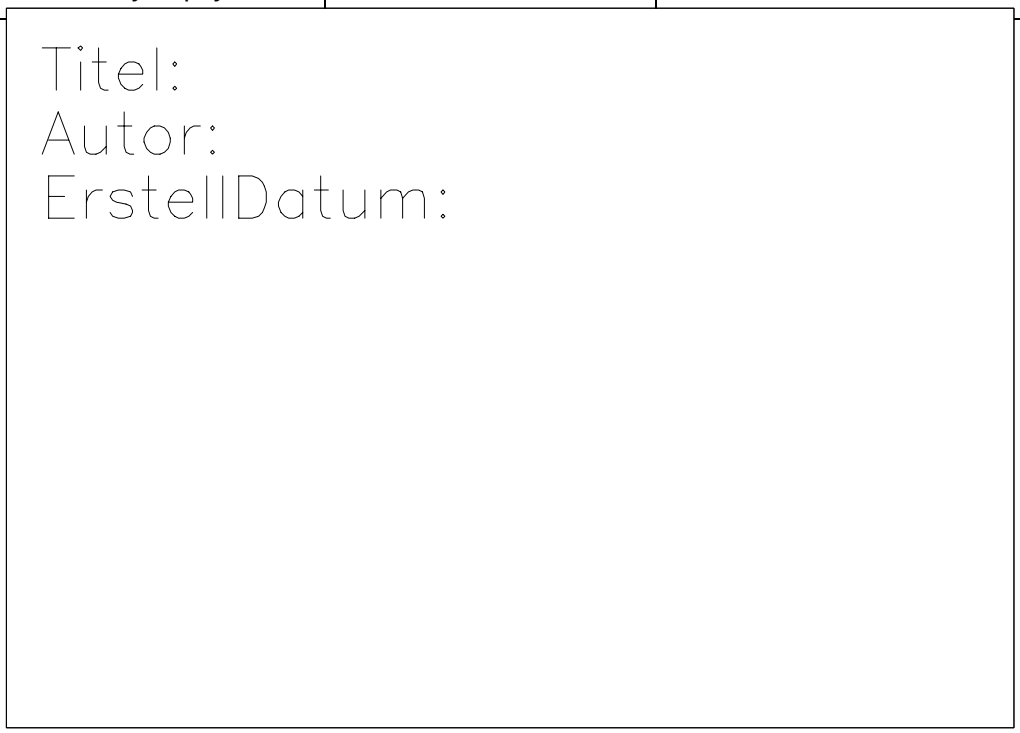

Fig. 8 Relationship between the input and NN derived concentration of *gelbstoff*

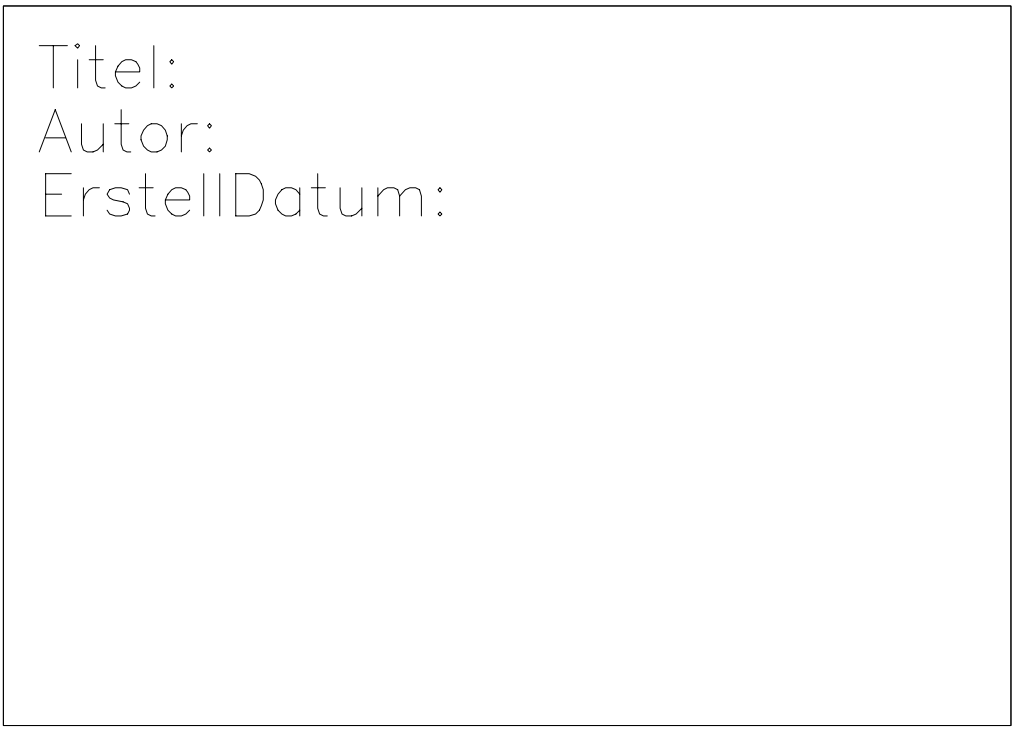

Fig. 9 Relationship between the input and NN derived concentration of suspended matter

Copyright © 1997 SCICON.

7.3.4.1 Definition of the scope

One can see that the error is acceptable at higher concentrations but increases strongly when the concentration becomes so low that the optical effect of that substance becomes neglectable small with respect to the high concentrations and strong fluctuations of the other two components. Thus the composition of water constituents defines here the scope of the algorithms; for turbid estuarine water it comprises about the following concentration range:

phytoplankton pigment (chl. a): 1 - 50 µg/l

gelbstoff absorption a(440): 0.1 - 2 m^{-1}

mineralic suspended matter: 1 - 50 mg/l

Obvious is the linear relationship within this scope and nearly the same error for all 3 components. The figure also shows that thanks to the construction of the `teaching'-sample the relative error of the derived quantities is nearly constant. The agreement seen there is sufficient for this range but can still be improved by Monte Carlo runs with more photons and a longer training phase. However outside the estimated scope there is little chance to improve the retrieval by better training due to the physical problem.

However, for other water types, such as the North Sea and Baltic Sea with less suspended matter and *gelbstoff* concentrations, the error is much smaller.

7.3.5 Application to Case I water

One major question of this ATBD is whether the same neural network as trained for case II water can also be used to retrieve the pigment concentration of case I water, which is water with very low concentrations of suspended matter and *gelbstoff*. For this test all cases were selected were the suspended matter concentration was below 0.06 mg/l and *gelbstoff* concentration below a(440) of 0.004 m^{-1}. Fig. 10 shows the result of this test. One can clearly sea that the NN responds linearly and with an acceptable error over the full concentration range of 4 decades, i.e. pigment concentration from 0.003 - 50 µg/l, which was used for training. Consequently, the same network can be used for case I and case II waters, provided that the inherent optical properties of phytoplankton in case I and case II areas are the same.

Copyright © 1997 SCICON.

Titel:
Autor:
ErstellDatum:

Fig. 10 Input and NN derived concentration of phytoplankton pigment for Case I water

7.3.6 Typical concentrations for North Sea water

The results for typical concentrations of the North Sea are given in fig. 11 -13.

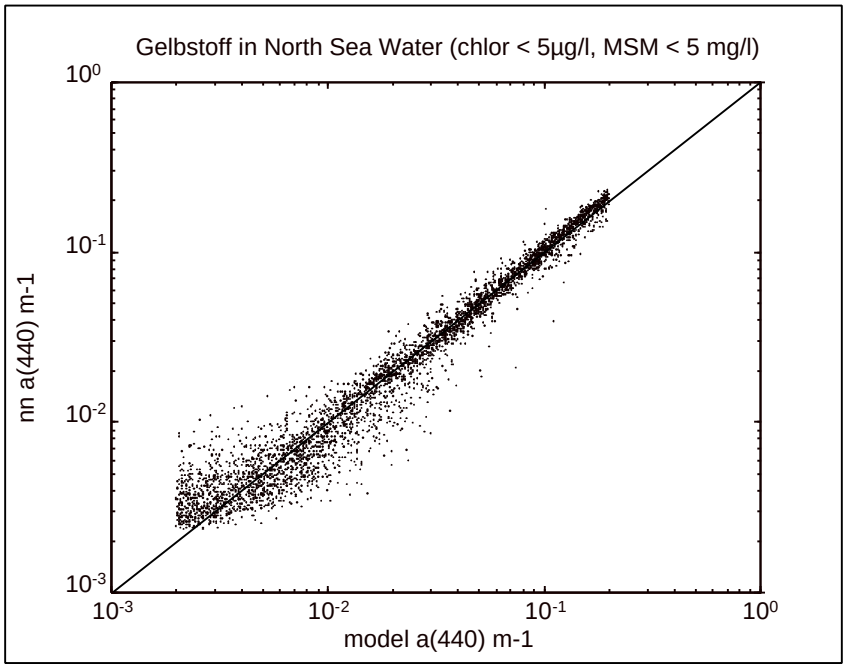

Fig. 11 Input and NN derived concentration of *gelbstoff* for typical north Sea water

Copyright © 1997 SCICON.

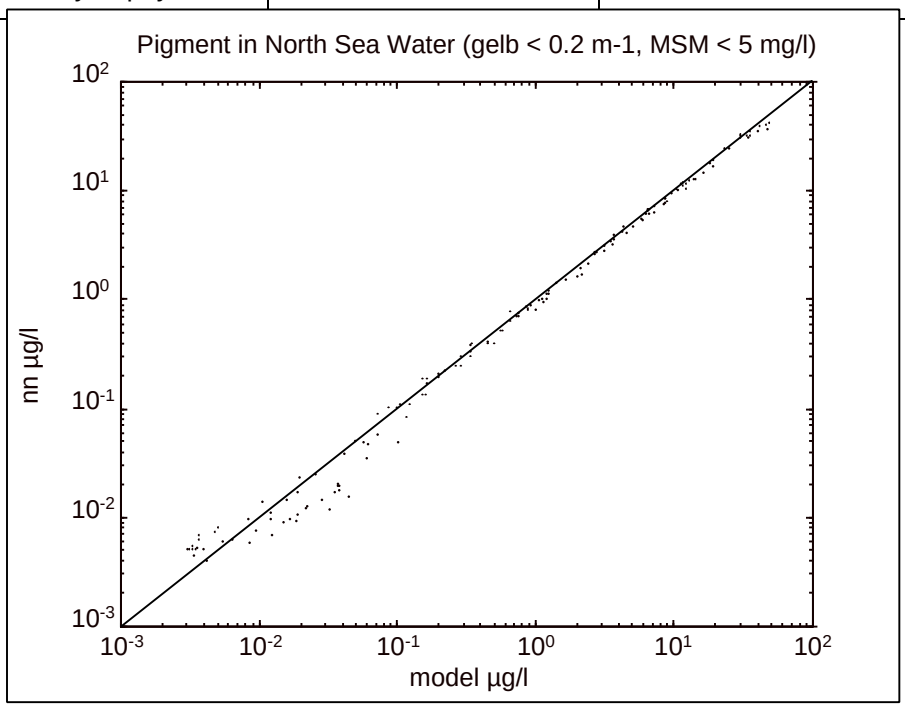

Fig. 12 Input and NN derived concentration of phytoplankton pigment (chlorophyll a) for typical North Sea water

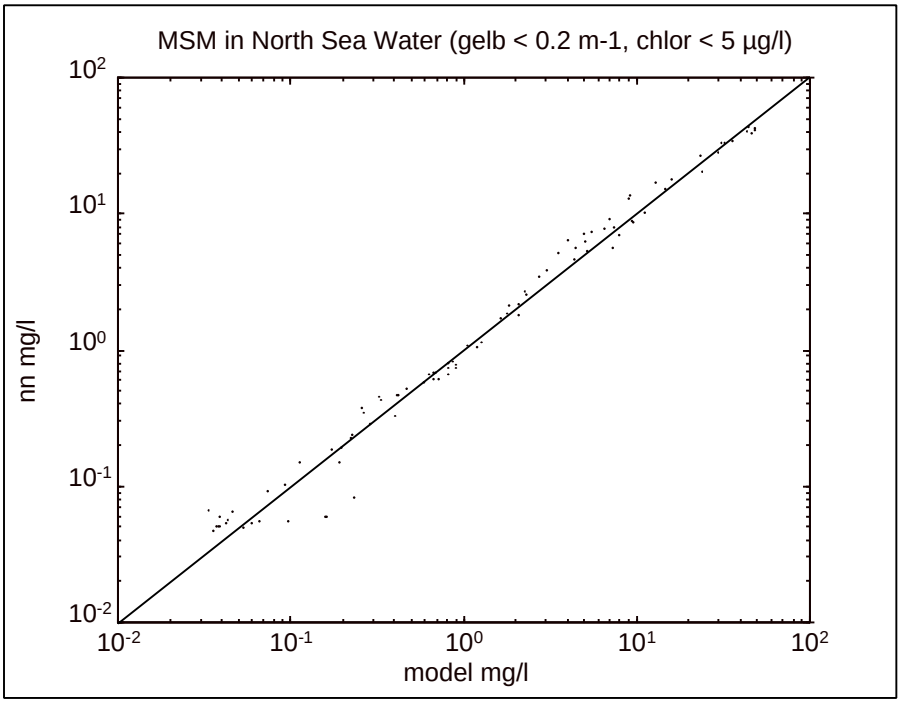

Fig. 13 Input and NN derived concentration of mineralic suspended matter for typical North Sea water

Copyright © 1997 SCICON.

7.3.7 Robustness against random errors of the input

A further important question is if the ffNN inversion method is robust against errors in the input, i.e. the reflectances. Two types of error tests have been performed.

In the first test series, the simulated MERIS test spectrum was changed by multiplying the whole spectrum with a N(1, 0.01)-distributed random number. In the second test series, the reflectance of each channel was multiplied with a N(1, 0.01)-distributed random number independently. For each test the spectrum was modified 500 times.

The envelope of the spectrum, which have been modified in total is given in fig. 14, the results of the error test in fig. 15-17. The results show that the output error (i.e. in terms of concentration) is very close to the input error for pigment and *gelbstoff*. However, since the algorithm concerning the suspended matter part is sensitive against the height of the reflectance of all channels, the variance of the output is large for suspended matter. The spectra where the channels were distributed independently are shown in fig. 18. The resulting concentration distributions for *gelbstoff* and pigments are given in fig. 19-20. We conclude that the stability of the approximating ffNN and its ability to interpolate is very high.

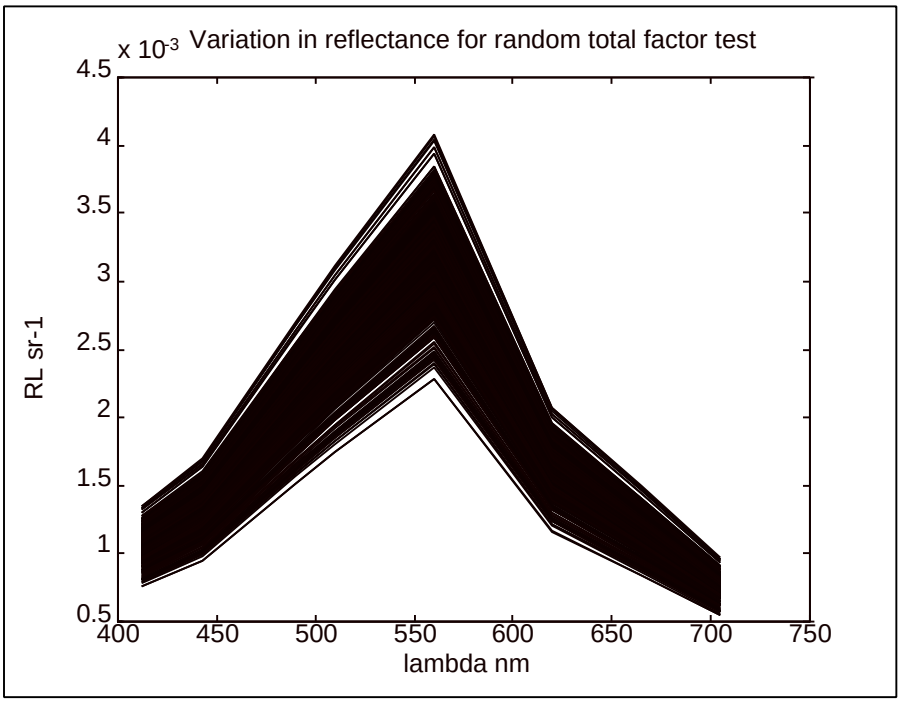

Fig. 14 Variation of reflectance spectra produced by multiplying the whole spectrum with a N(1, 0.01)-distributedrandom number. Target concentration for chlorophyll is 4 µg/l, NSP 2 mg/l and *gelbstoff* absorption at 440 nm of 0.5 m^{-1}.

Copyright © 1997 SCICON.

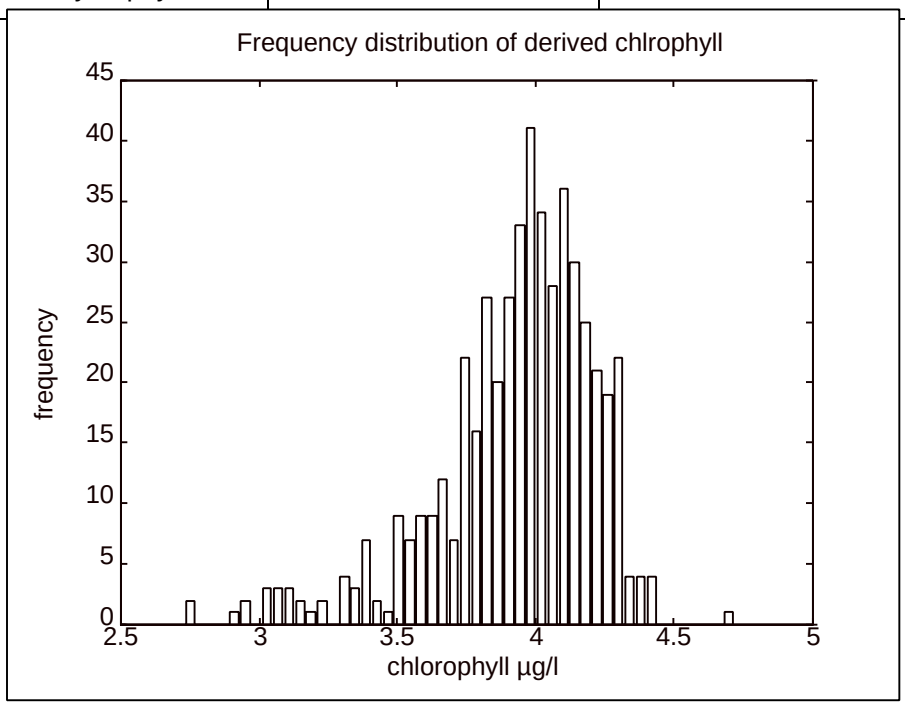

Fig. 15 Output error for chlorophyll caused by reflectances with a noise of 10%

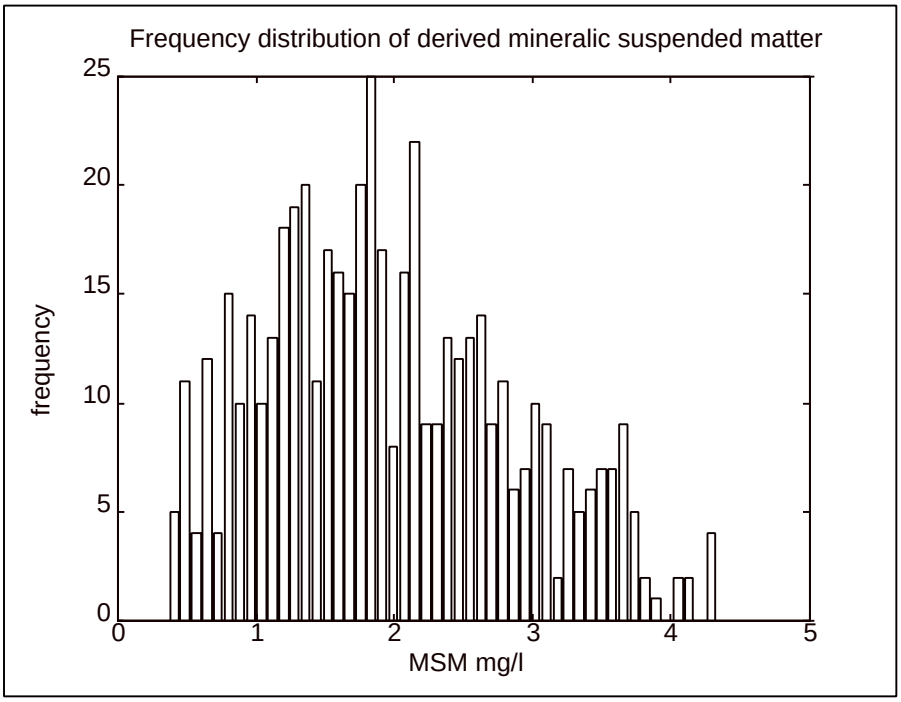

Fig. 16 Output error for suspended matter caused by reflectances with a noise of 10%

Copyright © 1997 SCICON.

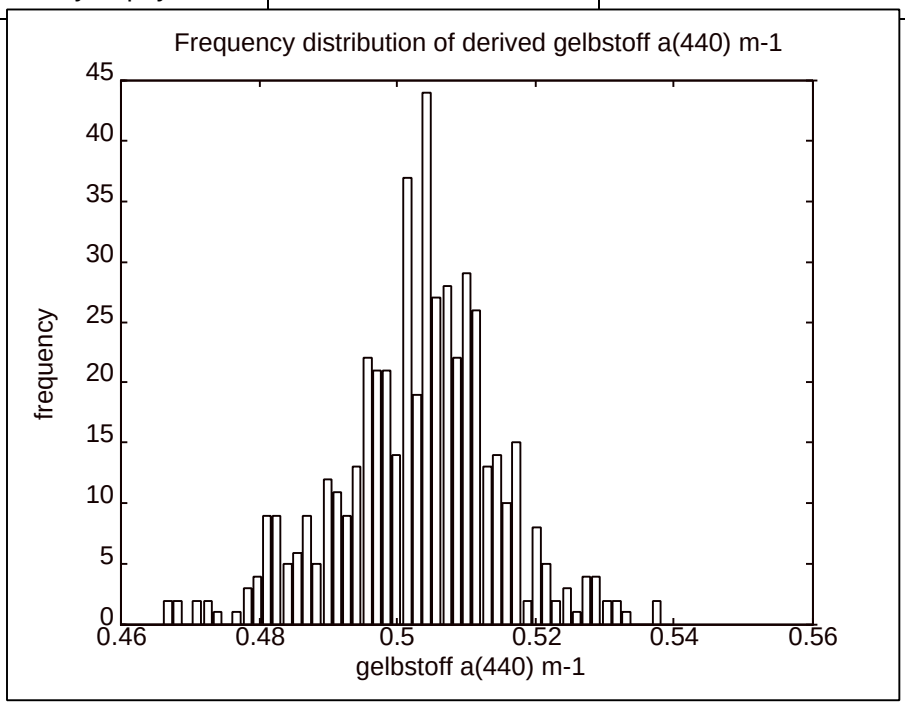

Fig. 17 Output error for *gelbstoff* caused by reflectances with a noise of 10%

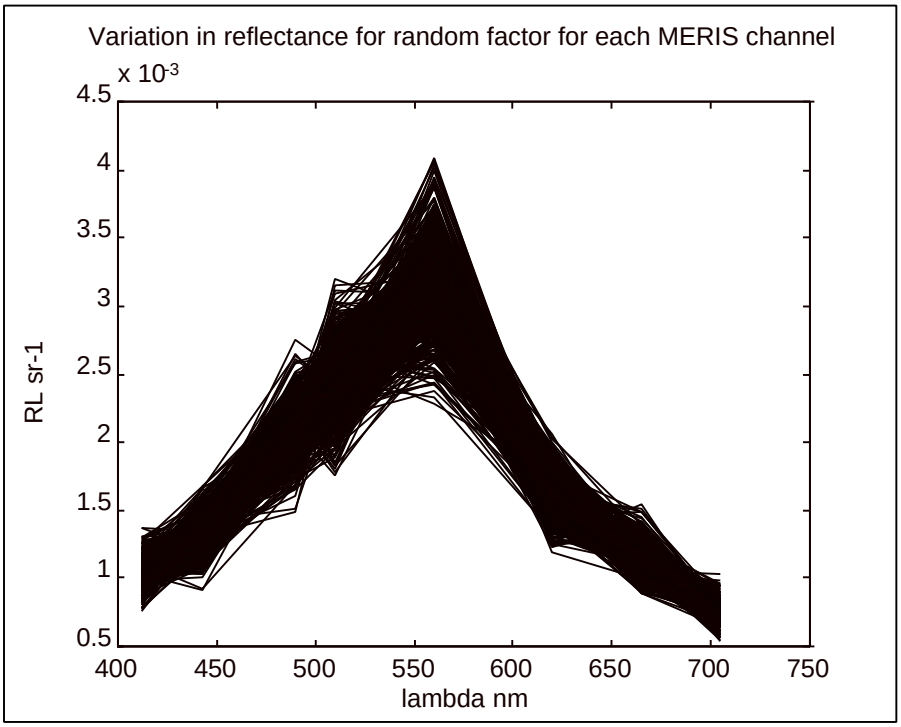

Fig. 18 Variation of the spectrum with random noise (standard deviation 10% of reflectance) independent for each channel

Copyright © 1997 SCICON.

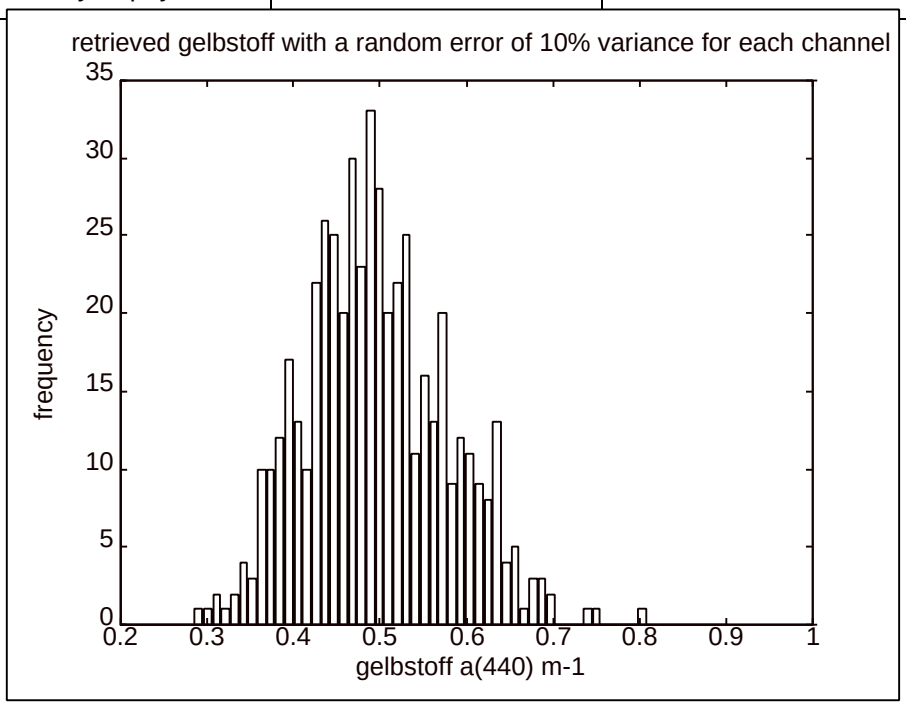

Fig. 19 Result for *gelbstoff*, target concentration is a(440nm) of 0.5 m^{-1}

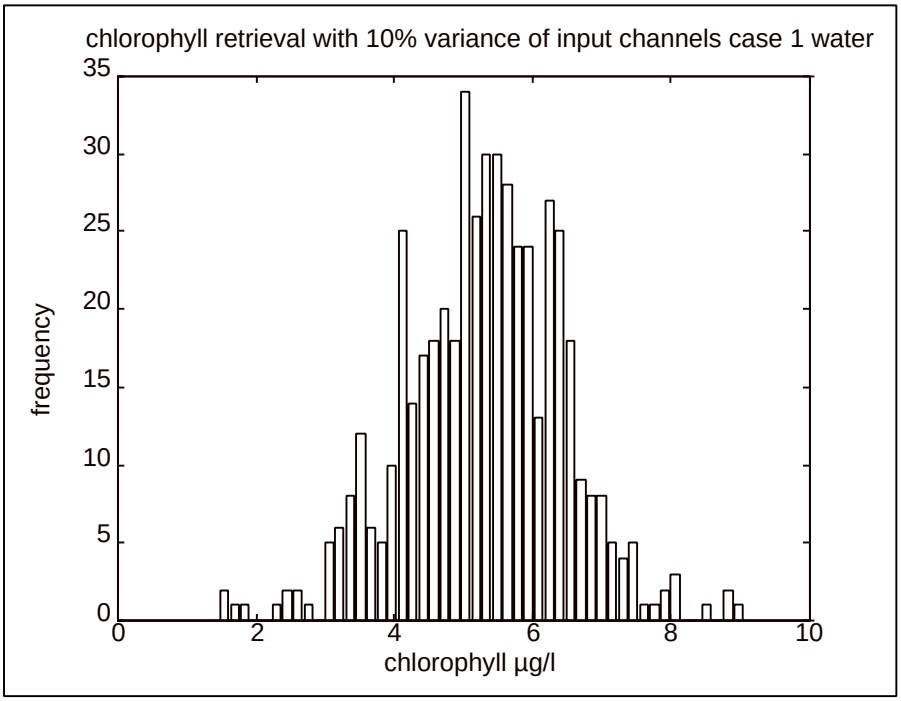

Fig. 20 Result for chlorophyll with a target concentration of 5.8 µg/l

Copyright © 1997 SCICON.

7.4 Practical Consideration

This part of the ATBD describes practical considerations for implementing the ffNN inverse modelling approach for mass production. The whole problem can be divided in the following parts:

1. Determination of the specific optical properties for different coastal areas and/or seasons.
2. Construction of a Neural Network for global application and, in addition as an option, special NN's for different areas and seasons resulting in a library of subroutines.
3. Test of the NN.
4. Implementation of the NN into the evaluation procedure, which requires the calculation of the water leaving radiance reflectances.

7.4.1 Programming and Procedural Considerations

One important step is the construction of the ffNN by training resulting in a subroutine (output in C-language) for implementation in the evaluation procedure. The training program we used is the Stuttgart Neural Network Simulator, version 3.1. During this training phase the scope of the algorithm is determined. It depends on the chosen range of concentration and the intervals as well as the number and nature of independent variables. The test, as shown above, provides the possibility to restrict the scope for a defined acceptable error for different water cases. With present available workstations the training phase is rather time consuming (see above). But since the training has to be performed only once, this part of the work is comparable small compared to the time used for mass production. Future computer systems will allow a much faster training. Because the high number of entries for the training we have selected for the first issue a simple radiative transfer model. The application of more sophisticated and thus more accurate models such as developed in this issue requires more computational effort. However, the runtime of the ffNN is independent of the complexity of the training model.

7.4.2 Computational effort

The calculation of the data set for training and testing of the NN and the training phase itself is the most time consuming part of the procedure. The MC model version used for this ATBD required about 10 - 12 minutes per MC run on a SUN ULTRA SPARC I or a PENTIUM 166 MHZ PC, from which 5 spectra with different viewing directions were computed. For the training of the NN about 12000 MC runs with 60 000 spectra were produced, 20% of these cases were used for testing, i.e. the production of the table costs about 1800 - 2000 hours, corresponding to about 80 days. Since we used about 15 workstations for this task running in the background, the time reduced to 1 week for producing the tables. Another week of computing time was necessary for training the NN (3 workstations used in parallel).

The emulation of the inverse model by the NN is very fast: 10^6 calls (corresponding to pixels, image with 1000 * 1000 cloud free water pixels) spent about 2 minutes at a SUN ULTRA SPARC 1. The ffNN is about 10^6 times faster than the forward model. It must be mentioned that the time needed by the ffNN is independent from the model; it would not be larger even if the model to be inverted includes more processes such as fluorescence or polarisation). The accuracy and the speed of the ffNN allow its operational usage. However, more sophisticated models need more computational effort for calculating the training set. Since the training has

Copyright © 1997 SCICON.

to be performed only once or whenever an update is necessary due to improved knowledge or regional aspects the training time is of minor importance. A retraining of the NN such as for other optical properties requires significantly less computations.

7.4.3 Calibration, Initialisation, and Validation

The main requirement is the knowledge of the specific optical properties of water constituents. These have to be determined by laboratory and field measurements. The validation of remotely sensed data of coastal waters is rather difficult because of the high dynamics. A direct comparison between the results of individual pixels and water samples is only possible in waters with low exchange rates. Another possibility is to use ship-borne measurements of radiance spectra to test the inverse modelling procedure.

Data of the specific optical properties have to be sampled in different areas in order to build a mean ffNN representing a mean coastal water and the library of regional adapted ffNNs.

7.4.4 Quality Control and Diagnostics

As proposed in the theoretical part, we propose to test the result of the ffNN inverse modelling on a random basis or whenever changes in the water mass occurs by using the resulting concentrations in a forward model and then compare the model reflectances with the measured. Furthermore, the inverse modelling procedure can be analysed with respect to its error behaviour for various compositions of water constituents. It has been shown, that the accuracy of the retrieval of one substance depends very much on the concentrations of the other constituents. The accuracy and thus the scope of the algorithm for a given type of water will be predicted by model calculations.

7.4.5 Operational runtime checks of the ffNN

In the operational usage of the ffNN one should plan to check the results regularly by using the calculated concentrations as input of a forward model. The resulting reflectances should be in agreement with the measured reflectances. Deviations could arise e.g. when the water constituents have optical properties not included in the model at the time of construction and training of the ffNN. Then the reflectances measured by the satellite when given to the ffNN still would result in some concentrations. But reflectances calculated by the model using these concentrations as input will disagree with those measured. This check should be made outside the normal production stream, since it requires time consuming forward calculations.

The procedure would include two steps:

1. use the concentrations c_{NN} obtained by the ffNN from r_{meas}. as input to the model to calculate r_{Mod} .
2. if $(r_{meas} - r_{Mod})^2$ exceeds a prescribed threshold flag the results of the region as invalid.

7.4.6 Exception Handling

The input (reflectances, angles) and output (concentrations) of the routine are checked if they are within the range used for the generation of the training table. This check is included in the NN subroutine which contains the lower and upper limits of all variables of the training set. If one of the input or output variables is outside its range, an error code is set which identifies the variables which are outside. It should be used to flag this pixel with the "out of scope flag".

Copyright © 1997 SCICON.

A further enhancement of this procedure could consider the concentrations of all three substances. If for the concentration of one substance the concentration of one of the other substance is too high to give a result within the acceptable error range, an additional warning flag "out of error range" could be set. Although the realisation of this feature is not difficult, it is implemented only as a dummy in the present version, before a detailed error study has been made.

7.4.7 Regional differences

In this study the model was used with optical parameters for suspended matter etc. which are very general. In order to improve the described method for specific areas a regionalization will be necessary. Obviously one needs the optical parameters of the water constituents for the different regions of interest. Then for these regions the function or subroutine representing the ffNN can be constructed as described above by retraining the net (which much less training time than used for the original net). It would be possible to set up a library with a standard ffNN subroutine and dedicated ffNN routines for different coastal regions of the world and then, whenever an image covers the region, the specific subroutine is selected. One could either use a general ffNN-procedure which reads a file with the net-parameters for the region in question or one could switch between different ffNN's with built-in-parameters.

7.4.8 Data Dependencies

The data required for the procedure are:

- specific optical properties of water constituents (absorption and scattering coefficients, phase functions of phytoplankton and suspended matter)
- typical mean spectral properties of the atmosphere (only for calculating the downwelling radiance distribution at the surface)
- Input to the procedure are: the water leaving radiance reflectances of 8 MERIS bands at the following central wavelengths 412, 442, 490, 510, 560, 620, 665, 705 nm, the viewing and solar zenith angle and the difference between the azimuth of the solar and viewing direction.
- ancillary data as listed in chapter 4.2.2.
- Flags: shallow water, sun glitter

7.4.9 Dependencies on other procedures

The algorithms depends on an atmospheric correction routine which converts TOA reflectances into water leaving radiance reflectances. Issue 3 of the ATBD will include the atmospheric correction part.

7.4.10 Output Products

The output products of this algorithm are:

- concentration of phytoplankton pigment [µg/l]
- concentration non-absorbing suspended matter [mg/l]
- *gelbstoff* absorption *a(440 nm)* [m^{-1}]

Copyright © 1997 SCICON.

- an error code, if one of the input variables or the retrieved concentrations is outside the range of the training table or is outside the acceptable error. The code identifies these variables.
- optional signal depth and or depth of euphotic zone [m].

a further variable which can be computed is the organic part of the suspended matter [%]. However, this requires additional sensitivity studies and the definition of its specific optical properties.

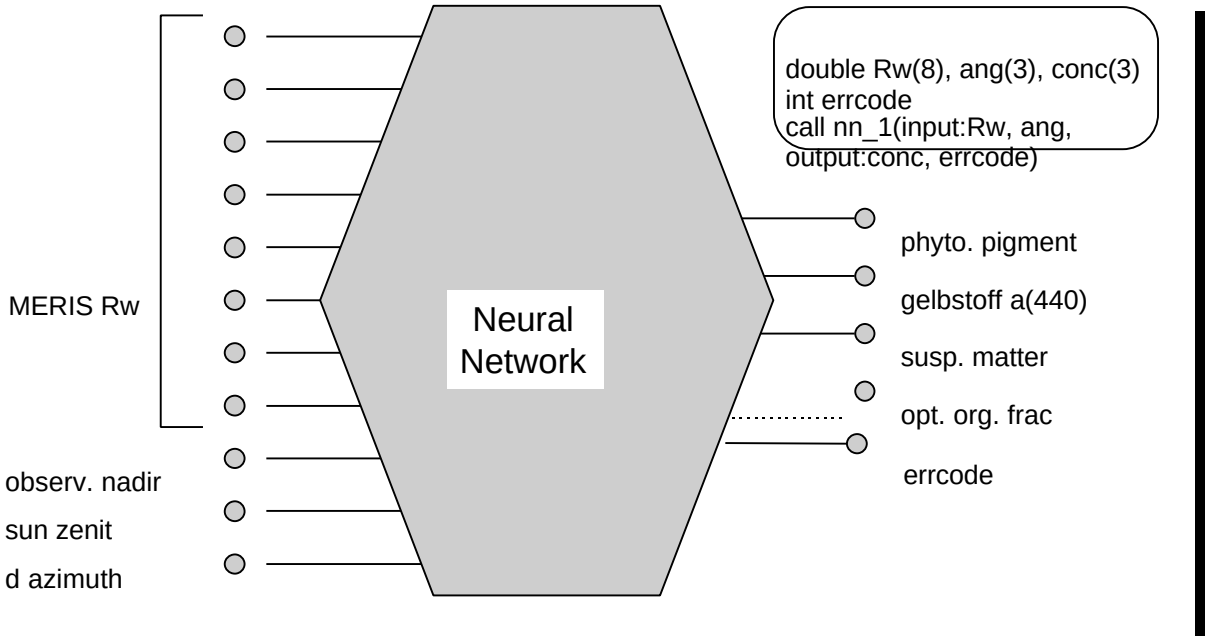

8. Assumptions and Constraints

The present version of the ffNN inverse modelling approach has the following assumptions and constraints:

- the atmospheric correction is not included. In some very turbid waters the atmospheric path radiance may not be determined independently from the retrieval of the substances.
- Polarisation, fluorescence of phytoplankton and *gelbstoff* and Raman scattering are not included.
- The wave slope distribution is assumed to be isotropic with respect to the azimuth angle.

9. Test and validation of the procedure

The final preparation of the algorithm requires extensive sensitivity studies in particular with respect to the three components which represent actual water constituents. Furthermore the algorithm has to be validated with simulated and real data. A detailed validation plan is given in Appendix B.

Copyright © 1997 SCICON.

9.1 Test of the Monte Carlo Model

The model is tested by using the canonical test cases for hydro-optical models as described in Mobley et al. (1993). These tests were applied to a number of different models including Monte Carlo, Variance Imbedding and Matrix Operator Models. The following tests are applied to the MC model used here:

- test 1: pure Rayleigh scattering water with an ω_0 of 0.2 and 0.9, no atmosphere, flat surface
- test 2: suspended matter scattering with an ω_0 of 0.2 and 0.9, no atmosphere, flat surface
- test 4: as test 2 with ω_0 of 0.9, but with atmosphere
- test 5: as test 2 with ω_0 of 0.9,but with rough sea surface, solar zenith angle 80^o

In addition the radiance distribution was compared , as given in Fig. 8 of Mobley et al.(1993) for the upward directed radiance hemisphere for problem 2.

All test were passed, results were within the deviations between the models as published in the test report.

9.2 Test of the Neural Network

The neural network is tested with a test data set which is independent from the training data set. More than 11000 different constellations of concentrations and angles have been used and applied to the NN. The resulting concentrations have been compared with the concentrations used to model the water leaving radiance reflectances (s. results above).

The error behaviour is tested by modifying the specific optical properties for each channel independently as well as altogether according to a Gaussian noise curve.

9.3 Test with real data

Radiance measurements from a ship and low flying aircraft will be used to test the procedure. This data for the MERIS channels is available at GKSS from various flights and cruises in the North Sea. However, the inherent optical properties of the water constituents of the test area have to be known. One further possibility for such a test is the COASTLOOK data set, expected by 1998.

10. Future Actions

For improving the present ffNN inverse modelling version the following investigations, developments and tests are necessary:

- Improvement of the forward calculations (reduction of statistical errors, particularly for the test cases)
- Improvement of the model by including polarisation and inelastic scattering
- Detailed error analysis of the model for MERIS
- Definition of the scope of the algorithm for different water cases
- Atmospheric correction using NN techniques as for the retrieval of water constituents

Copyright © 1997 SCICON.

- Mixing factor between different aerosols as another independent variable for improvement of the imbedded atmospheric correction
- Analysis of the effects of cirrus clouds in addition to aerosols
- Set-up of a data bank of specific optical properties for different coastal regions, partly by regional networks.
- Validation of the procedure using MERIS data simulated with aircraft data or from other satellites (MOS and SeaWiFS are now available).

11.

Copyright © 1997 SCICON.

12. References

ACRI (1996): Specifications for Case II coastal water reference model. Doc. No. PO-TN-MEL-GS-0016. (23 July 1996), (ACRI, 260, Route du Pin Montard, B.P. 234, 06904 Sophia Antipolis Cedex, France)

Buckton,Daniel; Danaher,Seán; O'Mongain,Eon (1995): Simulation of the MERIS instrument and constituent estimation. SPIE 2586(Global process monitoring and remote sensing of the ocean and sea ice), 12.

Cox,C; Munk,W (1954): Some problems in optical oceanography. J. Mar. Res. 14, 63-78.

Cox,C; Munk,W (1954): Statistics of the sea surface derived from sun glitter. J. Mar. Res. 13, 198-227.

Doerffer,Roland (1979): Untersuchungen über die Verteilung oberflächennaher Substanzen im Elbe-Aestuar mit Hilfe von Fernmeßverfahren. Arch. Hydrobiol. Suppl. 43 Elbe-Aestuar 4 2/3, 119-224.

Doerffer,Roland (1992): Imaging spectroscopy for detection of chlorophyll and suspended matter. In: Imaging spectroscopy: fundamentals and prospective applications. (Eds: Toselli,F; Bodechtel,J) ECSC, EEC, EAEC (Kluwer), Brussels and Luxembourg, 215-257.

Doerffer,Roland; Fischer,Jürgen (1994): Concentrations of chlorophyll, suspended matter, and *gelbstoff* in case II waters derived from satellite coastal zone color scanner data with inverse modeling methods. Journal Geophysical Research 99(C4, 15 April), 7457-7466.

Doerffer,Roland; Schiller,Helmut (1994): Inverse modeling for retrieval of ocean color parameters in case II coastal waters - an analysis of the minimum error. SPIE 2258(Ocean Optics XII), 887-893.

Elterman,L (1968): UV, visible, and IR attenuation for altitudes to 50 km. Environmental Research Papers ed. Vol. N° 285, AFCRL-68-0153. Airforce Cambridge Research Laboratories, Cambridge, USA. 49 pages.

Fischer,Jürgen (1984): Remote Sensing of Suspended Matter, phytoplankton and yellow substances over coastal waters, 1, aircraft measurements. Mitt. Geol. Palaeontol.Inst. Univ. Hamburg 55, 85 pp.

Fischer,Jürgen; Doerffer,Roland (1987): An inverse technique for remote detection of suspended matter, phytoplankton and yellow substances from CZCS measurements. Adv. Space Res. 7(2), 21-26.

Fischer,Jürgen; Graßl,Hartmut (1984): Radiative transfer in an atmosphere-ocean system: an azimuthally dependent matrix-operator-approach. Applied Optics 23, 1032.

GKSS (1994): MERIS data simulation using ROSIS flight data. ESA Contract AOP/WK/316601 ed. GKSS Forschungszentrum, 21502 Geesthacht.

Gordon,Howard R (1994): Modelling and simulating radiative transfer in the ocean. In: Ocean Optics. (Eds: Spinrad,Richard W; Carder,Kendall L; Perry,Mary Jane) Oxford University Press, Oxford, 3-39.

Gordon,Howard R; Morel,André (1983): Remote assessment of ocean color for interpretation

Copyright © 1997 SCICON.

of satellite visible imagery. A review. (Lecture notes on coastal and estuarine studies.) Springer Verlag, New York, Berlin.

Jain,SC; Miller,JR (1976): Subsurface water parameters: optimization approach to their determination from remotely sensed water color data. Applied Optics 15, 886-890.

Kalle,Kurt (1949): Fluoreszenz und *Gelbstoff* im Bottnischen und Finnischen Meerbusen. Dtsch. Hydrogr. Z. 2, 117-124.

Kronfeld,Ulrike (1988): Die optischen Eigenschaften der ozeanischen Schwebstoffe und ihre Bedeutung für die Fernerkundung von Phytoplankton. Ph.D. Dissertation, GKSS Report 88/E/40, GKSS Forschungszentrum, 21502 Geesthacht, Germany. 159 p.

Mobley,Curtis D (1994): Light and Water, Radiative Transfer in Natural Waters. Academic Press, San Diego.

Mobley,Curtis D; Gentili,Bernard; Gordon,Howard R; Jin,Zhonghai; Kattawar,George W; Morel,André; Reinersman,Phillip; Stamnes,Knut; Stavn,Robert H (1993): Comparison of numerical models for computing underwater light fields. Applied Optics 32(36), 7484-7504.

Morel,André; Gentili,Bernard (1991): Diffuse reflectance of oceanic waters: its dependence on Sun angle as influenced by the molecular scattering contribution. Applied Optics 30(30), 4427-4438.

Morel,André; Gentili,Bernard (1993): Diffuse reflectance of oceanic waters. II. Bidirectional aspects. Applied Optics 32(33), 6864-6879.

Nelder,JA; Mead,R (1965): A simplex method for function minimization. Comput.J. 7, 308-313.

Puls,Walter; Doerffer,Roland; Sündermann,Jürgen (1994): Numerical Simulation and Satellite Observations of Suspended Matter in the North Sea. IEEE Journal of Oceanic Engineering 19(1), 3-9.

Rumelhard,DE; Hinton,GE; Williams,RJ (1986): Learning internal representations by error propagation. In: Parallel distributed processing: explorations in the microstructure of cognition. Vol. Vol.I, Foundations. (Eds: Rumelhard,DE; McClelland,JL) The MIT Press, Cambridge, Ma, USA, 318-362.

Schiller,Helmut; Doerffer,Roland (1993): Fast computational scheme for inverse modeling of multispectral radiances: application for remote sensing of the ocean. Applied Optics 32(18, 20 June), 3280-3285.

Schiller,H; Doerffer,R (1997): Neural Network for emulation of an inverse model - operational derivation of case II water properties from MERIS data. Int. J. Remote Sensing (submitted).

Shettle,EP; Fenn,RW (1979): Models for the aerosols of the lower atmosphere and the effects of humidity variations on their optical properties. Environmental Research Papers ed. Vol. AFGL-TR-79-0214. AFGL, Hanscom, Ma., USA.

SNNS (1995): Stuttgart Neural Network Simulator, User Manual. Version 3.1.,University of Stuttgart, Institute for parallel and distributed high performance systems (anonymous ftp ftp.informatik.uni-stuttgart.de (129.69.211.2))

Copyright © 1997 SCICON.

Spitzy,A; Ittekkott,V (1986): *Gelbstoff*: an uncharacterized fraction of dissolved organic carbon. In: The influence of yellow substance on remote sensing of sea-water constituents from space. (Eds: Doerffer,Roland; Fischer,Jürgen; Graßl,Hartmut) GKSS Forschungszentrum Geesthacht, 21502 Geesthacht, Germany, 31.

World Climate Research Program (1986): A preliminary cloudless standard atmosphere for radiation computation. Vol. WCP-112, WMO/TD-N° 24. Int. Ass. for Meteor. and Atm. Phys., Radiation Commission, Geneva.

13.

Copyright © 1997 SCICON.

14. Appendix A: Example of a ffNN procedure (C - language)

14.1 Example for the usage of the NN

```
#include <stdio.h>
#include <math.h>
#include "macro_basis.c"

#define NVARS 14

#include "nnfr.c"

/* generate file to compare model input with NN output */

void
main(argc, argv)
      int             argc;
      char           *argv[];
{
      long             i, j, ndat;
      long        flagres;
      FILE           *fpin1, *fpres1;
      double           var[NVARS], out[3], dum;

      if (argc != 3) {
            fprintf(stderr, "call with model_res  to_plot\n");
            exit(-1);
      }
      if ((fpin1 = fopen(argv[1], "r")) == NULL) {
            fprintf(stderr, "%s read-open error\n", argv[1]);
            exit(-1);
      }
      if ((fpres1 = fopen(argv[2], "w")) == NULL) {
            fprintf(stderr, "%s write-open error\n", argv[2]);
            exit(-1);
      }
      ndat=57240;
      loop(i, ndat) {
            if ( (i%5) != 0 ) {
                  loop(j, NVARS) fscanf(fpin1, "%lf", &var[j]);
                  fscanf(fpin1,"%lf",&dum);
            } else {
                  loop(j, NVARS) fscanf(fpin1, "%lf", &var[j]);
                  fscanf(fpin1,"%lf",&dum);
                  nnfr(var,out,&flagres);
                  if(flagres == 0) {
                        fprintf(fpres1,"%7.3lf %7.3lf %7.3lf %7.3lf %7.3lf
%7.3lf\n",
                              var[11],var[12],var[13],
                              out[0], out[1], out[2]);
                  } else {
                        printf("flagres=%ld\n",flagres);
                  }
            }
      }
}
```

Copyright © 1997 SCICON.

14.2 Example of the subroutine which checks the errors and calls the NN generator

```
#include "50x12.202.c" /* this is the nn routine generated by the training
run */

void nnfr(double *nn_in,double *nn_out,long *flag)
/*
      nn_in input to NN:
            0     sun_theta   rad
            1     view_theta  rad
            2     view_phi    rad
            3-10  reflectances

      nn_out result from NN:
            0     conc. chlorophyll mug/l
            1     conc. gelbstoff         a(440 nm) m^-1
            2     conc. susp. matter      mg/l

      *flag indicates problems:
            0     no problem
            bit 1 nn_in[0]<loinp[0]
            bit 2 nn_in[0]>hiinp[0]
            bit 3 nn_in[1]<loinp[1]
            bit 4 nn_in[1]>hiinp[1]
            .....
            bit 21      nn_in[10]<loinp[10]
            bit 22      nn_in[10]>hiinp[10]

            bit 23      nn_out[0]<lores[0]
            bit 24      nn_out[0]>hires[0]
            .....
            bit 27      nn_out[2]<lores[2]
            bit 28      nn_out[2]>hires[2]

following three bits are presently not used, but for future version can be
used for flagging out of error range as output parameter

            bit 29      nn_out[0] res[0] out of error range
            bit 30      nn_out[1] res[1] out of error range
            bit 31      nn_out[2] res[2] out of error range
*/
{
      double loinp[11]={      0.000574,0.000000,0.000141,0.000052,
                        0.000061,0.000076,0.000086,0.000108,
                        0.000068,0.000049,0.000023    };
      double hiinp[11]={      1.309000,0.715600,3.142000,0.172700,
                        0.178200,0.159300,0.124200,0.084930,
                        0.025000,0.016750,0.008868    };
      double lores[3] ={      0.003006,0.002001,0.030017    };
      double hires[3] ={      49.84908,1.999906,49.89895    };
      long i, fl;

      (*flag)=0;
      fl=1;
      for(i=0;i<11;i++) {
            if(nn_in[i]<loinp[i]) (*flag)+=fl;
            fl*=2;
            if(nn_in[i]>hiinp[i]) (*flag)+=fl;
            fl*=2;
      }
```

Copyright © 1997 SCICON.

```
      nn_calculate(nn_in, nn_out);

      for(i=0;i<3;i++) {
            nn_out[i]=exp(nn_out[i]);
            if(nn_out[i]<lores[i]) (*flag)+=fl;
            fl*=2;
            if(nn_out[i]>hires[i]) (*flag)+=fl;
            fl*=2;
      }

}
```

14.3 Example of a subroutine produced by the NN generator

(only first and last sections of the function are given)

```
#define NEURON_FL double
#include <math.h>
void nn_calculate(in,out) NEURON_FL *in, *out;
/* generated from 50x12.202.neted and mcrange.res */
{
  NEURON_FL out1;
  NEURON_FL out2;
  NEURON_FL out3;
.
.
.
  NEURON_FL out72;
  NEURON_FL out73;
  NEURON_FL sum;

  out1=(in[0]-0.000574)*0.764277;
  out2=(in[1]-0.000000)*1.397429;
  out3=(in[2]-0.000141)*0.318283;
  out4=(in[3]-0.000052)*5.792132;
.
.
.
.
+out72*(9.918880)
     +out73*(0.329040)
     ;
  out[1]=-6.214000+6.907100/(1.0+exp(-(-1.182050+sum)));
  sum=out62*(0.078510)
     +out63*(-3.247670)
     +out64*(4.673970)
     +out65*(-1.852820)
     +out66*(2.711750)
     +out67*(-1.967490)
     +out68*(0.022500)
     +out69*(2.033660)
     +out70*(2.069980)
     +out71*(-2.124820)
     +out72*(3.086220)
     +out73*(-0.428700)
     ;
  out[2]=-3.506000+7.418000/(1.0+exp(-(0.798560+sum)));
}
```

Copyright © 1997 SCICON.

15.

Copyright © 1997 SCICON.

16. Appendix B: Validation Plan for case II water algorithm

Validation Plan for the Case II water IMT-NN algorithm for the retrieval of water constituent concentrations from MERIS water leaving reflectance data

Roland Doerffer

GKSS

21. November 1997

Version 0.1

- Draft -

16.1 Reference Documents

RD5. Specification for Case II Coastal Water Reference Model, PO-TN-MEL-GS-0016

RD6. Algorithm Theoretical Basis Document, PO-TN-MEL-GS-0005

16.2 Introduction

One major part of the development of a case II water algorithm for the Medium Resolution Imaging Spectrometer MERIS is the algorithm validation. It will prove if the theory and the model, on which the algorithm is based, is correct and it will demonstrate how the algorithm performs under various simulated and measured conditions. The result of the validation will be used to set up an error budget and to define the scope of the algorithm. This information will enable the user of the data to assess under which conditions he can expect results with an acceptable error and which conditions he has to check when using MERIS data of case II water. Furthermore, the algorithm should indicate conditions which are out of its scope.

The results of the validation will be documented in the Algorithm Validation document (AVD).

16.3 Basic Scope of the Algorithm

The case II water algorithm (RD6) is based on a water model which was defined to represent a mean global case II water (RD5). Because it is known that such mean optical properties do not exist and that coastal waters include a large range of different constituents with different optical properties which deviate significantly from these mean properties, it was decided to represent case II water by three components which are not necessarily identical with real substances. These components are:

- pure sea water
- mean global phytoplankton pigment
- a scattering component to represent any suspended matter

Copyright © 1997 SCICON.

- absorbing component, to represent *gelbstoff* and the absorbing organic component of suspended matter (organic detritus)

The validation of the algorithm has to demonstrate if these components represent the main three optical classes of sea water constituents (phytoplankton, suspended matter (SPM) and *gelbstoff*) in a proper way and if the derived concentrations can be related to the actual concentrations.

Conversion factors between scattering or absorption and concentration units have been used to provide concentrations in the data product rather than optical units. However, it may be necessary for the user to recalculate the concentrations with other conversion factors depending on his local conditions.

Furthermore, the scope of the algorithm is defined by:

- deep ocean (water depth >> signal depth z90 at spectral channel with minimum attenuation)
- homogenous vertical distribution
- homogenous horizontal distribution within one pixel
- neglectable influence due to inelastic scatting (fluorescence, Raman scattering)

16.4 Validation

16.4.1 Validation with simulated data

Simulated water leaving radiance reflectances which are based on the same model as used for training are the only test data which are strictly within the scope of the algorithm. Furthermore they provide the possibility to simulate well defined errors and study the sensitivity of the algorithm. The following tests will be performed:

16.4.1.1 Sensitivity to reflectance errors

Errors in reflectances (random per channel and random per total spectrum) will be simulated and tested

16.4.1.2 Sensitivity to geometry

Random errors in viewing geometry will be simulated and tested

16.4.1.3 Sensitivity to wind

The directional water leaving radiance reflectance is computed for training for "standard" ocean and atmosphere conditions including a rough water surface at wind speed of 7 m/s. The roughness of the sea surface is based on the Cox and Munk model for wave slope distribution. The sensitivity for different wind speeds will be studied using radiative transfer simulations computed for different wind speeds for typical case I and case II water conditions.

Copyright © 1997 SCICON.

16.4.1.4 Sensitivity to IOP

The algorithm will be tested with simulated water leaving radiance reflectances which are based on the specific optical properties as determined from COASTLOOC and similar data sets of the Mediterranean Sea and the North Sea.

16.4.2 Validation with field measurements

Water leaving radiance reflectances will be determined from radiance spectra measured from above the water surface. Since the water leaving radiance and the water leaving radiance reflectance can not be measured directly, the following measurements will be performed for each sample:

The water surface radiance (Lwr) is measured from above the water surface under an angle with minimum sky and sun glitter (20 degree off nadir, azimuth opposite to sun). Since this measurement includes the radiance which leaves the water body and the specularly reflected skylight, the radiance of that piece of sky (Lsky) is measured which is reflected by the water surface into the sensor. Subtracting this sky radiance using a specular reflectance of 0.02 the water leaving radiance can be computed (Lw = Lwr-Lsky*0.02). Third measurement is the radiance of a calibrated spectralon reflection plate (Lref), which represents the downwelling irradiance (direct sun and sky light) when multiplied by PI.

The water leaving radiance reflectance is then determined from these three measurements as:

$$Lwr = (Lwat-Lsky*0.02)/(Lref*PI)$$

These water leaving radiance reflectances will be used as test spectra for the neural network. The concentrations derived from simultaneously taken water samples will be compared with the result of the NN routine.

Prerequisite for these measurements are cloud-free sky conditions, a sun elevation > 20 degree and a wind speed of < 4 m/s.

16.4.3 Validation with airborne measurments

Radiance spectra measured from an aircraft flying in low altitude (150 - 300 m) will be used to test if the three groups of substances can be separated in a proper way under realistic conditions of case II water. The flight transects will follow the salinity gradient from the coast to the open sea to meet various water bodies with high and low concentrations of each constituent. The data will be corrected for Rayleigh scattering of the atmosphere. Although single spectra cannot be validated directly by in situ measurements, the concentration profile along the transect can be compared with the known horizontal distribution of substances in the German Bight: *gelbstoff* follows a gradient from the Elbe estuary into the North Sea which corresponds inversely to the gradient in salinity; concentration of suspended matter is high in the estuary and above shallow areas (reflects the topography) and phytoplankton pigment is variable and independent from the distribution of the two other groups.

The flights will be performed preferably during MOS overflight in order to check the atmospheric correction of MOS radiances.

Copyright © 1997 SCICON.

Prerequisites are a cloudless atmosphere and a low aerosol content (horizontal visibility > 20 km).

16.4.4 Validation with MOS data

The imaging spectrometer MOS offers the opportunity to test MERIS algorithms, because it has similar spectral bands and with 500 m a similar pixel size. MOS flies on board the Indian Earth observation satellite IRSP3; it was designed and is operated by the German Aerospace Centre (DLR). Different are the swath width with only +- 7 degrees and the bands in the near infrared range.

Since only level 1b data are provided by DLR, it is necessary to apply an atmospheric correction procedure prior to the test of the case II water algorithm. Presently an atmospheric correction algorithm is under development at GKSS under contract from ESRIN. As soon as this algorithm is available and tested, water leaving radiance reflectance data of MOS can be provided for testing the case II water algorithm.

For the retrieval of water constituents MOS bands 1-6 will be applied. Band 7 (650 nm) has an offset error which occurrence cannot be predicted and, thus, be corrected.

16.5 Out of scope tests

The neural network case II water algorithm includes a test which proves if the incoming reflectances and computed concentrations are within the range which was used for training the net. An out of training range flag is set, when either a reflectance or a concentration value is outside this range. This flag will be tested by using simulated data which are out of the training range and with real data (shipborne, airborne, MOS) which include exceptional conditions such as exceptional plankton blooms (red tides).

16.6 Determination of Errors

The error of the concentration of a water constituent derived from remote sensing data depends on mainly four conditions:

1. Agreement between the water model and the actual conditions, in particular concerning the following:

- The model components represent the actual composition of water constituents,
- Specific inherent optical properties of water constituents,
- Vertical and horizontal within-pixel distribution is homogenous,
- Water depth >> signal depth (reflectance by sea bottom can be neglected),
- No floating substances including foam.

2. concentration of other water constituents which are described in the model
3. accuracy of the input data, i.e. the water leaving radiance reflectances, which depends on instrumental errors and errors in atmospheric correction.
4. Accuracy and sensitivity of the neural network

Copyright © 1997 SCICON.

Any deviations summarized under (1) may lead not only to quantitative errors but also to errors with respect to a correct identification of a substance (e.g. suspended matter is interpreted as phytoplankton). Thus, the user has to verify for his area the conditions described under "Scope of algorithm". He has to characterize his area with respect to water depth, typical optical depth, typical vertical distribution, within-pixel patchiness, typical specific optical properties and compare with model assumptions.

However, during the validation, the sensitivity of the algorithm against these conditions will be tested for some European areas which, however, represent already a wide range of possible conditions.

The errors induced by 2-3 will be determined by a systematic test using simulated errors. This minimum error of the algorithm will be defined by using the test data set. It is computed with the same Monte Carlo code and parameters as used for the training set with random polls of concentrations from the test range.

16.7 Determination of the Scope of Algorithm

The scope of the algorithm is mainly defined by the water model which is used for the forward radiative tranfer calculations to compute the training table. Strictly, any deviations from this model produce a condition which is out of scope. However, since a certain error will be tolerated by the algorithm, the scope of the algorithm depends on the acceptable error, which, furthermore, depends on the scientific problem and the relationship of this error to the natural variability within the area and period under research. Consequently, different acceptance ranges around the true value have to be defined for calculating the scope of algorithm. Here, the scope is defined for 3 error ranges, (1) an error range of +- 0.405 on the logarithmic scale, which is a factor of 1.5, (2) of ln +-0.693 which corresponds to a factor of 2 and (3) an error of ln +- 2.31 which corresponds to one order of magnitude.

The scope of algorithm for these three error ranges will be computed as a function of the error of the input reflectance and the concentration of other substances.

17.

Copyright © 1997 SCICON.

18. Appendix C: Case II water model (by M. Babin and R. Doerffer)

Title: SPECIFICATIONS FOR CASE II COASTAL WATER REFERENCE MODEL

Doc. no: PO-TN-MEL-GS-0016

Issue: Draft

Revision: 0

Date: 23 July 1996

	Function	Name	Company	Signature	Date
Prepared:		M. Babin	ACRI		
		R. Doerffer	GKSS		
Approved:	Project Manager	F. Montagner	ACRI		
Released:			ESA		

Change Record

Issue	Revision	Date	Description	Change pages
Draft	0	23/07/96	Initial Draft	-

Copyright © 1997 SCICON.

18.1 1. - Purpose

The specification provided here will be used in the frame of MERIS Level 2 Algorithms development, for case II water radiative transfer calculations and for testing of algorithms. They are selected from various measurements and calculations in coastal and open sea. Actual optical properties may deviate from the given values.

It should be noted that the files mentioned in the text below, will become available on the "anonymous ftp" server **`acri.cica.fr`**.

18.2 2. - Coastal Water Optical Properties

18.2.1 2.1 - Remotely sensed layer

The geometrical thickness of the vertical water layer from which 90% of the remotely sensed ocean colour signal comes from (denoted Z_{90}; m) can be approximated by (Gordon and McCluney 1975):

$$Z_{90} = 1/K_d \qquad (1)$$

at all wavelength, where K_d (m^{-1}) is the vertical attenuation coefficient for downward irradiance. Here, we assume that:

$$z >> Z_{90}$$

where z (m) is the geometrical thickness of the water column.

18.2.2 2.2 - Water constituents

The apparent optical properties of surface sea waters will be determined according to the concentrations and inherent optical properties of 4 groups of substances: pure sea water, phytoplankton (and associated organic matter), total non-chlorophyllous suspended matter, and coloured dissolved organic matter (yellow substance or *gelbstoff*).

The concentration units are:

phytoplankton (and associated organic matter): expressed by the concentration of chlorophyll *a* (mg m^{-3}).

total non-chlorophyllous suspended matter: it is assumed that this component is solely represented by non-absorbing mineral particles and its concentration is expressed by its total scattering coefficient at 550 nm [$b_P(550)$; m^{-1}][3].

coloured dissolved organic matter (yellow substance or *gelbstoff*): expressed by its absorption coefficient at 440 nm [$a_Y(440)$; m^{-1}].

[3] If desired, it can be *a posteriori* converted into mass concentration per unit volume using a given mass-specific total scattering coefficient [$b_P^*(550)$].

18.2.3 2.3 - Vertical distribution

It is assumed that all substances are homogeneously distributed in the water column. For many coastal waters, this is a realistic assumption, especially when considering the Z_{90} layer.

18.2.4 2.4 - Inherent optical properties of water and its constituents

Sea water apparent optical properties will be determined from the individual spectral absorption and elastic scattering properties, i.e. the absorption coefficient, $a(\lambda)$, and the volume scattering function, $b(q, l)$. The latter is expressed as:

$$\beta(\theta,\lambda) = \frac{d\Phi(\theta,\lambda)}{\Phi_o(\lambda)} \frac{1}{d\omega dr} \qquad (2)$$

where $\Phi_o(\lambda)$ is the radiant flux on the cross-sectional area, $d\Phi(q,\lambda)$ is the radiant flux scattered in the element of solid angle $d\omega$ oriented at angle q, and dr is the thickness of the volume element. Here, the volume scattering is expressed through:

$$\beta(\theta,\lambda) = b(\lambda)\tilde{\beta}(\theta) \qquad (3)$$

where $b(\lambda)$ is the total scattering coefficient and $\tilde{\beta}(\theta)$ is the normalised volume scattering function[4]:

$$\tilde{\beta}(\theta) = \frac{\beta(\theta)}{b} \qquad (4)$$

Note that the wavelength dependency of $\tilde{\beta}(\theta)$ is neglected. Thus, the bulk sea water inherent optical properties will be input in radiative transfer calculations as $a(\lambda)$, $b(\lambda)$ and $\tilde{\beta}(\theta)$. $a(\lambda)$ and $b(\lambda)\tilde{\beta}(\theta)$ can be broken into individual contributions by the different water constituents:

$$a(\lambda) = \sum_{n=1}^{N} a_n(\lambda) \qquad (5a)$$

$$b(\lambda)\tilde{\beta}(\theta) = \sum_{n=1}^{N} b_n(\lambda)\tilde{\beta}_n(\theta) \qquad (5b)$$

where n denote a given sea water constituent.

---

[4] Note that the **phase function**, $p(q)$, is equal to $4\pi\tilde{\beta}(\theta,\lambda)$.

18.2.4.1 2.4.1 - Pure sea water and phytoplankton

In Case I waters, the relative proportions of phytoplankton and related derivatives are well correlated with chlorophyll *a* concentration ($[chl]$) (Carder *et al.* 1986), and *a* and *b* are tightly correlated with $[chl]$ (see Morel 1987). Therefore, absorption and scattering coefficients for case I waters, respectively $a_1(\lambda)$ and $b_1(\lambda)$, can be expressed as:

$$a_1(\lambda) = a_w(\lambda) + a_{chl}(\lambda)$$

$$b_1(\lambda)\beta_1(\theta) = b_w(\lambda)\beta_w(\theta) + b_{chl}(\lambda)\beta_{chl}(\theta) \quad (6)$$

where the subscripts "*w*" and "*chl*" denote pure sea water, and phytoplankton and derivatives, respectively. Here, $a_1(\lambda)$ and $b_{Chl}(\lambda)$ are determined as a function of chlorophyll concentration as described by Morel (1988) and Morel and Antoine (1994):

$$a_1(\lambda) = K_d(\lambda)u(\lambda) \quad (7)$$

where $K_d(\lambda)$ is total vertical attenuation coefficient, which is given as a function of $[chl]$ by Morel (1988) and Morel and Antoine (1994), from 300 to more than 1000 nm. *u* is determined iteratively as described by Morel (1988). $b_w(\lambda)$ is determined from (Morel 1974):

$$b_w = 0.00288(\lambda / 500)^{-4.32} \quad (8)$$

and $b_{chl}(\lambda)$ from (Gordon and Morel 1983):

$$b_{chl}(\lambda) = 0.30[chl]^{0.62}(550 / \lambda) \quad (9)$$

Here, the normalised volume scattering function of pure sea water (refraction index = 1.334) adopted is that published by Morel (1966), which can be expressed as:

$$\tilde{\beta}_w(\theta,\lambda) = \frac{3}{4\pi(3+p)}(1+p\cos^2\theta) \quad (10)$$

where the parameter *p* equals 0.84. For phytoplankton and derivatives $\beta_{chl}(\theta)$, the normalised volume scattering function given by Petzold (1972) must be applied. Petzold's $\tilde{\beta}(\theta)$ values are listed in Table 2.4.1-1 below and plotted in Fig. 2.4.1-1.

q	$\underline{\tilde{\beta}(\theta)}$	q	$\underline{\tilde{\beta}(\theta)}$
1.00E-01	1.77E+03	5.00E+01	2.28E-02
1.26E-01	1.30E+03	5.50E+01	1.70E-02
1.58E-01	9.50E+02	6.00E+01	1.31E-02
2.00E-01	6.99E+02	6.50E+01	1.05E-02
2.51E-01	5.14E+02	7.00E+01	8.49E-03
3.16E-01	3.76E+02	7.50E+01	6.98E-03
3.98E-01	2.76E+02	8.00E+01	5.84E-03
5.01E-01	2.01E+02	8.50E+01	4.95E-03
6.31E-01	1.44E+02	9.00E+01	4.29E-03
7.94E-01	1.02E+02	9.50E+01	3.78E-03
1.00E+00	7.16E+01	1.00E+02	3.40E-03
1.26E+00	4.96E+01	1.05E+02	3.12E-03
1.58E+00	3.40E+01	1.10E+02	2.91E-03
2.00E+00	2.28E+01	1.15E+02	2.80E-03
2.51E+00	1.52E+01	1.20E+02	2.69E-03
3.16E+00	1.00E+01	1.25E+02	2.57E-03
3.98E+00	6.58E+00	1.30E+02	2.48E-03
5.01E+00	4.30E+00	1.35E+02	2.38E-03
6.31E+00	2.81E+00	1.40E+02	2.33E-03
7.94E+00	1.82E+00	1.45E+02	2.31E-03
1.00E+01	1.15E+00	1.50E+02	2.36E-03
1.50E+01	4.89E-01	1.55E+02	2.51E-03
2.00E+01	2.44E-01	1.60E+02	2.66E-03
2.50E+01	1.47E-01	1.65E+02	2.83E-03
3.00E+01	8.61E-02	1.70E+02	3.03E-03
3.50E+01	5.93E-02	1.75E+02	3.09E-03
4.00E+01	4.21E-02	1.80E+02	3.15E-03
4.50E+01	3.07E-02		

Table 2.4.1-1. Normalized volume scattering function published by Petzold (1972).

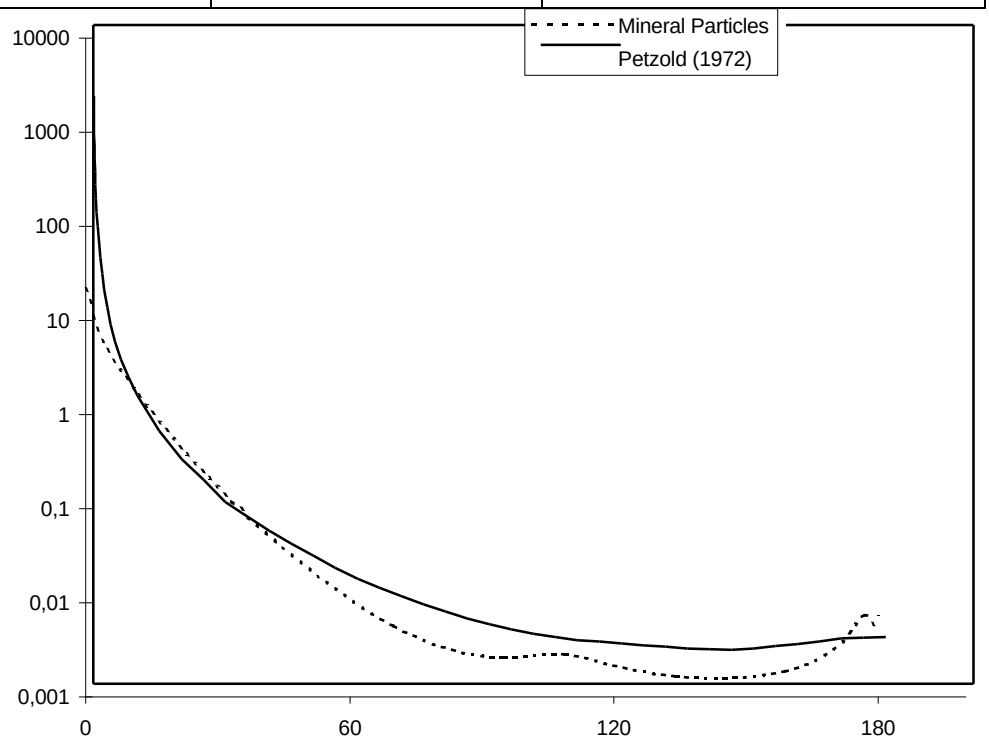

Figure 2.4.1-1. Normalized volume scattering function published by Petzold (1972), and computed for mineral particles as described below in Section 2.4.2.

18.2.4.2 2.4.2 - Non-chlorophyllous suspended sediments and gelbstoff

In case II waters, humic and fulvic acids from terrestrial origin (often collectively denoted "yellow substance" or "*gelbstoff*"), which represent about 70% of dissolved organic matter (Spitzy and Ittekkot 1986), are a major contributor in light absorption by non-chlorophyllous matter. In coastal waters and, in some cases, in areas neighbouring upwelling regions (Carder *et al.* 1991), *gelbstoff* absorption often largely exceeds that of phytoplankton. Therefore, it strongly influences reflectance. High suspended sediment load is also often observed in the vicinity of river runoffs (river plumes) and near the coast line due to re-suspension of sediments. Such suspended mineral sediments have high scattering coefficients and, depending on the site, i. e. on their chemical composition, various contributions to absorption (Whitlock *et al.* 1981, Ahn 1990). In this study, we computed *gelbstoff* absorption and sediment scattering as described in Sathyendranath et al. (1989):

$$a_y(\lambda) = a_y(440)e^{-0.014(\lambda-440)} \qquad (11)$$

$$b_x = b_x(550)(\lambda/550)^{-n} \qquad (12)$$

where $a_y(\lambda)$ is the *gelbstoff* absorption coefficient, $b_x(\lambda)$ is the sediment scattering coefficient, n is a constant that determines the spectral dependency of $b_x(\lambda)$.

Thus, the bulk absorption and scattering properties of sea water can be expressed as:

$$a(\lambda) = a_1(\lambda) + a_y(\lambda) \quad (13)$$

$$b(\lambda)\tilde{\beta}(\theta) = b_1(\lambda)\tilde{\beta}_1(\theta) + b_X(\lambda)\tilde{\beta}_X(\theta) \quad (14)$$

using Eqs. 6 to 12. For mineral particles, a phase function ($\tilde{\beta}_X(\theta)$) was determined from Mie calculations assuming a particle size spectrum following a Junge distribution with the exponent, m, equal to 4 and a size range going from 0.45 to 20 µm, and a refraction index equal to 1.15. For such particles, *n* in Eq. 12 equals 0.812. Corresponding $\tilde{\beta}(\theta)$ values are listed in Table 2.4.2-1 below and plotted in Fig. 2.4.1-1 above.

Table 2.4.2-1. Normalized volume scattering function adopted for mineral particles.

q	$\underline{\tilde{\beta}(\theta)}$	q	$\underline{\tilde{\beta}(\theta)}$	q	$\underline{\tilde{\beta}(\theta)}$
0	2.18E+01	61	1.02E-02	121	2.09E-03
1	1.67E+01	62	9.49E-03	122	2.04E-03
2	1.03E+01	63	8.85E-03	123	1.99E-03
3	7.50E+00	64	8.26E-03	124	1.94E-03
4	5.89E+00	65	7.72E-03	125	1.90E-03
5	4.83E+00	66	7.22E-03	126	1.86E-03
6	4.05E+00	67	6.78E-03	127	1.83E-03
7	3.43E+00	68	6.37E-03	128	1.80E-03
8	2.93E+00	69	5.99E-03	129	1.77E-03
9	2.52E+00	70	5.65E-03	130	1.74E-03
10	2.17E+00	71	5.34E-03	131	1.72E-03
11	1.87E+00	72	5.05E-03	132	1.69E-03
12	1.62E+00	73	4.79E-03	133	1.67E-03
13	1.41E+00	74	4.56E-03	134	1.66E-03
14	1.22E+00	75	4.34E-03	135	1.64E-03
15	1.06E+00	76	4.14E-03	136	1.63E-03
16	9.28E-01	77	3.96E-03	137	1.61E-03
17	8.11E-01	78	3.79E-03	138	1.60E-03
18	7.10E-01	79	3.64E-03	139	1.60E-03
19	6.24E-01	80	3.51E-03	140	1.59E-03
20	5.49E-01	81	3.38E-03	141	1.58E-03
21	4.84E-01	82	3.27E-03	142	1.58E-03
22	4.27E-01	83	3.17E-03	143	1.58E-03
23	3.78E-01	84	3.08E-03	144	1.58E-03
24	3.36E-01	85	3.00E-03	145	1.58E-03
25	2.98E-01	86	2.92E-03	146	1.58E-03
26	2.66E-01	87	2.86E-03	147	1.59E-03
27	2.37E-01	88	2.80E-03	148	1.60E-03
28	2.12E-01	89	2.76E-03	149	1.61E-03
29	1.90E-01	90	2.72E-03	150	1.62E-03
30	1.70E-01	91	2.69E-03	151	1.63E-03

31	1.53E-01	92	2.66E-03	152	1.65E-03
32	1.37E-01	93	2.64E-03	153	1.67E-03
33	1.23E-01	94	2.63E-03	154	1.70E-03
34	1.11E-01	95	2.63E-03	155	1.73E-03
35	1.01E-01	96	2.63E-03	156	1.76E-03
36	9.08E-02	97	2.64E-03	157	1.79E-03
37	8.22E-02	98	2.65E-03	158	1.83E-03
38	7.45E-02	99	2.67E-03	159	1.88E-03
39	6.75E-02	100	2.70E-03	160	1.93E-03
40	6.13E-02	101	2.73E-03	161	1.99E-03

Table 2.4.2-1. (Continued)

q	$\tilde{\beta}(\theta)$	q	$\tilde{\beta}(\theta)$	q	$\tilde{\beta}(\theta)$
41	5.57E-02	102	2.76E-03	162	2.06E-03
42	5.07E-02	103	2.79E-03	163	2.14E-03
43	4.61E-02	104	2.81E-03	164	2.23E-03
44	4.21E-02	105	2.83E-03	165	2.33E-03
45	3.84E-02	106	2.85E-03	166	2.45E-03
46	3.50E-02	107	2.85E-03	167	2.59E-03
47	3.20E-02	108	2.84E-03	168	2.76E-03
48	2.93E-02	109	2.82E-03	169	2.95E-03
49	2.69E-02	110	2.79E-03	170	3.20E-03
50	2.46E-02	111	2.74E-03	171	3.47E-03
51	2.26E-02	112	2.68E-03	172	3.85E-03
52	2.08E-02	113	2.61E-03	173	4.33E-03
53	1.91E-02	114	2.54E-03	174	4.97E-03
54	1.76E-02	115	2.47E-03	175	5.85E-03
55	1.62E-02	116	2.39E-03	176	6.96E-03
56	1.50E-02	117	2.33E-03	177	7.48E-03
57	1.38E-02	118	2.26E-03	178	7.29E-03
58	1.28E-02	119	2.20E-03	179	5.89E-03
59	1.18E-02	120	2.14E-03	180	7.09E-03
60	1.10E-02				

18.3 3 - Sea surface state

The effect of the air-sea interface shape on Fresnel reflection and refraction will be accounted for by applying statistics of Cox and Munk (1954, 1955) and assuming an isotropic distribution of waves and a wind speed of 7 m s^{-1}. White caps are not accounted for.

18.4 4 - Atmospheric properties

The following MERIS bands are considered here:

Channel number	Wavelength
1	(412 nm)
2	(443)
3	(490)
4	(510)
5	(560)
6	(620)
7	(665)
8	(681)
9	(705)
13	(775)
14	(865)

No absorption by atmospheric gases is assumed for these bands. The radiation transfer is treated without polarisation.

18.4.1 4.1 - Air pressure at ground

1013.25 hPa

18.4.2 4.2 - Density Profiles & Rayleigh parameters

The vertical profile of the Rayleigh scattering coefficient is given by Elterman (1968), for a standard atmospheric pressure of 1013.25 hPa. The profiles with 50 1-km layers are tabulated for each MERIS channel in 11 files (rpmerxxx.txt), where xxx is the wavelength as listed above.

18.4.3 4.3 - Ozone layer

The vertical ozone profile is taken from Elterman(1968). The density profile given in cm ozone per km for a ground pressure of 1013.25 hp, is tabulated in the file ozprofel.txt. The total ozone column content is 0.34 cm. The extinction profiles with 50 1 km-layers are tabulated for each MERIS channel in 11 files (opmerxxx.txt), where xxx is the wavelength as listed above. The ozone absorption spectrum is given in file ozspek1.txt.

18.4.4 4.4 - Aerosol

To be consistent with case I water simulations and algorithms, a maritime atmosphere is defined also for case II water. The vertical profiles and optical properties are taken from WMO report 112.

18.4.4.1 4.4.1 - Aerosol type

Three aerosol types are used to model the case I and case II atmospheres:

- maritime aerosol with a humidity of 70% (Shettle & Fenn, 1979)
- continental aerosol (WMO report 112, 1986)
- stratospheric aerosol which is represented by a 75% solution of sulfuric acid in water (H_2SO_4) (WMO report 112, 1986)

The normalised extinction coefficients and single scattering albedos are tabulated for the 3 aerosol types and, in addition, for the urban aerosol type for each of the 11 MERIS bands in the files csmerxxx.txt, where xxx is the wavelength as listed above.

18.4.4.2 4.4.2 - Aerosol phase function & single scattering albedo

Aerosol phase functions and single scattering albedos were computed using the MIE code developed at LPCM, and the inputs (complex indices of refraction and particle size distributions) given in Shettle and Fenn (1979) and World Climate Research Program (1986) document 112 (1986).

The single scattering albedos and the phase functions for the 11 MERIS channels are tabulated in the following files with xxx the wavelength:

- maritime aerosol 70% humidity: gm70_xxx.txt
- continental aerosol: gcon_xxx.txt
- stratospheric aerosol: ghso_xxx.txt

The 75 angles are listed in file wink.txt. The single scattering albedos of these files are used for the calculations.

18.4.4.3 4.4.3 - Aerosol vertical profiles

The first two km (layers 1 and 2) consist of the maritime aerosol type with an aerosol extinction at 550 nm of 0.025 km-1. The layers 3-10 consist of the continental aerosol type with an extinction of 0.0025 km^{-1} and the layers 11-50 of stratospheric aerosol type. The extinction of the stratospheric aerosol is altitude dependent (s.table).

The vertical aerosol extinctions for these three types for 550 nm are tabulated in file profilma.txt.

18.4.4.4 4.4.4 - Sun irradiance

As all calculations are done in terms of reflectance, sun irradiance is assumed to equal 1.

18.5

18.6 5 - References

AHN, Y.-H. 1990 Propriétés optiques de particules biologiques et minérales présentes dans l'océan; Application: inversion de la réflectance. Thèse de Doctorat, Université Pierre et Marie Curie, Paris, 214 pp.

CARDER K.L., S.K. HAWES, K.A. BAKER, R.C. SMITH, R.G. STEWARD and B.G. MITCHELL. 1991. Reflectance model for quantifying chlorophyll *a* in the presence of productivity degradation products. Journal of Geophysical Research, 96: 20 599-20 611.

CARDER K.L., R.G. STEWARD, J.H. PAUL and G. A. VARGO; 1986. Relationships between chlorophyll and ocean color constituents as they affect remote-sensing reflectance models. Limnology and Oceanography, 31: 403-413.

COX, C. and W. MUNK. 1954. Statistics of the sea surface derived from sun glitter. J. Mar. Res., 13: 198-227.

COX, C. and W. MUNK. 1954. Some problems in optical oceanography. J. Mar. Res., 14: 63-78.

ELTERMAN L. (1968). UV, visible, and IR attenuation for altitudes to 50 km, Air Force Cambridge Research Laboratories, Environmental Research papers, N° 285, AFCRL-68-0153, 49pp.

GORDON, H. R. and W. R. McLuney. 1975. Estimation of the depth of sunlight penetration in the sea for remote sensing. Applied Optics, 14:413-416.

GORDON, H. R. and A. MOREL. 1983. Remote assessment of ocean color for interpretation of satellite visible imagery. A review. Lecture Notes on Coastal and Estuarine Study, Vol. 4, Springer Verlag.

MOREL, A. 1966. Etude expérimentale de la diffusion de la lumière par l'eau, les solutions de chlorure de sodium et l'eau de mer optiquement pure. J. Chim. Phys., 10: 1359-1366.

MOREL, A. 1974. Optical properties of pure water and sea water. In : Optical aspects of Oceanography, N. G. Jerlov and E. Steemann-Nielsen, N. G. Jerlov and E. Steemann-Nielsen, Academic, pp. 1-24.

MOREL, A. 1987. Chlorophyll-specific scattering coefficient of phytoplankton. A simplified theoretical approach. Deep-Sea Res., 34: 1093-1105.

MOREL A. 1988. Optical modeling of the upper ocean in relation to its biogenous matter content (case I waters). Journal of Geophysical Research, 93: 10 749-10 768.

MOREL A. and D. ANTOINE. 1994. Heating rate within the upper ocean in relation to its bio-optical state. J. Phys. Oceanogr., 24: 1652-1665.

PETZOLD, T. L. 1972. Volume scattering functions for selected ocean waters. San Diego: Scipps Inst. Oceanogr., Ref. 72-78, 79 pp.

SATHYENDRANATH, S., L. PRIEUR and A. MOREL. 1989. A three-component model of ocean colour and its application to remote sensing of phytoplankton pigments in coastal waters. Int. J. Remote Sensing, 10: 1373-1394.

SHETTLE E.P. and R.W. FENN. 1979. Models for the aerosols of the lower atmosphere and the effects of humidity variations on their optical properties. Environmental Research Papers, AFGL-TR-79-0214, 20 September 1979, AFGL, Hanscom, MA.

SPITZY A. and V. ITTEKOTT. 1986. *Gelbstoff* : An uncharacterized fraction of dissolved organic carbon. *In* the influence of yellow substances on remote sensing of sea-water consitutents from space (GKSS Geesthacht Research Center, Geesthacht, FRG), VOl. II, pp 31.

WHITLOCK, C. H., L. R. POOLE, J. W. USRY, W. M. HOUGHTON, W. G. WITTE, W. D. MORRIS and E. A. GURGANUS. 1981. Comparison of reflectance with backscatter and absorption parameters for turbid waters. Appl. Opt., 20: 517-522.

WORLD CLIMATE RESEARCH PROGRAM. 1986. A preliminary cloudless standard atmosphere for radiation computation. Int. Ass. for Meteor. and Atm. Phys., Radiation Commission, March 1986, WCP-112, WMO/TD-N° 24.

Addendum 1

to

„MAPP Data Products Definition and Algorithm Specification Algorithm Theoretical Basis Document (ATBD) Regionalized Case-II Water products and algorithms“

Abstract

This addendum is based on experiences/findings achieved in the final MERIS groundsegment validation phase. Topics discussed are

Utilization of a realistic error model for reflectances

Exploitation of field campaign data to reduce inversion ambiguities

Improvement of run time checks and exception handling

Conclusions are drawn and proposals are made for these topics in the MAPP context, respectively. Concerned sections of the ATBD are identified.

1. Utilization of a realistic error model for reflectances

1.1 Motivation

The `Regionalized pigment index, sediment and gelbstoff retrieval from directional water leaving radiance reflectances using inverse modelling technique‘ relies on Neural Nets (NN‘s) emulating the inverse model. The parameters of the NN are fixed during a training phase when patterns of reflectances & concentrations of water constituents (training set) are presented to the NN. As a result the NN `learns‘ the mapping from reflectance- to soncentration-space.

Now, NN‘s are known to have good *interpolation* capabilities but to perform poorly if forced to *extrapolate*. Therefore when preparing the training set it is very important to ensure that at least the region in reflectance space is covered which will be covered during the real retrieval. To achieve this the spectra derived from the forward model have to be modified by adding contributions sampled from an as realictic as possible error model.

1.2 The error model

A simple error model above Case 2 waters for the water-leaving reflectance retrieval was developed by ACRI using the MERIS Level 2 processing prototype MEGS. It is attached at the end of this document for completeness.

1.3 Implementation of the error model

A pvwave/IDL-procedure was written to accomplish the necessary modification of the reflectance spectra:

```
function error_model, rndvec, logrho, rholim
       noisy=exp(logrho)*!pi
       dr=dblarr(8)

       fn=2.  ; to get really smearing over region to cover

       if noisy(1) lt 0.045 then dr(1)=-0.000722037+fn*rndvec(1)*0.000285548 $
                          else dr(1)=0.000519828+fn*rndvec(1)*0.001925612
       slopeb=[1.12563275, 0.69503953, 0.656062369, 0.572462264,$
                           0.395084137, 0.42286848, 0.326793601]
       biasb=[-0.001579045, 0.000291421, 0.000348122, 9.92006E-05,$
                           0.000171224, 0.000130715, 2.71495E-05]
       noiseb=[0.000648182, 0.000539528, 0.000505556, 0.00052479,$
                           0.00036472, 0.000366768, 0.000320552]
       for i=0, 6 do begin
              k=i
              if i gt 0 then k=i+1
              dr(k)=biasb(i)+slopeb(i)*dr(1)+fn*noiseb(i)*rndvec(k)
       endfor
       nedr=[1.6e-4, 1.1e-5, 9.6e-5, 9.2e-5,$
             7.8e-5, 6.9e-5, 6.0e-5, 6.1e-5]
       for i=0, 7 do begin
              noisy(i)=(noisy(i)+dr(i)+nedr(i)*rndvec(8+i))/!pi
              if noisy(i) lt rholim(i) then noisy(i)=rholim(i)
       endfor
       return, alog(noisy)
end

;usage:

common forw_NN, NNforwlun, NNforw_input, NNforw_output
forw_nn_init
```

```
NN_in=dblarr(6,nsamp)
orig_refl=dblarr(nshow,8)
noisy_refl=dblarr(nshow,8)
rg=randomn(seed,nsamp,16)

rholim=exp([-8.018819 ,-7.603442 ,-6.901749 ,-6.690072,$
           -6.859725 ,-8.654559 ,-9.296165 ,-9.947495 ])
       forw_NN
       noisy_forw_output=error_model(rg(n,*), NNforw_output, rholim)
```

1.4. Conclusion

Twice time the above error model should be added to the reflectance spectra obtained from any forward model calculations to be used as training set for `regional‘ NN. For the standard MERIS retrieval this turned out to generate quite a robust NN performing well when inverting reflectance data which were modified by one times the error model. But even when the spectra were modified by three times the error model the NN still gave a reasonable response.

1.5 Concerned ATBD section

7.3.3

2 Exploitation of field campaign data to reduce inversion ambiguities

2.1 Motivation

For MAPP several `regional' NN's have to be generated using training sets obtained from forward model calculations using as input different inherent optical properties of water constituents. Then it might happen (and indeed it happened with the standard MERIS procedure) that the training of the NN emulating the inverse model does not converge. Such a convergence failure can be due to ambiguities inherent to the inversion. To overcome such situation one can proceed, *mutatis mutandis*, like with the MERIS standard procedure.

2.2 The source of ambiguities

If definitely distinct concentration combinations result in more or less the same reflectance spectra then, strictly speaking, there is no inverse model and a concentration retrieval is impossible:

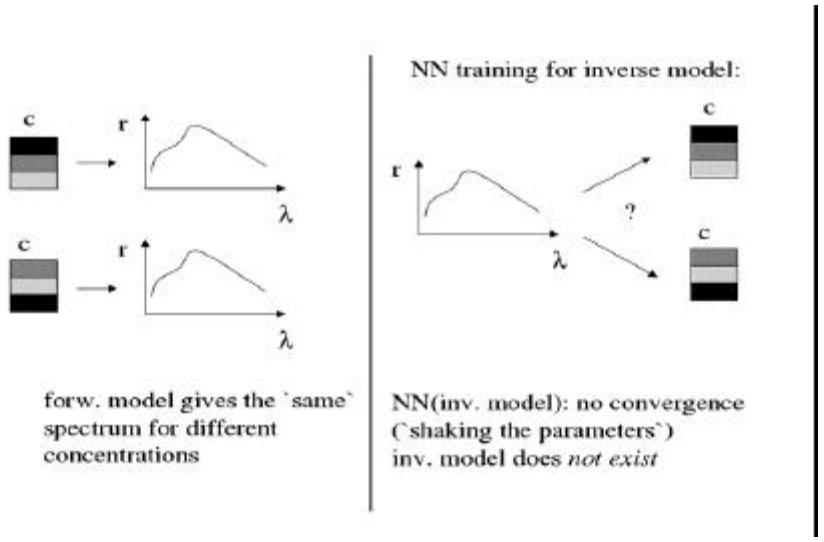

That such situations really occur is illustrated in **fig. 1** where the small difference of two spectra belonging to distinct concentrations is displayed:

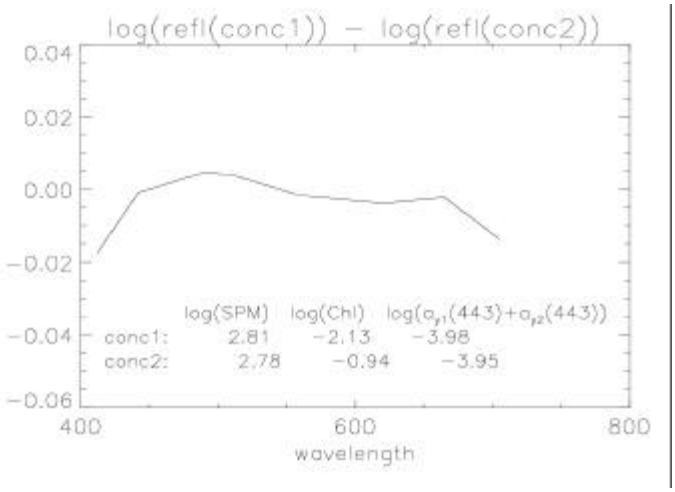

fig. 1 example of ambigous spectra

2.3. Avoiding the ambiguities

The approach chosen to avoid the ambiguities was to restrict the concentration region according to COAST*l*OOK findings.

The logic of this work was like follows:

1 produce a new NN emulating the forward model (`forw_NN`).

2 determine the region in concentration space which is covered by the COAST*l*OOC data (finding center of gravity and covariance matrix)

3 use `forw_NN` to generate a training data set covering the COAST*l*OOC data range and generate a NN emulating the inverse model (`inv_NNcl`) - this is a test whether the restriction in concentration space diminishes the ambiguities

4 use `forw_NN` and a realistic error model for reflectances to generate a training data set covering the COAST*l*OOC data range and generate a NN emulating the inverse model (`inv_NNnoise`). If the error model is correct this will exclude situations where the `inv_NNnoise` is forced to extrapolate

2.3.1 The analysis

2.3.1.1 NN emulating the forward model (`forw_NN`)

For generation of the NN emulating the forward model we use the table described in `**Technical Note: MERIS Case 2 IMT Neural Net Training Set generated at ACRI**'.

The input to the six input neurons are

`log(SPM), log(Chl), log(a_{y2}(443)), theta_s, theta_v, Delta_Phi`

and the eight output neurons produce

`log(R_{Lw}(412)),...,\log(R_{Lw}(705)).`

The two hidden layers contain 10 and 12 neurons, respectively. The rms of the output neuron error is 0.0042. The performance of the forward model emulation is exemplified in fig. **2** together with examples of spectra derived from the forward NN.

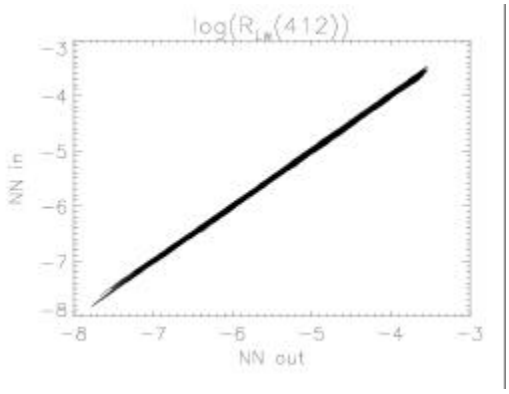

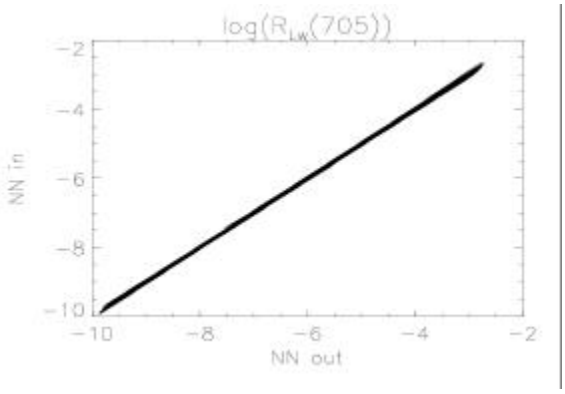

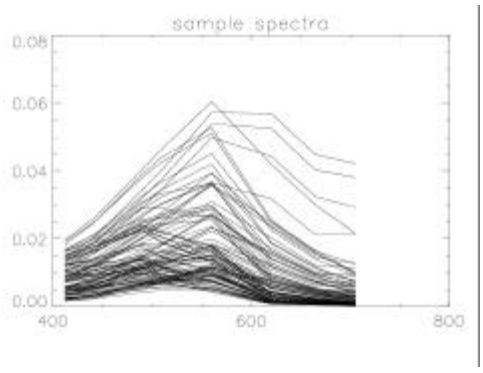

fig. 2 Performance of forward model emulation by `forw_NN` and example spectra derived from the forward model

2.3.1.2 Covariance analysis

After removing from the COAST*l*OOC data base (424 lines) lines where one or more of the concentrations are missing we are left with 332 valid triples. Scatter plots from this sample are shown in `fig. 3`.

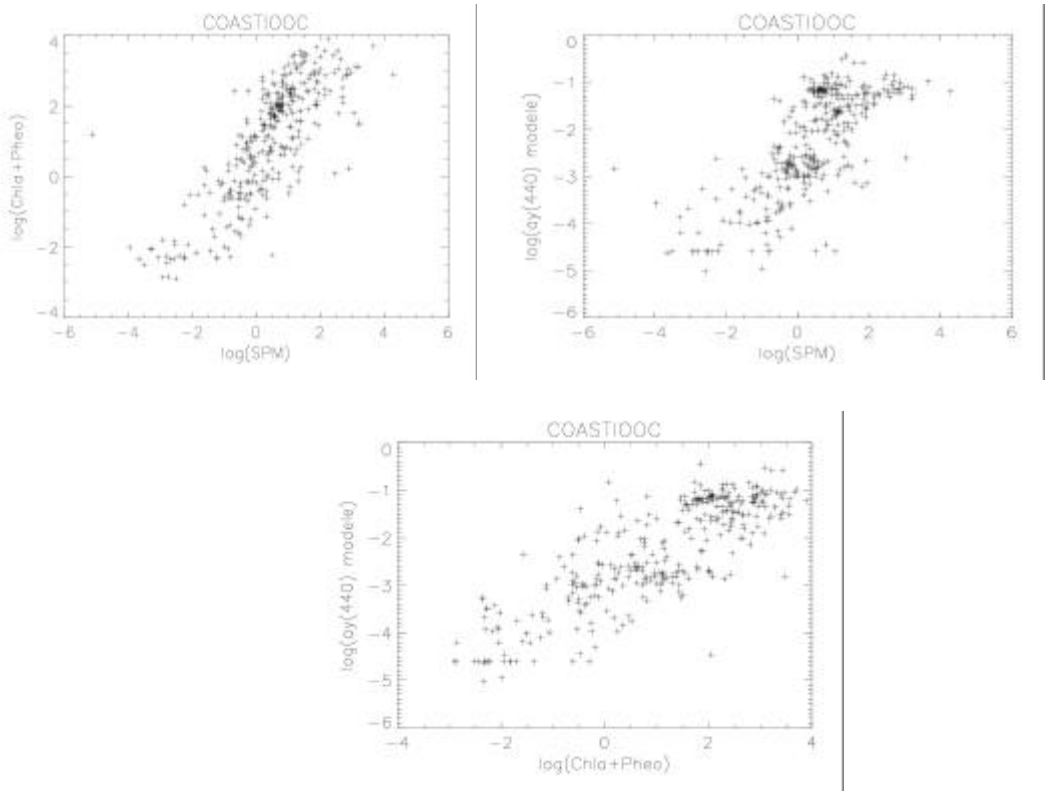

fig. 3 Concentrations from COAST*l*OOC data base with complete concentration triples

The centre of gravity of the log's of concentrations is

$$\vec{c} = (0.390774 \quad 1.03039 \quad -2.30769)^T$$

and the covariance matrix is

$$C = \begin{pmatrix} 1.91538 & 1.75238 & 1.10757 \\ 1.75238 & 2.63181 & 1.45859 \\ 1.10757 & 1.45859 & 1.19810 \end{pmatrix}$$

For training data generation we generate triples of random numbers uniformly distributed in [-1.386, 4.605] x [-3.506, 3.912] x [-5.298, 0.182] and accept them as log's of concentrations if

$$\sqrt{(\vec{c}-\vec{\bar{c}})^T C^{-1}(\vec{c}-\vec{\bar{c}})} < 3$$

A subsample of concentrations obtained by this procedure is shown in `fig. 4` together with the original COAST*l*OOC points (the SPM cut was necessary to fit the limits used in **`Technical Note: MERIS Case 2 IMT Neural Net Training Set generated at ACRI''**).

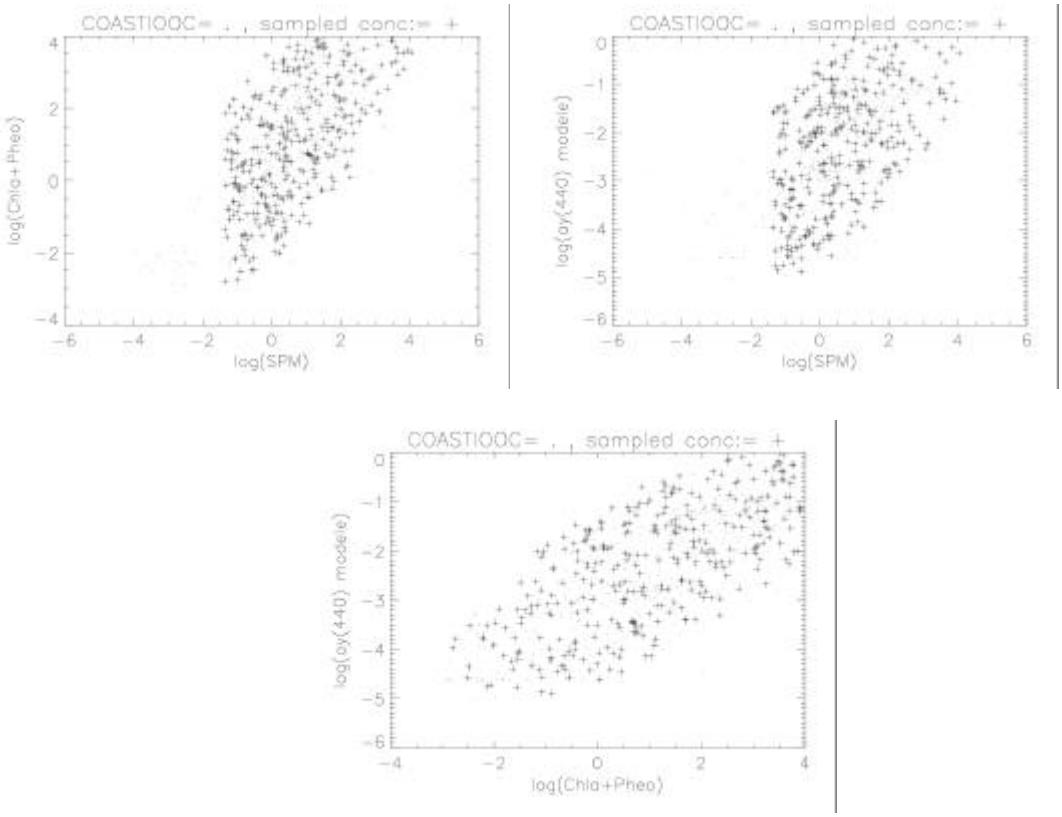

fig. 4 Sampled concentrations (+), concentrations from COAST*l*OOC (.)

2.3.2 NN's emulating the inverse model

For both NN's, *i.e.* without and with error model, the input to the eleven input neurons is
`theta_s, theta_v, DeltaPhi, log(R_{Lw}(412)),... ,log(R_{Lw}(705))`
and the three output neurons produce
`log(SPM), log(chl), log(a_{y2}(443)).`

2.3.2.1 NN emulating the inverse model using concentrations from COAST*l*OOC and noisefree spectra (`inv_NNcl`)

A sample of 50K concentrations was generated as described above and used together with uniformly sampled angles from the respective ranges as input to `forw_NN` to generate a new trainings/test-sample.
We trained a NN with four hidden layers containing 25, 20, 15, 10 neurons, respectively. The rms of the output neuron error is 0.003. The good performance of the NN (see `fig. 5`) shows that there is essentially no problem with ambiguities.

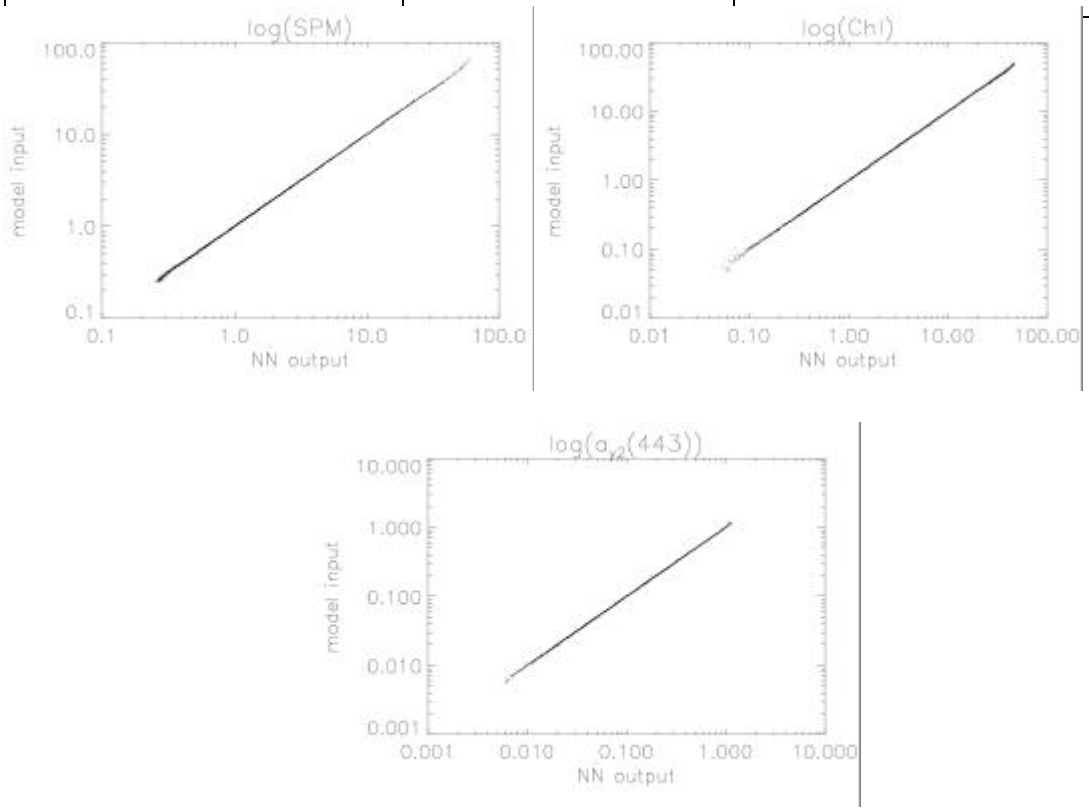

fig. 5 Performance of inverse NN trained with noisefree data

2.3.2.2 NN emulating the inverse model using concentrations from COAST*l*OOC and spectra with simulated errors (`inv_NNnoise`)

A sample of 200K concentrations was generated as described above and used together with uniformly sampled angles from the respective ranges as input to `forw_NN`. But now the resulting spectra were made noisy before including them into the trainings/test-sample. To simulate the noise we used the error model described in **`Technical note: A simple reflectance error model above Case 2 waters'** from ACRI (23/12/1999). Simulating the errors we used *twice* the error model to ensure that real spectra will be subject of *interpolation* by the NN.

For comparison with the figures in the technote about the error model the corresponding distributions are shown in `fig. 6` and `fig. 7` for a subsample of the trainings/test-sample.

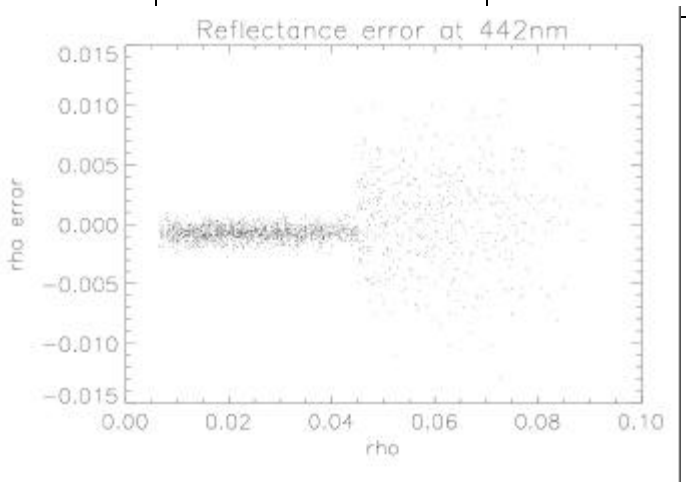

fig. 6 Error resulting from *twice* the error model

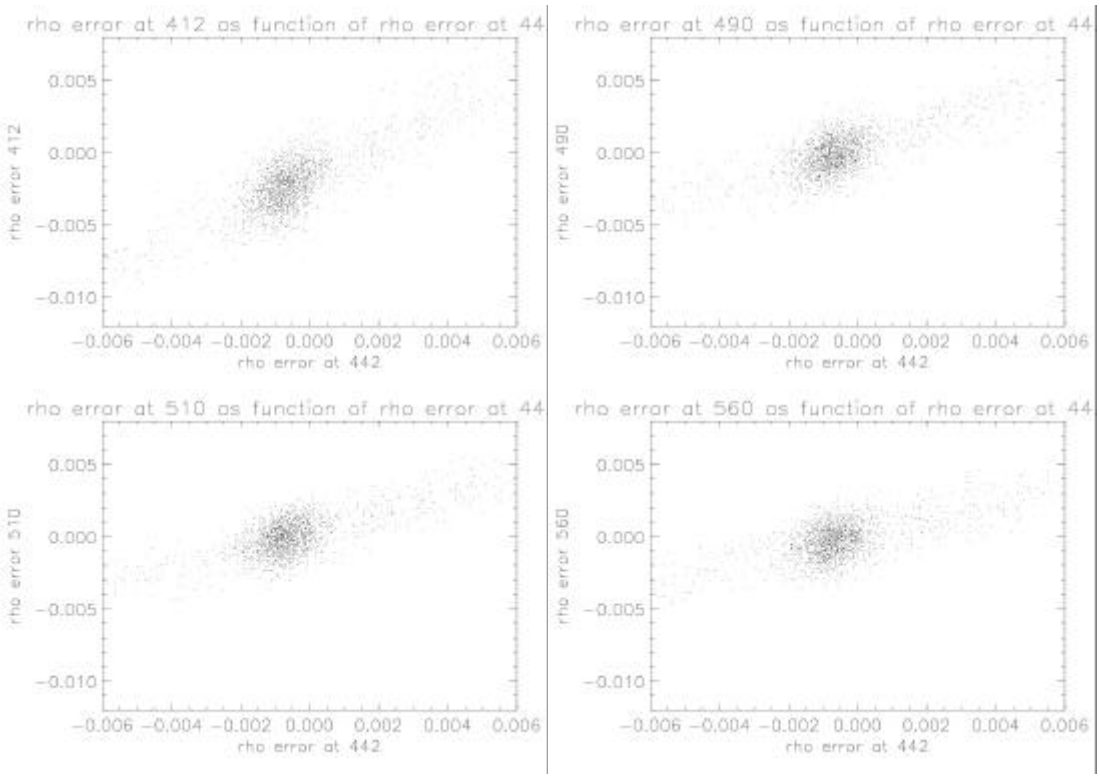

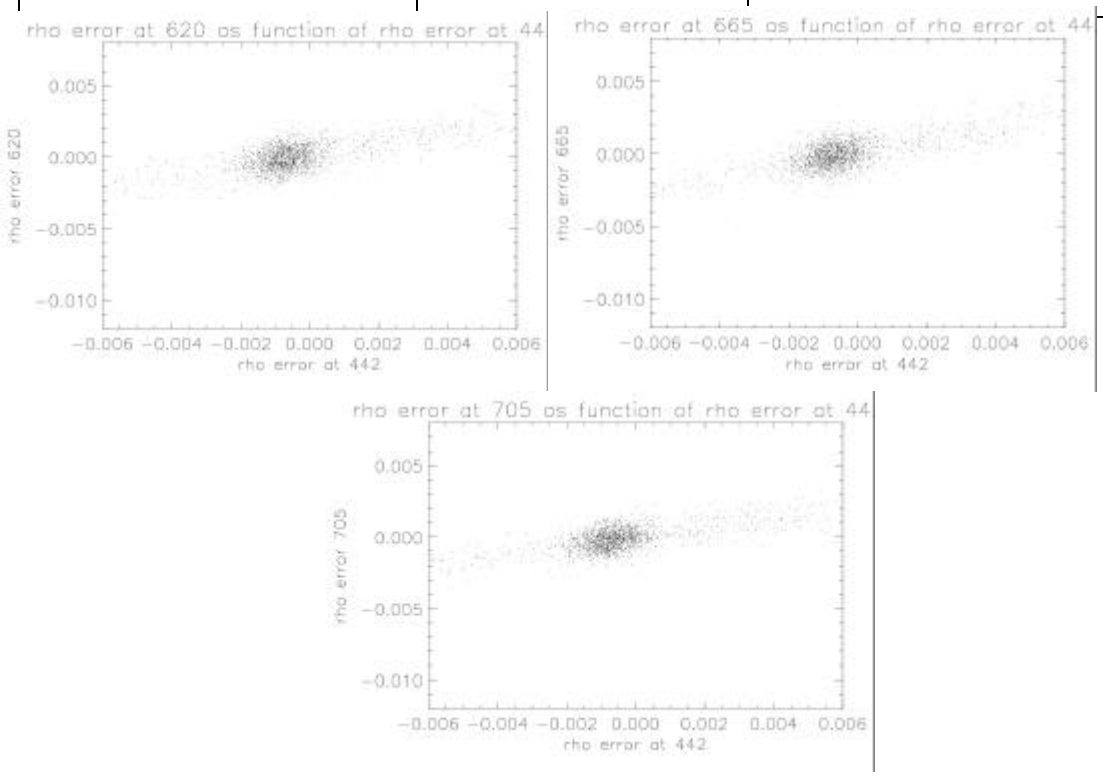

fig. 7 Error resulting from *twice* the error model

We trained a NN with five hidden layers containing 25, 20, 15, 10 and 5 neurons, respectively. The rms of the output neuron error is 0.028. In `fig. 8` the NN performance is shown: two independent test data sets were generated using the original error model as well as using three times the error model.
Obviously now the NN is quite robust with respect to erronous reflectance spectra.

2.4 Conclusion

For a region with new inherent optical properties of water constituents the forward model run should be made within the complete cartesian product of the concentrations of the respective water constituents. Next one should train a NN emulating rhe forward model. Then, if the training of the inverse NN does not converge, the forward NN can be used to generate spectra corresponding to a restricted subregion in concentration space, which should be adjusted to regional findings of concentrations of the water constituents.

2.5 Concerned ATBD sections

7.2.7, 7.3.4.1

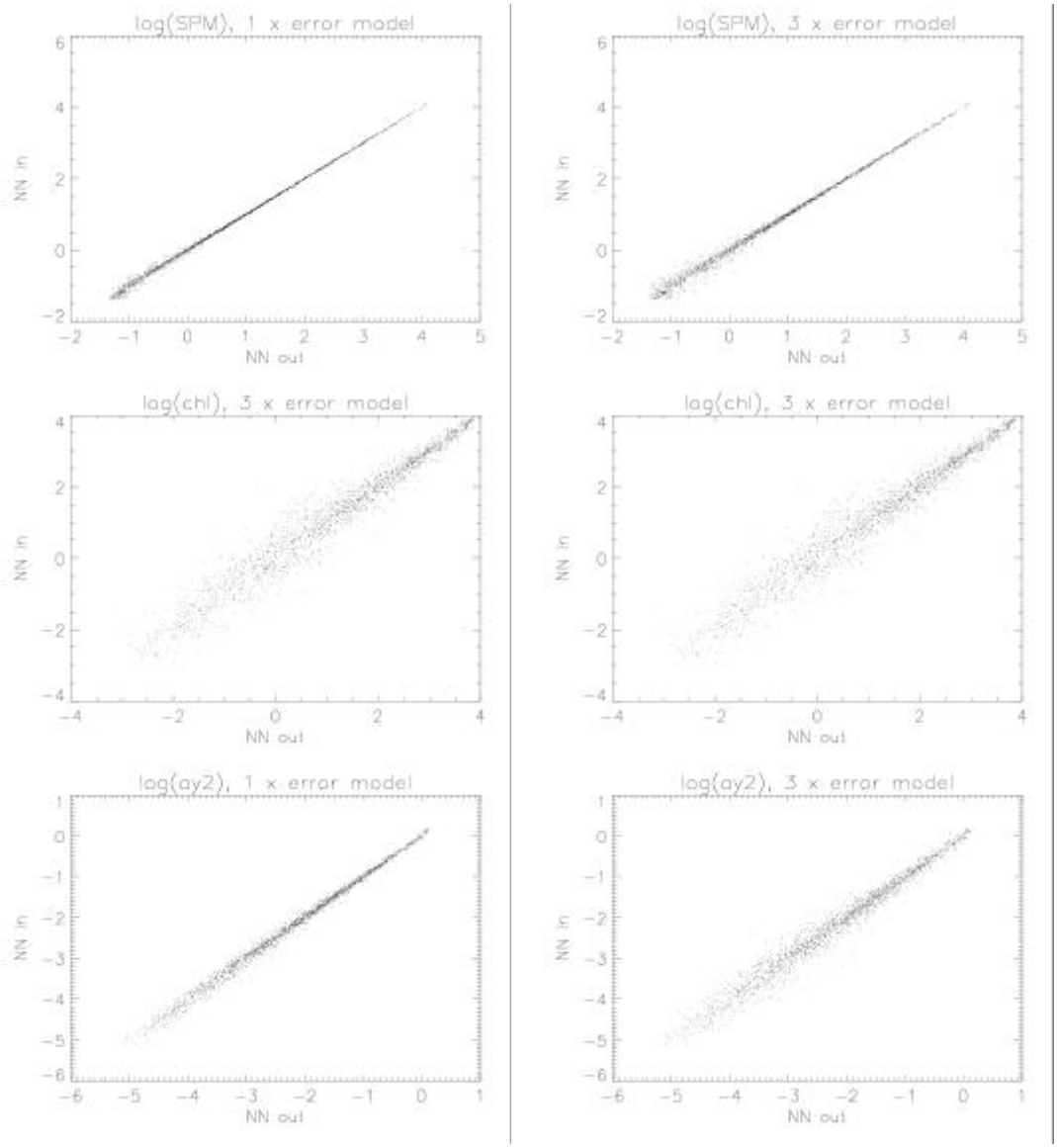

fig. 8 Performance of `inv_NNnoise` for test data with noise corresponding to the error model (left) and 3 times the error model (right)

3. Improvement of run time checks and exception handling

In the original MERIS ATBD a rather simple scheme do detect out of scope situations was planned. The high accuracy of NN's emulating the forward model made possible an extension of the idea descibed in section 7.4.5 of the MAPP ATBD: a check with the help of the forward model can now be performed operationally for all pixels.

3.1 The new MERIS scheme

In the MERIS groundsegment the `out of scope flag' now is derived according to the scheme indicated in `fig. 9`, where **r,r'** stands for the logarithm of the reflectances.

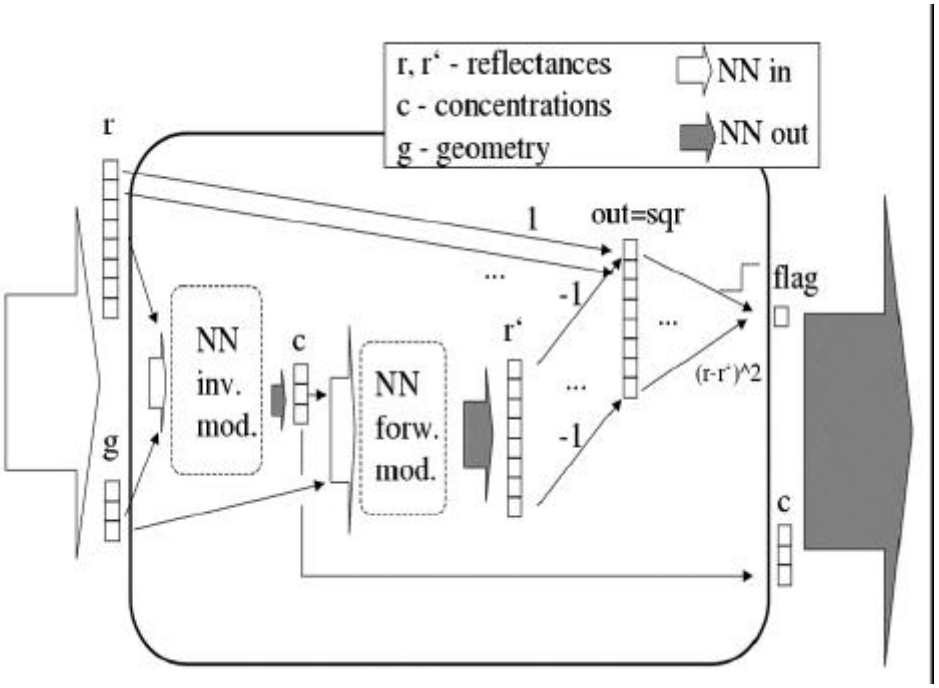

fig. 9 New scheme to derive `out of scope flag'

The concentrations obtained by the inverse NN `inv_NNnoise` together with the angles are fed into the forward NN `forw_NN` to derive reflectances which are compared with the measured ones. Let `dsq` the sum of the squared deviations.
For the MERIS groundsegment the threshold value `dsq=dsq_cut` at which the flag for 'out of scope' is raised was determined from `fig. 10`.

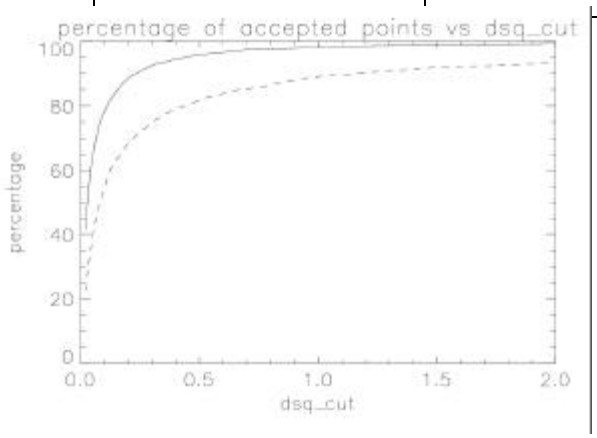

fig. 10 Percentage of points with `dsq<dsq_cut` as a function of `dsq_cut` is shown for the test samples corresponding to the error model (line) and to 3 times the error model (dashed)

The choice `dsq_cut=0.7` removes 2.5% from the sample corresonding to the original error model but removes 15% from the sample corresponding to three times the error model. In `fig. 11` an example is given of the improvement due to the cut: the rms of the deviation in this plot goes from 0.3 to 0.35.

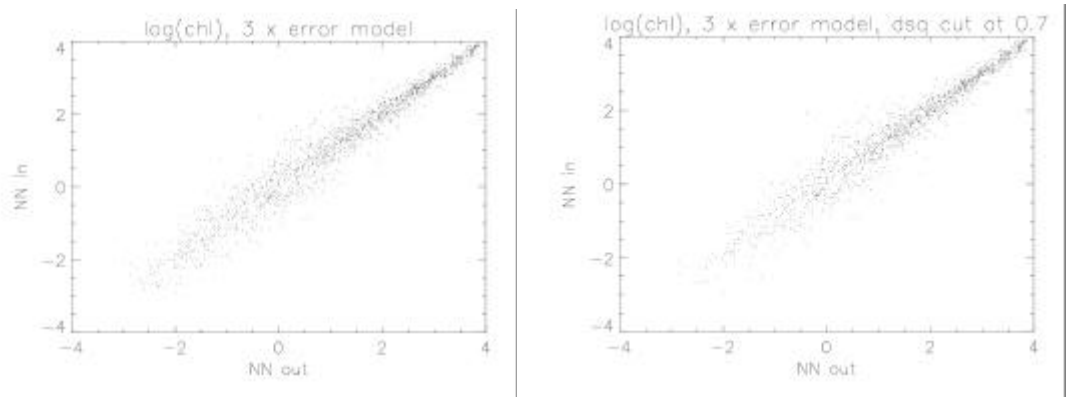

fig. 11 Improvement of the NN retrieval due to cut `dsq<0.7` using the test sample corresponding to three times the error model

3.2 Conclusion

The new MERIS scheme to find ‘out of scope’ situations is certainly more powerful compared to the original one. But for MERIS due to the fixed architecture it was not possible to use more then a bit to signal the result of the check. In MAPP a more detailled information about the value of `dsq` should be given to the user.

3.3 Concerned ATBD sections´

7.4.5, 7.4.6, 7.4.10, 14.2, 14.3, 16.5